UNIVERSIDAD POLITECNICA DE VALENCIA

ESCUELA POLITECNICA SUPERIOR DE GANDIA

MASTER EN INGENIERIA ACUSTICA

LINE ARRAY DESIGN

TRABAJO FIN DE MASTER

Autor:
Diego Hernández García

Directores:
Jin Huang (FCU)
Rubén Picó (UPV)

Junio de 2012

逢 甲 大 學

電 聲 碩 士 學 位 學 程

碩 士 論 文

Line array design

指導教授：黃錦煌

研究生：Diego Hernández

中 華 民 一 百 零 一 年 六 月

Contents

List of figures

Abstract

This master thesis is devoted to study the acoustic and psycho-acoustic characteristics of binaural reproductions on speaker line arrays. The main goal is to study the beamforming theory and its validation by comparing with measured results. In addition, some applications for line speaker arrays are presented.

Beamforming and its applications have been investigated in recent decades. However, the rapid growth of technology requires smaller speakers in order to install them in devices like flat televisions, laptops, cell-phones or electronic tables. Therefore, this thesis work will focus in small size speakers and low power applications suitable for domestic and portable audio reproduction.

With transaural audio reproduction it is possible to provide a virtual environment where the source locations are perceived at positions where no physical sources exist. Headphones can be used to reproduce binaural signals due to the low crosstalk they offer. Even thought, in some applications for convenience loudspeakers are preferred, undesired signal arrives to the contralateral ear. To improve the crosstalk and sensation of separated channels this thesis presents the using of line arrays for binaural audio reproduction. Psychoacoustic cues to guess where the sound source is located or Head Related Transfer Functions are used in combination with beamformers to obtain trans-aural audio reproduction.

In order to design and simulate line arrays Graphical User Interfaces will be presented. Programmed by Matlab, they offer a tool to design and study the beamformers. By introducing the characteristics of the line array, different directivity representations and useful parameters will be given. It also allows the simulation by using real speaker directivities previously measured.

To validate the simulation of line arrays, different measurements will be carried out in an anechoic chamber by using a turn table controller. This thesis describes an audio system composed of signal processor, amplifiers and speaker line array that can be used to generate directional steerable beams and transaural audio reproduction. In order to amplify the signal to the speakers, the design and construction of an eight-channel amplifier will be explained in detail.

Keywords: beamforming, line array speaker, 3D audio, transaural audio

1 Introduction

This master thesis is a result of research carried out at the Electro-Acoustics Department of Feng Chia University in Taichung, Taiwan; under an international student exchange program with the Polytechnic University of Valencia, Spain. During the thesis period, it has been maintained a close cooperation with Merry Electronics, a worldwide leader company in acoustic devices manufacturing.

1.1 Motivation

Beamforming and its applications have been deeply researched during the last decades. The rapid growth of technology in multimedia and electronic devices requires considering smaller speakers. Therefore, this thesis work focus the applications for small size speakers and low power applications suitable for domestic and portable audio reproduction such as laptops, flat televisions, electronic tables or cell-phones among others. Thanks to the evolution in Digital Signal Processors, the processing of multiple channels simultaneously is easily implementable. Then, elaborated audio algorithms can be tested and measured in order to validate the presented simulations.

1.2 Structure of the thesis

This thesis is composed of seven chapters. After this introduction, beamforming theory will be explained in detail in Chapter 2. Chapter 3 will present the algorithms to obtain electrical steering. Several applications and trans-aural audio reproduction for beam-formers will be explained. In chapter 4, different methods to simulate the beam forming theory will be presented. Chapter 5 is devoted to explain the audio system designed to test and measure the proposed algorithms. A validation of the simulated results by comparing with measurements will be presented in Chapter 6. Finally, conclusions and directions for future work will be given in Chapter 7.

1.3 Background

Beamforming is a signal processing method to obtain desired directivity patterns. It is based on constructive and destructive interferences formed on the wave front. The technique is widely used in multiple applications for electromagnetic waves or mechanical waves, both transmitter and receptors. Wireless communications, radar, antennas ultrasound scanners, sonar, noise cancelling… any application that requires focusing the energy in an angular direction (Figure 1-1). Beamforming in this thesis is devoted to audible frequency produced by a speaker line array. The most common application of speaker arrays is live sound reinforcement [1], where several speakers can be arrayed in order to focus the sound pressure level on specific areas. This work

considers arrays composed of small speakers, in order to use them in High Fidelity or domestic applications.

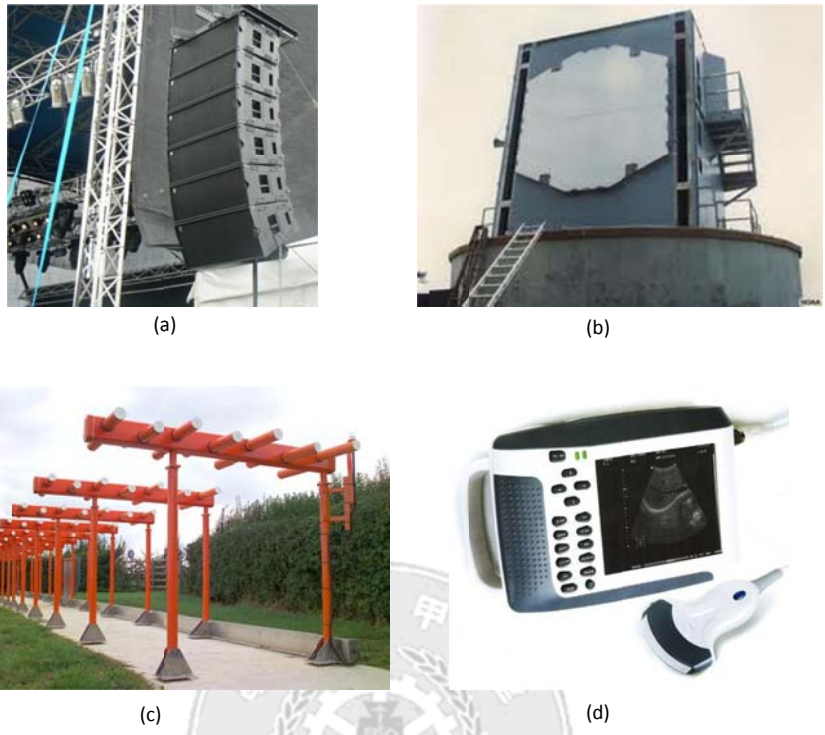

(a) (b) (c) (d)

Figure 1-1 Beamforming applications: (a) Live sound (b) Radar (c) Antennas (d) Ultrasound scanners

During the last decades many different audio systems have been developed. Considering loud-speaker sound systems, the most simple is a mono-phonic system, which is not able of reproducing spatial characteristics. Stereo-phonic offers an audio reproduction of sound images distributed between the two speakers. Depending on the angle, the listener will have wider stereo reproduction. To obtain the maximum stereo angle the speakers have to be located in front of each ear, but this configuration is difficult to achieve in most of the situations. The goal of 3D audio applications is to recreate natural environments on stereo-phonic audio systems by using signal processing. Stereo audio system can be considered as binaural reproduction, where undesired signal arrives to the contralateral ear. The basic trans-aural crosstalk canceller is based in Head Related Transfer Functions and cues to guess where the sound source is located. This technic assumes the sources are omnidirectional. Therefore, this thesis work presents trans-aural crosstalk cancellation on speaker line arrays, which provide reduction of the crosstalk previously presented due to its directional proprieties.

1.4 Literature review

Physical acoustics and sound engineering books, such as "*Sound system engineering"* [2] and "*Fundamentals of physical acoustics*" [3], devote sections to introduce readers to the

beamforming theory. These books provide the beamforming theory via mathematical formulation. Furthermore, other books like "*Electroacoustic Devices Microphones and Loudspeakers*" [4] and "*Sound Systems Design and Optimization"* [5], focus in beamforming for live sound applications. That is, long distances applications by using arrays composed of high power multi-via loudspeakers. This thesis adopts their concepts, and utilizes them to Hi-Fi domestic applications.

The concepts of Quarter Power Angle (-6 dB angle) and far field estimation proposed by Ureda [12, 14, 15], are considered in this thesis. Other authors like Smith [6, 7] and Meyer [13, 21] published papers related to discrete line arrays and optimization, focused in live sound. Wooh and Shi have published several papers related to beamforming in ultrasounds [8, 9, 10]. Their results will be adopted in this thesis to calculate the frequency working range of the line array.

The concept of 3D audio is a knowledge researched topic. The basic principle of transaural audio reproduction was presented by Bauer in 1961 and first implemented by Atal and Schroeder in 1966. Binaural signal is filtered by Head Related Transfer Functions (HRTF) and crosstalk cancellation. Gardner [27] and Huopaniemi [29] offered a deep research in 3D audio. Furthermore, Guldenschuh and Sontacchi [26] used beamforming to obtain transaural audio reproduction. The thesis applies their concepts to develop an algorithm for 3D sound by using line array speaker sources.

Self published several books related with audio electronics. This thesis considers "*Audio Power Amplifier Handbook*" [34] as a reference to study audio amplification. For the electronic design, the datasheet of the IC provided by the manufacturer [39] has been used. Additionally, sound system equipment standards for amplifier [40] and loudspeaker [41] measurements have been considered.

2 Beamforming theory

2.1 Introduction

Speakers can be arrayed in order to produce directivity patterns that may not be possible from a single speaker. The main benefit of line array is the ability to obtain a desire steered angle by electrical steering, in other words, by applying delayed signals to each speaker [1, 2, 3]. Furthermore, a speaker array can be employed to increase the sound pressure level, although it is not the main purpose in this study.

The objective of this thesis is to study and analyze the physical behavior of beamforming in order to optimize the design, and obtain a desired performance. The equations and methods described in this chapter will be used to develop a Graphic User Interface (GUI) and predict the directivity function of a real loudspeakers line array configuration.

The consideration in this study is restricted to time-harmonic radiation in the far field. The distance between the source and the listener is not too large, hence the air absorption is not considered. The directional sources are one way speakers provided by Merry Electronics (Taiwan), and the examples shown will be related with them.

First, a simple two elements array will be presented in order to introduce the discrete array. Then, the continuous array will be used to analyze the phased array. Lastly, other relevant points will be explained in order to find a method to design line arrays and obtain its characteristics.

2.2 Representation of the directivity

There are different possibilities to present a directivity function on a graphic. The most common way is to plot the directivity factor on polar coordinates system, where the directivity is given for one frequency. Furthermore, this thesis also considers Cartesian coordinates and 3D representations.

2.2.1 Cartesian and polar coordinates

The X axis or angle information can be represented in Cartesian or polar coordinates. As shown in Figure 2.1 (a), the information is presented in polar representation by a distance and an angle. By using the angle in the polar system as the angle of the directivity, it results an easy and natural way to observe the directivity.

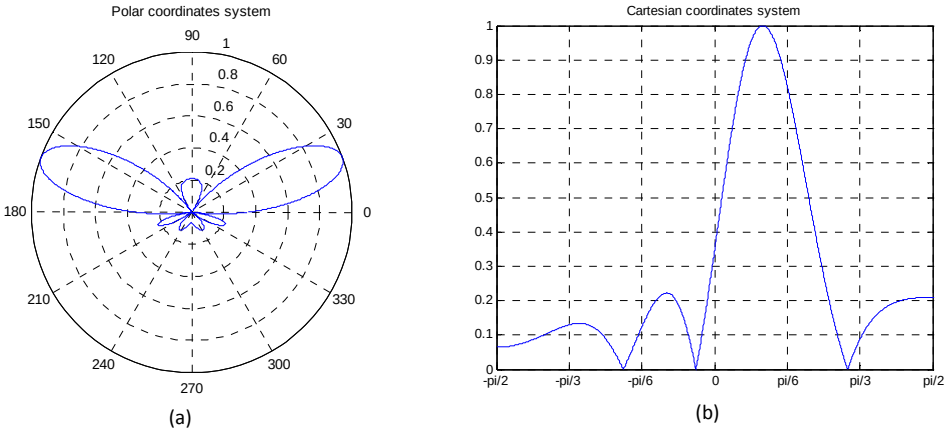

Figure 2.1 Directivity representations: (a) Polar coordinates (b) Cartesian coordinates

Polar system is convenience to obtain information of maximum lobes of the directivity pattern, but the lowest values can be too closed to be observed clearly. As shown in Figure 2.1 (b), Cartesian coordinate system displays the low values on the X axis becoming easier to observe the secondary lobes.

2.2.2 Directivity and sound pressure

The directivity at one frequency is the relation between the intensity at the angle and the maximum of all the angles. In other words, the directivity is normalized to the maximum in each frequency. In this case, the information of the pressure or frequency response for each angle is not considered. In order to observe the sound pressure distribution and the directivity, it is possible to represent the sound pressure on a decibel scale or normalize the directivity function to the maximum of all the frequencies and angles. This representation requires the frequency response of the source for each angle, and it is needed to be obtained previously. Figure 2.2 represents the measured directivity of a line array speaker at 2 kHz to compare the three representations.

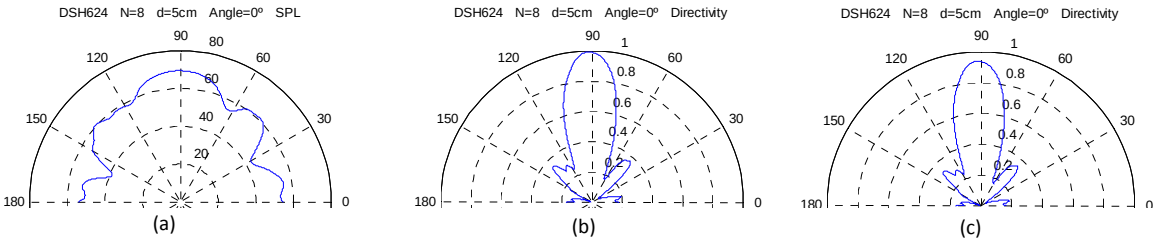

Figure 2.2 Directivity patterns: (a) Pressure (b) Directivity factor (c) Normalized to all frequencies maximum

2.2.3 Three-dimension representation

Lastly, frequency, angle and directivity can be plotted in a three-dimensional representation. The frequency axis can be expressed in linear or logarithmic and the Z axis represents the pressure in decibels or normalized, as shown in Figure 2.2 (a) and (b).

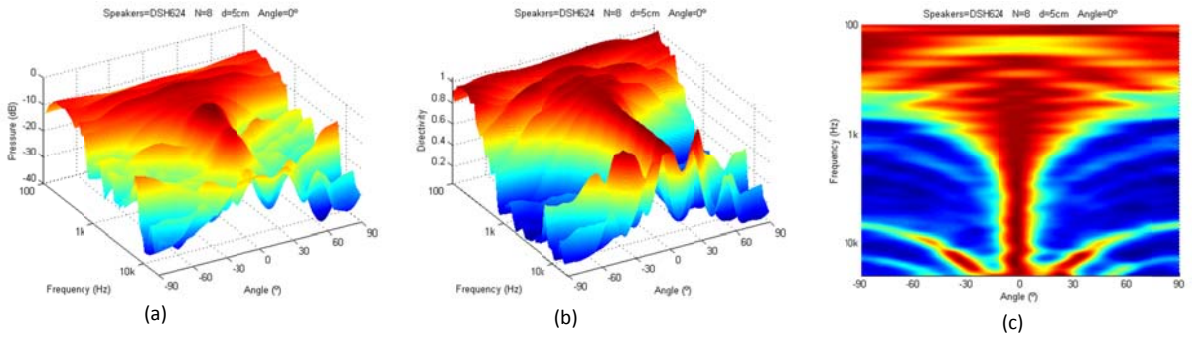

Figure 2.3 3D directivity patterns: (a) Pressure (b) Directivity factor (c) Top view

If the directivity function presents too many abrupt changes, the observation can be difficult. Even though it is possible to smooth the function, it is convenient to move the point of the observation to the top of the figure. As represented in Figure 2.3 (c), an easier visualization of Figure 2.3 (b) is obtained. Unless otherwise indicated, the pressure is displayed from -40 to 0 dB.

2.3 Array of two elements

The general solution for outward wave propagation is written as

$$p = \frac{A}{r} e^{j(\omega t - kr)} \tag{2.1}$$

where *A* is the amplitude and *r* the distance to the source. Because the receptor is in the far field the rays coming from the sources take parallel paths [3]. In a two element array each source radiates in the far field as

$$p = p_1 + p_2 = \frac{A}{r} e^{j(\omega t - kr)} \left[e^{j\theta} + e^{-j\theta} \right] = 2 \frac{A}{r} e^{j(\omega t - kr)} \cos\theta \tag{2.2}$$

$\theta = (kd/2)\ \sin\theta$ is half the difference in phase between the signals. Combining Eq. (2.1) and Eq. (2.2) the pressure becomes

$$p = 2 \frac{A}{r} e^{j(\omega t - kr)} \cos\left[\frac{kd}{2} \sin\theta \right] \tag{2.3}$$

The acoustic pressure of the Eq. (2.3) is the product of three different factors. The first, factor *A/r,* denotes the amplitude term and factor $\cos[kd/2\ \sin\theta]$ represents the directivity term. That is, the pressure is in relation to direction and frequency. The factor $e^{j(\omega t - kr)}$ describes wave propagation [3].

The general directivity function is the relation between the pressure at angle θ and the maximum pressure. The directivity function of two sources line array is

$$D(\theta) = \left|\frac{P(r,\theta)}{P(r,\theta_{max})}\right| = \left|\frac{2\frac{A}{r}e^{j(\omega t - kr)}\cos\theta}{2\frac{A}{r}e^{j(\omega t - kr)}}\right| \tag{2.4}$$

$$D(\theta) = \left|\cos\left(\frac{kd}{2}\sin\theta\right)\right| = \left|\cos\left(\frac{\pi d}{\lambda}\sin\theta\right)\right| \tag{2.5}$$

Figure 2.4 explains a detailed evolution of the directivity obtained by varying the inter-element spacing d.

a) If $\pi d/\lambda \ll 1$ ($d \ll \lambda$) the two sources practically coincide, and yield an omnidirectional directivity pattern (Figure 2.4 (a)).
b) As $\pi d/\lambda$ increase from near zero ($d < \lambda/2$) the pattern begins to emerge on axis (Figure 2.4 (b)).
c) When $\pi d/\lambda = \pi/2$ ($d = \lambda/2$) the lobe on axis becomes a null in the normal direction and an eight directivity pattern results. The radiation is null in the direction because the two signals emitted in that direction are exactly $180°$ out of phase (Figure 2.4 (c)).
d) If $\pi d/\lambda$ is increased further ($\lambda/2 < d < \lambda$), the beam narrows, the null moves to lower angles and side lobes appear (Figure 2.4 (d)).
e) When $\pi d/\lambda$ reaches the value π ($d = \lambda$), the sidelobes become as big as the main lobes at $0°$ and $180°$ (Figure 2.4 (e)).

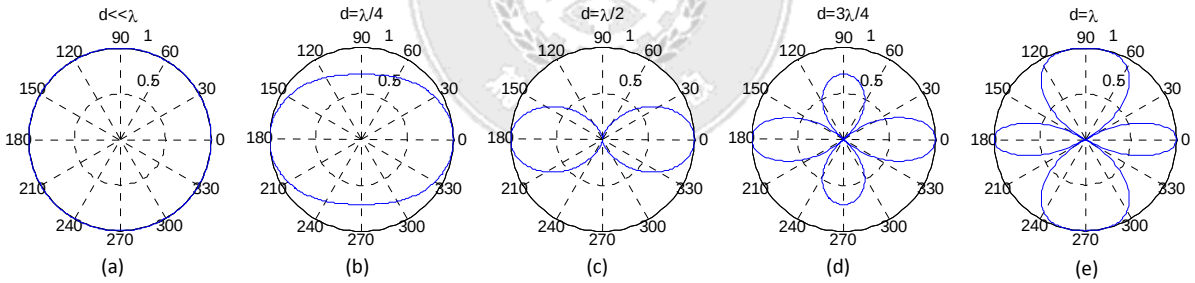

Figure 2.4 Two elements array: inter-element spacing evolution

Considering the phase shift, it is possible to provide an electrically beam steering. The difference in phase between two sources is $2\theta_s$. Then, the directivity becomes

$$D(\theta) = \left|\cos\left(\frac{kd}{2}\sin(\theta - \theta_s)\right)\right| \tag{2.6}$$

As shown in θ evolution in Figure 2.5, the major lobe now appears at $\theta = \theta_{max} = \sin^{-1}(2\theta_s/kd)$. When $\theta_s = \pi/2$, the two sources are out of phase with each other, their contributions cancel in the normal direction $\theta = 0°$. Then, directivity function becomes an eight pattern, also called as end-fire.

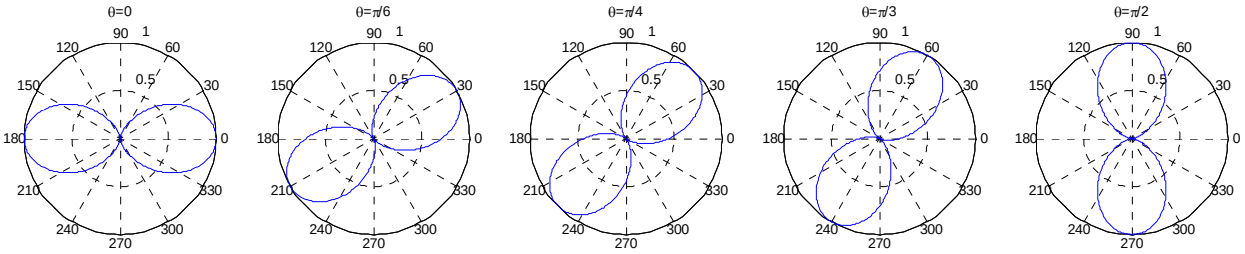

Figure 2.5 Two elements array: steering angle evolution

2.4 Discrete array

A discrete line array is defined as an array of omnidirectional point sources [2, 4, 6]. Figure 2.6 illustrates an array of N elements where *L* represents the array length, θ_s is the steered angle and *d* is the inter-element spacing.

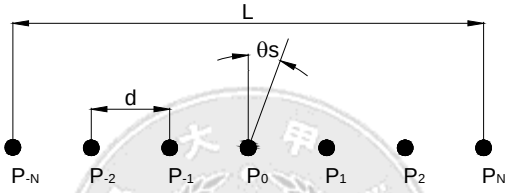

Figure 2.6 Discrete line array

Considering an equal inter-element spacing *d,* the pressure p_0 is the same as (2.1). For the point designated as P_{-1} is

$$\mathrm{P}_{-1} = \frac{\mathrm{A}}{\mathrm{r}} e^{j[wt-k(r+d\sin\theta)]} = p_0 e^{-j2\theta_s} \tag{2.7}$$

The pressure p of the N sources is a finite sum represented as

$$p = p_0\left[\ldots + e^{-j4\theta_s} + e^{-j2\theta_s} + 1 + e^{j2\theta_s} + e^{j4\theta_s} + \cdots\right] \tag{2.8}$$

Taking out the term $e^{-j(N-1)\phi}$ the equation is transformed to

$$p = p_0 e^{-j(N-1)\theta_s}\left[1 + e^{-j2\theta_s} + e^{-j4\theta_s} + \cdots + e^{-j2(N-1)\theta_s}\right] \tag{2.9}$$

Considering the geometric progression of the form $1 + x + x^2 + \cdots + x^{N-1}$ sums to $\frac{1-x^N}{1-x}$, then the pressure can be expressed as

$$p = p_0 \frac{e^{jN\theta}}{e^{j\theta}} \frac{1 - e^{jN\theta}}{1 - e^{j\theta}} = p_0 \frac{e^{jN\theta} - e^{-jN\theta}}{e^{j\theta} - e^{-j\theta}} = p_0 \frac{\sin N\theta}{\sin\theta} \tag{2.10}$$

On axis ($\theta = 0, \theta_s = 0$), the pressure is $p = Np_0$, then, the directivity function becomes

$$D(\theta) = \left|\frac{\sin N\theta}{N \sin \theta}\right|$$

Including the inter-element spacing and wavelength ($\theta = \pi d/\lambda \, sin\theta$), finally the directivity function for a discrete line array becomes

$$D(\theta) = \left|\frac{\sin\left(N\frac{\pi d}{\lambda} sin\theta\right)}{N \sin\left(\frac{\pi d}{\lambda} sin\theta\right)}\right| \quad \textbf{(2.11)}$$

Figure 2.7 shows the evolution of directivity corresponding to the number of elements (N) of the array. If the inter-element spacing keeps constant at $\lambda/2$ meanwhile the length of the array increases, it is observed that the directivity is increased as the number of elements increases. In other words, the line array becomes more directional as the length increases.

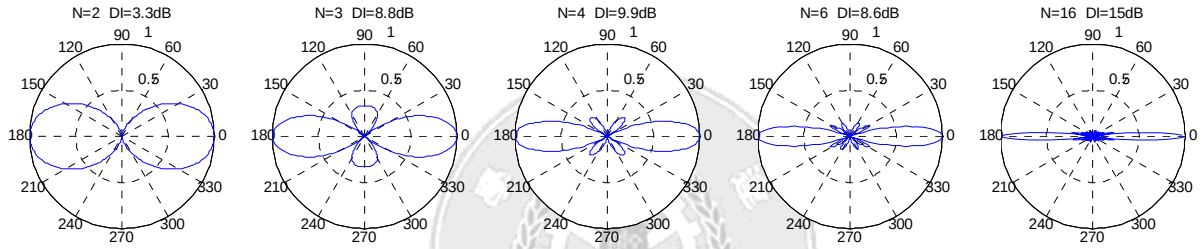

Figure 2.7 Discrete line array: number of elements evolution

The beam can be steered to a desire angle. Then, by including the phase in (2.11) the directivity function becomes

$$D(\theta) = \left|\frac{\sin\left(N\frac{\pi d}{\lambda}(\sin(\theta) - \sin(\theta_s))\right)}{N \sin\left(\frac{\pi d}{\lambda}(\sin(\theta) - \sin(\theta_s))\right)}\right| \quad \textbf{(2.12)}$$

Figure 2.8 shows the effect of increasing N with a fixed phase of $\pi/4$ (steered angle at 45 degrees). Again, the separation between the elements keeps constant at $\lambda/2$ meanwhile the length of the array increases.

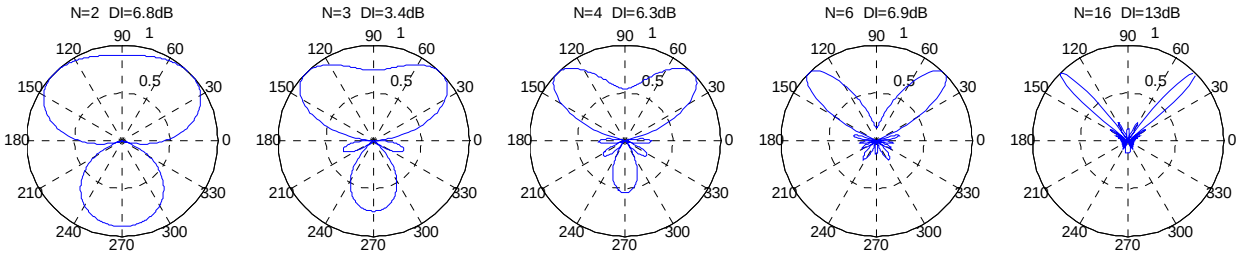

Figure 2.8 Discrete line array: N evolution for a steered angle

The benefit of high directivity can be obtained by increasing the length of line array. When the relation d/λ increases, secondary lobes appears [6, 7]. These lobes, called grating lobes, are as prominent as the main lobe, and severally degrade the overall directivity. To avoid this effect, it is possible decrease the inter-element spacing or the working frequency. Figure 2.9 shows an six-element array with different values of d/λ relation.

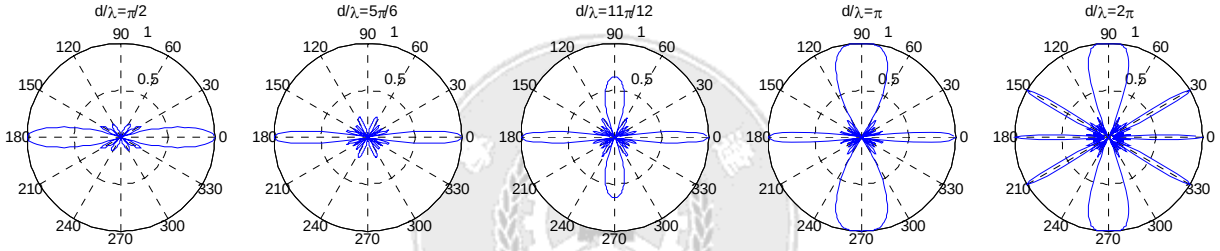

Figure 2.9 Discrete line array: the grating lobes apparition

2.5 Continuous array

Considering a discrete line array, if the inter-element spacing becomes very small and the number of elements (*N*) very large, a continuous line source can be formed [4, 9] as shown in Figure 2.10.

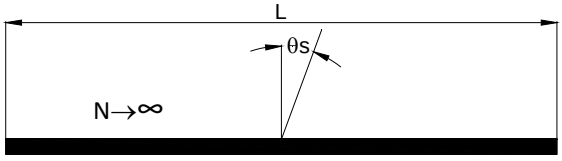

Figure 2.10 Continuous line array

To obtain the directivity function, d can be replaced by $L/(N-1)$ in (2.11).

$$D(\theta) = \left| \frac{\sin\left(\frac{N}{N-1}\frac{kL}{2}\sin\theta\right)}{N\sin\left(\frac{kL}{2(N-1)}\sin\theta\right)} \right| \tag{2.13}$$

In the limit $N \to \infty$, the directivity function becomes

$$D(\theta) = \left| \frac{\sin\left(\frac{1}{2}kL\sin\theta\right)}{\frac{1}{2}kL\sin\theta} \right| = \left| \frac{\sin\left(\frac{\pi}{\lambda}L\sin\theta\right)}{\frac{\pi}{\lambda}L\sin\theta} \right| \tag{2.14}$$

Considering the phase, for a steering angle θ_s the directivity function becomes

$$D(\theta) = \left| \frac{\sin\left(\frac{\pi}{\lambda}L(\sin(\theta_s) - \sin(\theta))\right)}{\frac{\pi}{\lambda}L(\sin(\theta_s) - \sin(\theta))} \right| \tag{2.15}$$

Now, the directivity function is a $\sin(x)/x = sinc(x)$ function; it behaves as an ideal line array source. Also this directivity function is the same of a piston of length *L*, which is useful to study the phased array. Figure 2.11 (a), (b) and (c) shows a comparison of discrete and continuous line array of same length at 3.5, 4 and 5 kHz, respectively. Note the grating lobes are totally avoided with the continuous array when the frequency is increased.

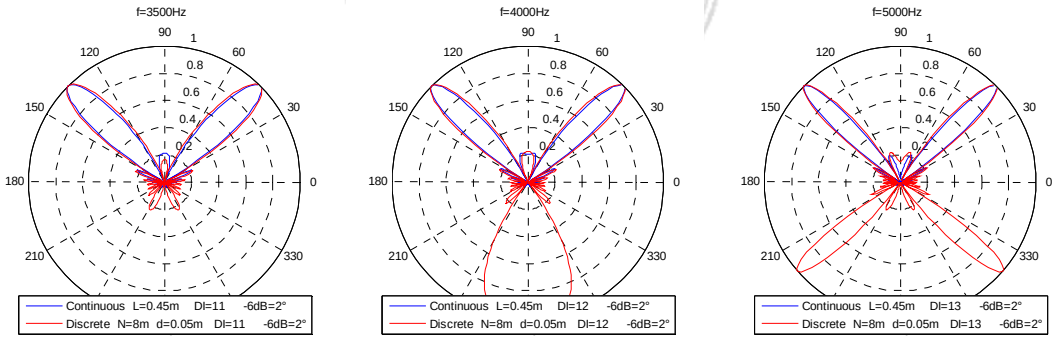

Figure 2.11 Comparison of discrete and continuous line array

It is interesting to obtain a uniform directivity model in order to study further array configurations. A line source can be defined, as shown before, as a continuous and infinite number of sources along a line. Then, the acoustic pressure radiated in the far field from it can be expressed as

$$p = \frac{1}{r}\int_0^L A(x)e^{-j(kr(x)+\theta(x))}\,dx \tag{2.16}$$

The general directivity function is the relation between the pressure at angle θ and the maximum pressure, as follows

$$D(\theta) = \left|\frac{p}{p_{max}}\right| = \left|\frac{\int_0^L A(x)e^{-j\left(kr(x)+\theta(x)\right)}\,dx}{\int_0^L A(x)\,dx}\right| \tag{2.17}$$

By substituting in Eq. (2.17) a constant amplitude ($A(x) = A$) and a constant phase ($\theta(x) = 0$), the directivity function obtained is the same that the obtained by Eq. (2.15).

2.6 Directional sources array

So far, ideal omnidirectional and line sources were considered. Real speakers with its own directivity can be used as represented in Figure 2.12.

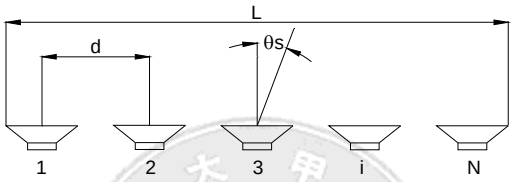

Figure 2.12 Directional source line array

When the directivity function of a speaker is considered, the calculations are based in the far field where the sound pressure level decreases linearly with the distance. After obtaining the directivity of the sources, and considering that all the elements of the array have the same directivity D_e, Eq. (2.1) becomes [4]

$$\mathrm{p_0} = \frac{\mathrm{A}}{\mathrm{r}} D_e(\theta) e^{j(wt-kr)} \tag{2.18}$$

With the replacement for p_0, the directivity equation can be expressed as

$$D(\theta) = D_e(\theta) D_a(\theta) \tag{2.19}$$

Where $D_a\,(\theta) = (\sin N\theta)/(N\,\sin\theta\,)$ is the array directivity and $D_e(\theta)$ the directivity of each element. The overall directivity is the product of the element directivity and the array directivity.

In this thesis work different speakers provided by Merry Electronics are used. Their directivity has to be measured before simulation and design. Also, other specifications like frequency response, impedance, dimensions, sensitivity, and power are considered. Next, specifications for the speakers HPS503, HPS131, DSH624 and DSH715 are presented in Table 2.1.

Table 2.1 Speaker specifications

Speaker	Power (W)	Dimensions (cm)	Impedance (Ω)	F_0 (Hz)	Sensitivity
HPS503	3	Ø 5	4	160	80 dB @ 1kHz/1W/1m
HPS131	3	Ø 5	8	160	80 dB @ 1kHz/1W/1m
DSH624	3	Ø 4	4	200	80 dB @ 1kHz/1W/1m
DSH715	1	2.3 x 1.2	4	800	77 dB @ 1kHz/1W/50cm

Due to the small dimensions the DSH715 micro-speakers are provided mounted in a 3 cc enclosure; this will offer versatility to test different configurations. The measured directivity for the speakers is presented in Chapter 6, where each directivity function is presented as a function of angle and frequency on 3D graphics. Also its directivity function is introduced in a Graphical User Interface in order to simulate directional sources. Figure 2-13 shows the images of the different speakers.

Figure 2-13 Speaker images: (a) HPS503 (b) HPS131 (c) DSH624 (d) DSH715

2.7 Phased array

Sometimes, it is not possible to obtain the directivity of the source. The speaker can be approximated to a piston. Then, the phased array is formed, as shown in Figure 2.14, by continuous line arrays of length *a* and inter-element spacing *d* [10].

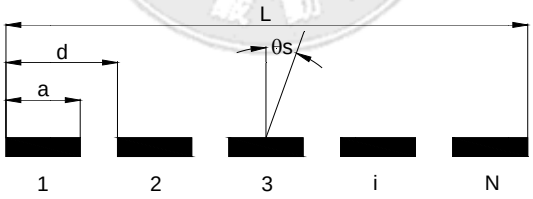

Figure 2.14 Phased array

A continuous line array of length *a* behaves as a piston of diameter *a*, the longer the diameter, the more directive the element. Then, the directivity function of one element can be expressed as

$$D_e(\theta) = \left| \frac{\sin\left(\pi\, a \sin\frac{\theta}{\lambda}\right)}{\pi\, a \sin\frac{\theta}{\lambda}} \right| \qquad \textbf{(2.20)}$$

The overall directivity of the phased array is the product of the element directivity and the discrete array directivity $D_a(\theta)$. By combining Eq. (2.12) and Eq. (2.15) overall directivity is obtained

$$D(\theta) = D_e(\theta)\, D_a(\theta)$$

$$D(\theta) = \left| \frac{\sin\left(\pi\, a \sin\frac{\theta}{\lambda}\right)}{\pi\, a \sin\frac{\theta}{\lambda}} \frac{\sin\left(N\frac{\pi d}{\lambda}(\sin(\theta) - \sin(\theta_s))\right)}{N \sin\left(\frac{\pi d}{\lambda}(\sin(\theta) - \sin(\theta_s))\right)} \right| \quad \textbf{(2.21)}$$

For small values of a/λ or θ_s the term $D_e(\theta)$ tends to one, then, the directivity function of the phased array can be approximated as the discrete array. This effect appears when the element is small enough to consider it an omnidirectional source. For the working frequency of the array the simplification could be applied only for low frequency.

In Figure 2.15 a comparison of discrete and phased array is illustrated. It is observed that the great benefit of the phased array, attenuating undesired lobes when the diameter is increased.

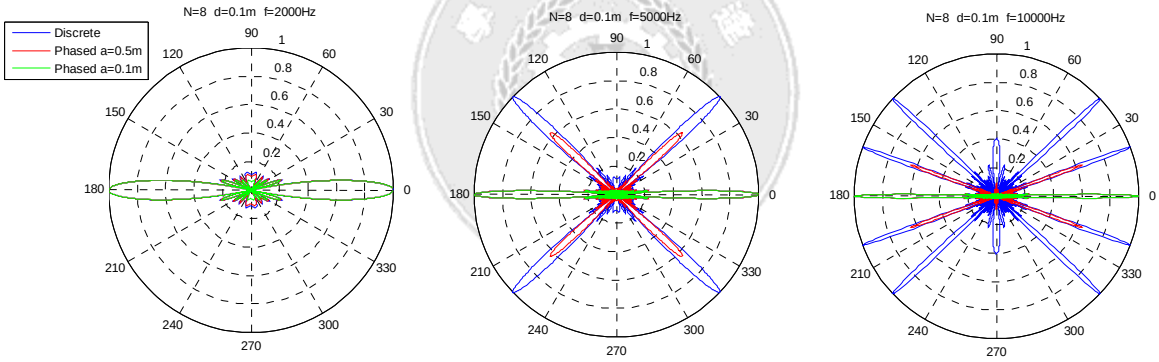

Figure 2.15 Discrete and phased array comparison

2.8 Steering limitations

In this section, the directivity pattern of the line array is analyzed in order to find a solution for an optimum beam steering. This means, to find a condition to produce maximum pressure at the steered angle and minimum in other directions. This limitations have to be valid in a defined frequency range, as far as possible, the working frequency range of the line array.

As the frequency increases, it is observed that the main lobe is surrounded by other smaller lobes appearing at both sides of the main lobe, these lobes are called side lobes. If the frequency increases, other lobes called grating lobes appear [10]. These lobes are as prominent as the main lobe, and its apparition has a strong secondary signal in other direction than the steered angle.

This effect produces a resulting spurious or confusing signal. In Figure 2.16, it is shown an example of a steered angle of 30° where main lobe, side lobes and grating lobes are represented.

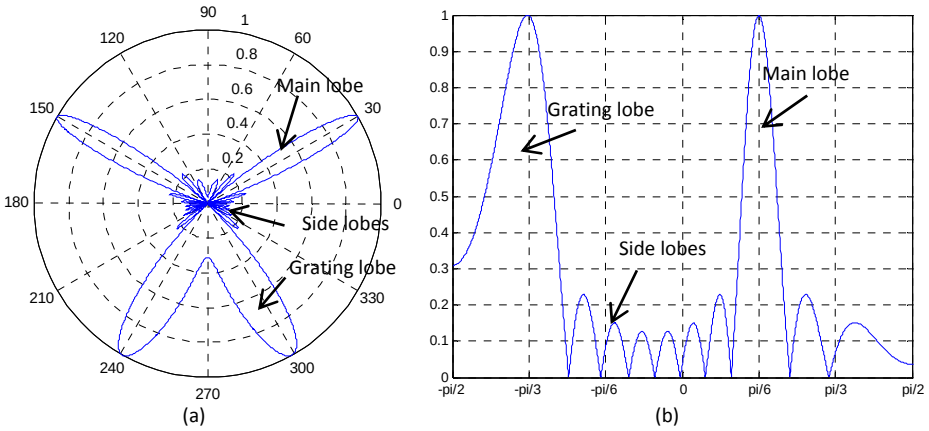

Figure 2.16 Main lobe, side lobes and grating lobes: (a) polar (b) Cartesian coordinates

The goal of an optimum design is to obtain a well-directed main lobe on the steered angle direction and the minimum of amplitude for the other directions. This can be achieved by minimizing the main lobe width and side lobes amplitudes. Lastly, the working frequency range can be restricted by finding where the grating lobes appear.

2.8.1 Main lobe width

It is important to minimize the main lobe width in order to obtain a high directivity. The width of a lobe is defined as the distance between the first zero crossing angles [11]. Then, setting the condition for D=0, the numerator on Eq. (2.21) becomes

$$\frac{N\pi d}{\lambda}(\sin\theta_s - \sin\theta) = m\pi \tag{2.22}$$

The value $m = -1$ represents the first zero for positive angles, and $m = 1$ for negative. Other values for $m = \pm 2, \pm 3, \ldots$ represent the next zero crossing are not considered. The zero-crossing locations can be found at the angles

$$\theta = \sin^{-1}\left(\sin\theta_s - \frac{m\lambda}{Nd}\right) \tag{2.23}$$

The width of the lobe is the angle between the values $m = \pm 1$, it can be obtained as

$$\Delta\theta = \sin^{-1}\left(\sin\theta_s + \frac{\lambda}{Nd}\right) - \sin^{-1}\left(\sin\theta_s - \frac{\lambda}{Nd}\right) \tag{2.24}$$

Figure 2.17 shows an example of a 1 m length discrete array with different number of elements N. It can be observed how the width of the main lobe is influenced by θ_s and N, the width is

increased by increasing θ_s or decreasing N. In other words, the directivity becomes higher when the angle of the steered beam and the inter-spacing are small.

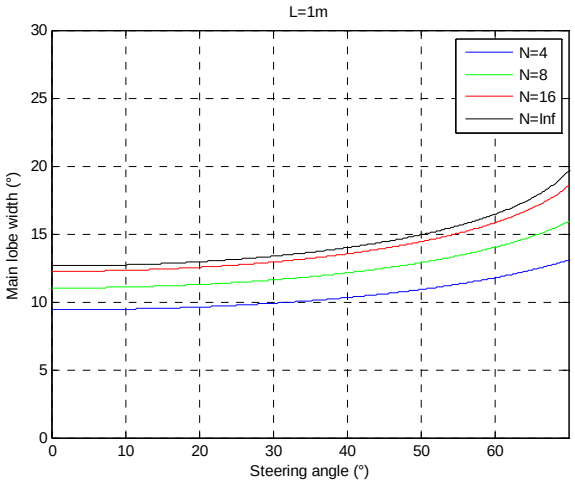

Figure 2.17 Main lobe width as a function of steering angle

2.8.2 Side lobes

It is desired to minimize the side lobes amplitude in order to minimize the leaking of acoustic energy in other directions than the main lobe [12]. According to Eq. (2.22), zero-crossing angles can be found for $m = \pm 1, \pm 2, \pm 3, \ldots$ Assuming that the peaks appear in the middle of the zero-crossings, the approximate locations of the peaks can be obtained as

$$\frac{N\pi d}{\lambda}(\sin\theta_s - \sin\theta) = \frac{(2m+1)\pi}{2} \tag{2.25}$$

$$\theta = \sin^{-1}\left(\sin\theta_s - \frac{(2m+1)\lambda}{2Nd}\right) \tag{2.26}$$

The first lobe (m=1) or peak side lobe has the maximum amplitude among the rest of side lobes, this amplitude is calculated as

$$H(\theta_{psl}) = \left|\frac{1}{N\sin\left(\frac{3\pi}{2N}\right)}\right| \tag{2.27}$$

The amplitude is a function of the number of elements only, in consequence the only way of suppressing the sides lobes is to increase N. In Figure 2.18, amplitude is plotted as a function of N. It is observed a quick convergence to -6.7 dB or 0.21. Increasing N beyond 16 does not improve the amplitude attenuation. Therefore, a line array with more than 16 elements suppresses at maximum the side lobes.

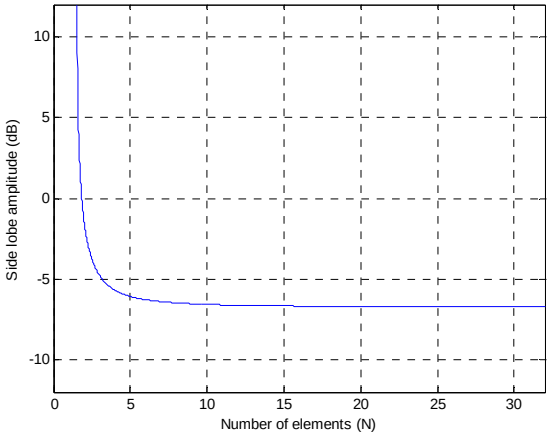

Figure 2.18 Side lobe amplitude as a function of number of elements

2.8.3 Grating lobes and maximum frequency

Finally, the most important is to know the frequency of the first grating lobes apparition. As shown before, the grating lobes are undesired and it is interesting to know how to attenuate them. In order to understand the calculation for phased or directional sources array, the explanation begins for the simplified case of discrete array.

2.8.3.1 Discrete array

The location of the peak can be obtained by finding the condition where the maximum of the lobe is reached [12]. Setting the Eq. (2.10) equal to 1 (maximum) the first grating lobe is founded as

$$\frac{\pi d\ (\sin\theta_s - \sin\theta)N}{\lambda} = \pi \tag{2.28}$$

$$\theta = \sin^{-1}\left(\sin\theta_s - \frac{\lambda}{d}\right) \tag{2.29}$$

The critical inter-element spacing can be obtained by finding the position of the peak value at $\theta = 90°$

$$d = \frac{\lambda}{1 + \sin\theta_s} \tag{2.30}$$

The inter-element spacing obtained indicates the apparition of the center of the lobe. The grating lobe is not completely eliminated; some portion of the lobe still appears in the directivity function. In order to remove the lobe completely, the first zero crossing of the grating lobe is moved further the 90° position. There are an exactly (N-2) number of sides lobes between the main and grating lobes, this condition can be obtained by adding a new term in the equations

$$d = \frac{\lambda}{(1+\sin\theta_s)}\frac{N-1}{N} \tag{2.31}$$

Then, the frequency where the grating lobe appears can be determinate by substituting $\lambda = c/f$.

$$f = \frac{c}{d\cdot(1+\sin\theta_s)}\frac{N-1}{N} \tag{2.32}$$

Also, it is interesting to know the maximum steerable angle as a function of frequency.

$$\theta = \sin^{-1}\left(\left(\sin\theta_s - \frac{c}{d\cdot f}\right)\frac{N}{N-1}\right) \tag{2.33}$$

Figure 2.19 (a) shows the relation d/λ as a function of θ_{max} for different number of elements N. It is observed that the angle increases with a higher N. Figure 2.19 (b) illustrates the maximum steerable angle of a 1 m length discrete array for different number of elements. To avoid grating lobes on high frequency, it is necessary to increase the number of elements.

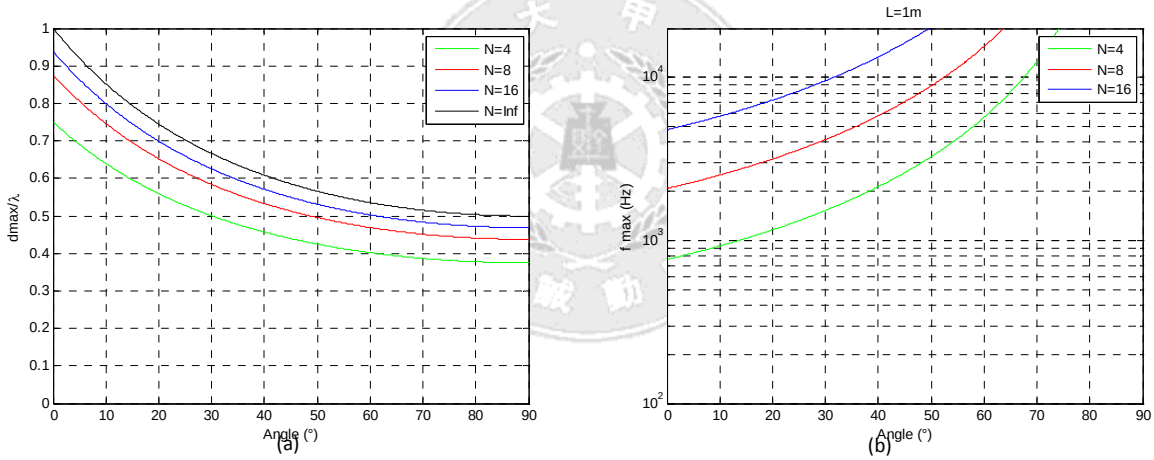

Figure 2.19 Discrete array: (a) Maximum inter element spacing (b) Maximum frequency

By representing the frequency range and steering angles together in a three-dimensional graphic, it is possible to observe the apparition of grating lobes. The examples presented in Figure 2.20 show several lobes apparition by increasing the frequency more than 3 kHz.

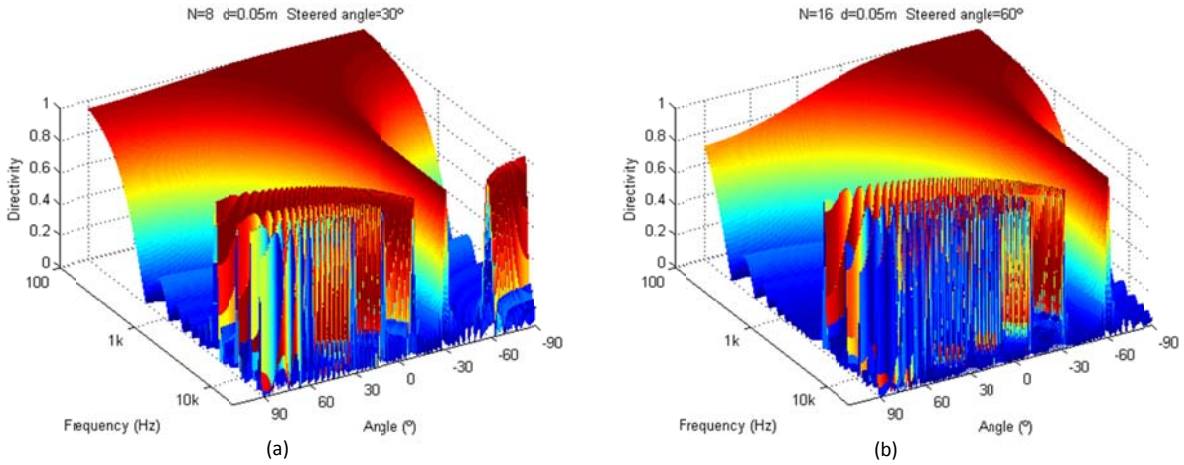

Figure 2.20 Grating lobes apparition in discrete array: Angle steered at (a) 30° and (b) 60°

2.8.3.2 Phased array

As previously shown, the phased array can attenuate or avoid the grating lobes. By the size element equal to the inter-element distance, it is possible to approximate the phased array to a continuous array, where grating lobes are totally omitted. If the size element is reduced, gaps between the elements will be introduced and the grating lobes will appear.

From the directivity function of the phased array shown in Eq. (2.21), the inter-element spacing can be numerically obtained. First the deviation of the grating lobe location $(x - x_0)$ has to be expressed in terms of a/λ, N, and θ_s. Then, d can be derived by assuming linear relation between d and x in the neighborhood of x_0 [12].

$$d = d^0 - (x - x_0)\left(\frac{\partial d}{\partial x}\right)_{x=x_0} \tag{2.34}$$

$$d = \frac{\lambda}{1 + \sin\theta_s} - \frac{3\lambda\left(1 - \frac{a\pi}{\lambda}\tan^{-1}\left(\frac{a\pi}{\lambda}\right)\right)}{\pi^2(N^2 - 1)} \tag{2.35}$$

The apparition of the grating lobe occurs almost at the same frequency due to the low influence of the second term in Eq. (2.35). By computer simulation, it is observed that the great benefit of the phased array is the attenuation of the grating lobes. Due to the directivity of the individual sources, the effect is higher for small angles, where the sources have higher directivity. In Figure 2.21, the directivity of a phased array with different element sizes is shown. The grating lobes are attenuated as the element size increases, but the penalty paid is that the attenuation also of the main lobe at high frequency.

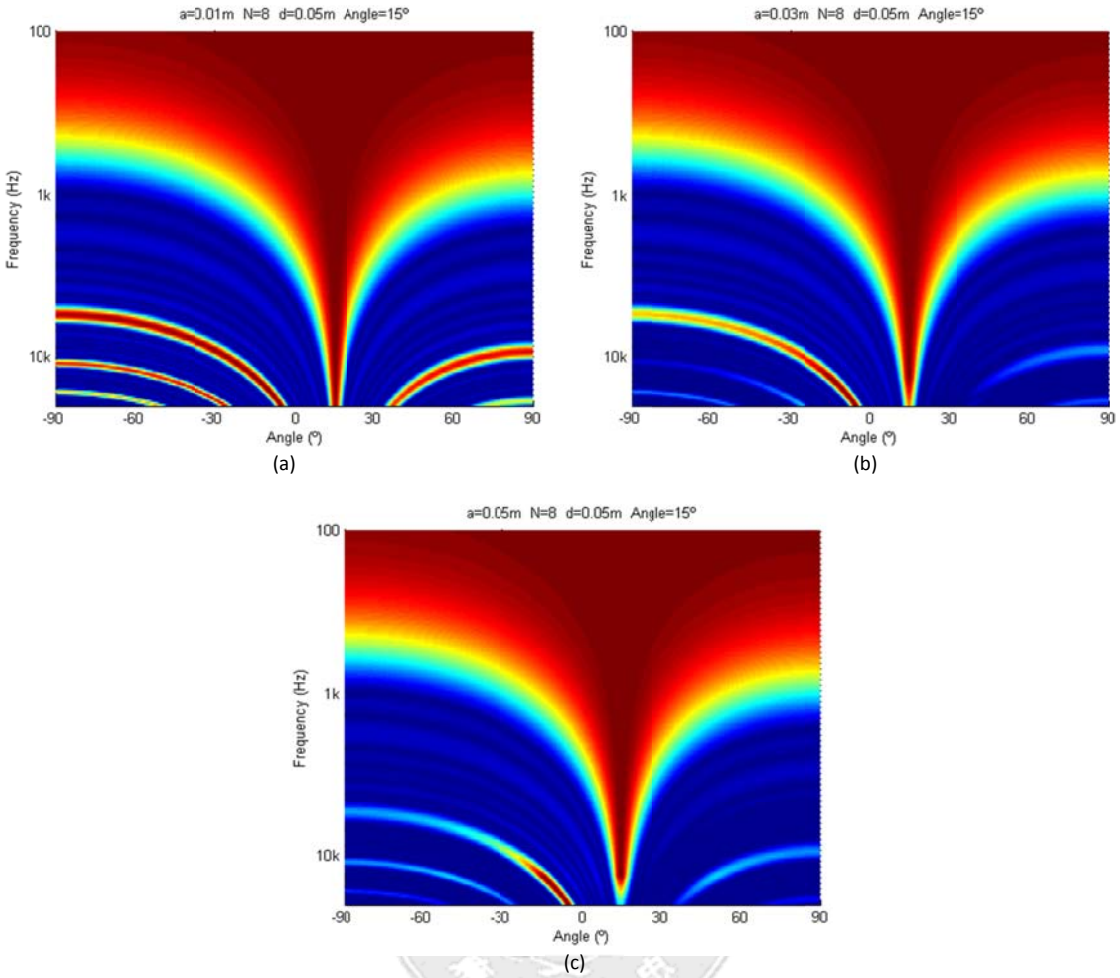

Figure 2.21 Grating lobes (a) a=1 cm (b) a=3 cm (c) a=5 cm

A practical method to find the high frequency limitation is by analyzing the directivity pattern as a function of angle and frequency. Then, a threshold is set on the amplitude at $\pm 90°$ or other angles depending on the reasonable degradation of the directivity accepted. Figure 2.22 (a) plots four different thresholds. Figure 2.22 represents a directivity pattern of a phased array with large element size (*a*), almost the same of the inter-element spacing (*d*). The grating lobes are presented but attenuated enough to not consider the maximum frequency given by Eq. (2.31).

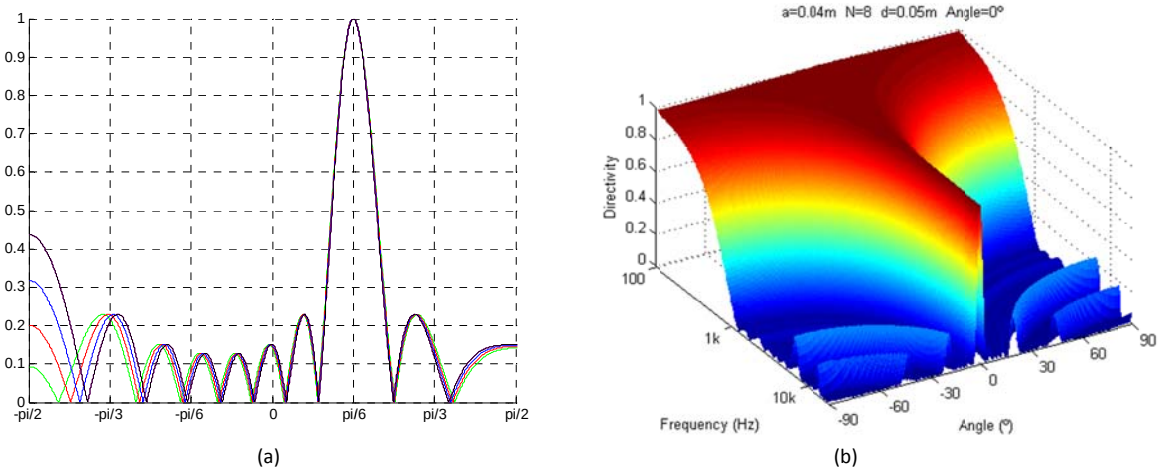

Figure 2.22 Apparition of the first grating lobe: (a) Cartesian coordinates (b) 3D representation

2.8.3.3 Directional sources array

Additionally, real speaker directivities can be considered. If previously obtained, the speaker directivity can be used to calculate the line array directivity function based on Eq. (2.29). But, measuring or obtaining the directivity of the speaker is not always possible, then the source can be simplified as a piston or small uniform array. By defining an effective diaphragm diameter as element size, the simulation result can be obtained by using Eq. (2.21). The use of directional sources always improves the attenuation of grating lobes for all the effective diameters. Therefore, a bigger diaphragm provides better grating lobes attenuation.

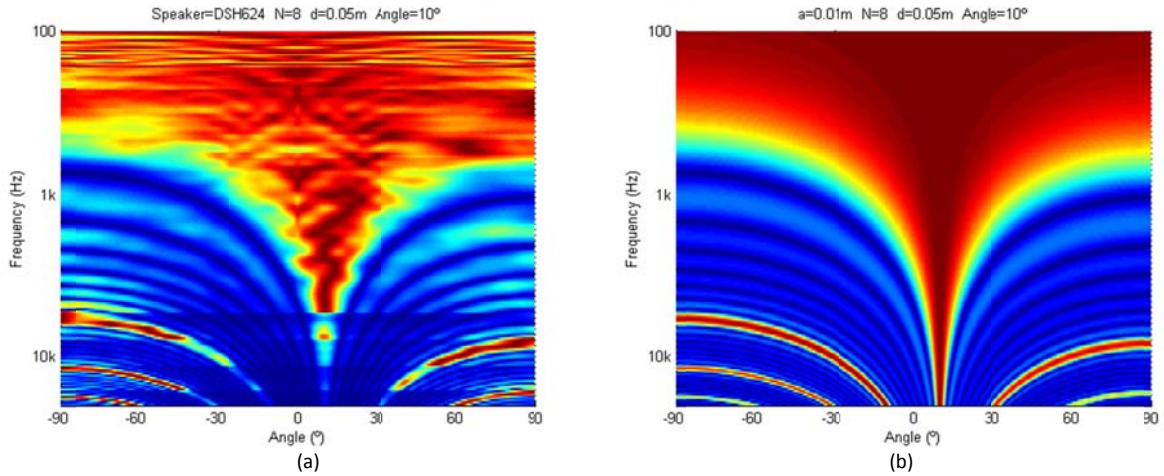

Figure 2.23 Directivity comparison: (a) directional array (b) phased array

2.9 Minimum frequency

The minimum frequency depends on the length of an array. The longer the array is, the more directive at low frequencies. But different criterion can be applied to find the minimum, by defining a threshold for directivity index the quarter power angle does not offer guarantees of

grating lobes avoidance. In this study the minimum frequency limit is defined by finding the first zero-crossing on the directivity function. By setting $m = 1$ and $\theta = 90°$ in Eq. (2.22), the frequency can be expressed as

$$f = \frac{c}{dN \cdot (1 + \sin\theta_s)} \tag{2.36}$$

Considering the half size element a of the phased array introduced at each side of the discrete array the minimum frequency is calculated as

$$f = \frac{c}{(a + dN) \cdot (1 + \sin\theta_s)} \tag{2.37}$$

The frequency depends on a, θ_s, d and N. Figure 2.24 (a) represents the frequency as a function of the length. It is observed how the directivity at low frequency can be obtained by increasing it. Figure 2.24 (b) illustrates an example with several line array lengths. A big influence of the steering angle on the minimum frequency is also observed.

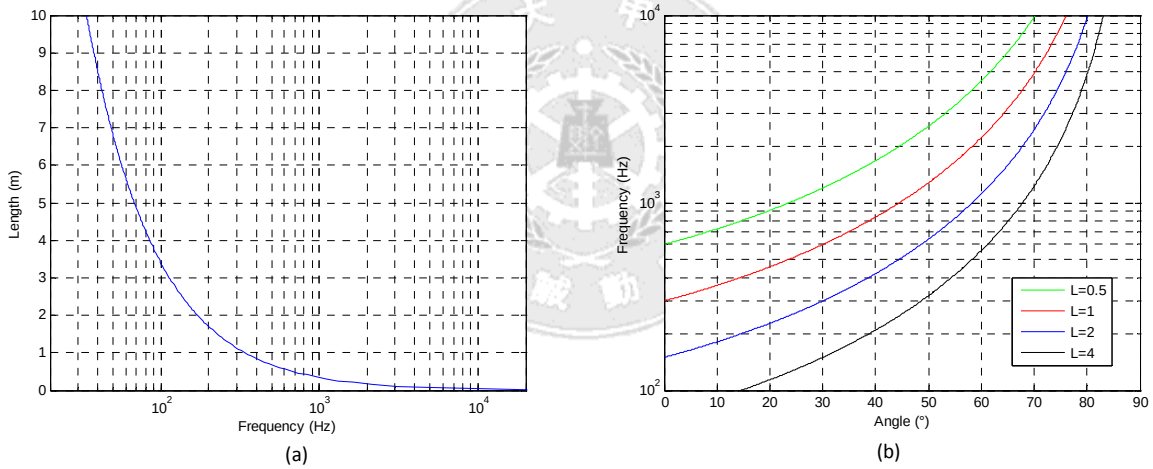

Figure 2.24 (a) Frequency as a function of length (b) Frequency as a function of angle

2.10 Directivity Index

The Directivity Index (DI) is a measurement of the degree of concentration of acoustical power in one direction. In other words, DI is a performance indicator of the directivity. When it is considered time-harmonic radiation in the far field, the intensity can be defined as a relation between pressure and acoustic impedance.

$$I = \frac{P_{rms}^2}{\rho_0 c_0} \tag{2.38}$$

In a directional source, where the intensity varies as a function of angle, the relation between the maximum intensity and the average of all the angles is known as Directivity Factor.

$$D_i = \frac{I_{max}}{I_{ave}} \tag{2.39}$$

Then, the Directivity Index, in decibels, is defined as

$$DI = 10 \log Di \tag{2.40}$$

The Directivity Index is useful to analyze the directivity of a line array. Figure 2.25 illustrates an example of several lengths of uniform line arrays, where Directivity Index is plotted as a function of frequency. When the wavelength decreases (frequency increases) the DI increases linearly, until the main lobe is formed. Then, the variation of amplitude of the grade lobes undulates the DI response. The longer the line array is, the higher DI will be at low frequency.

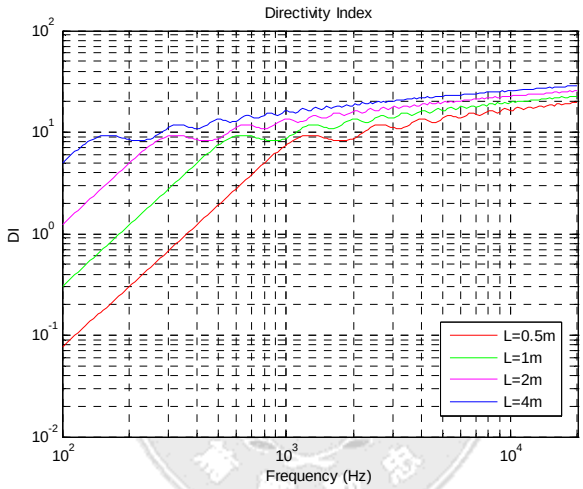

Figure 2.25 Directivity Index frequency response for several line array lengths

On discrete line array secondary main lobes are presented when the frequency increases. These lobes degrade severally DI because they can be as prominent as the main lobe. As an example, Figure 2.26 (a) shows a 0.5 m discrete line array with different number of elements *N*. It is observed that the undulation of the DI is more severe than the continuous array case. For a phased array with the grating lobes avoided, as shown on Figure 2.26 (b), the overall DI is increased and the undulation attenuated.

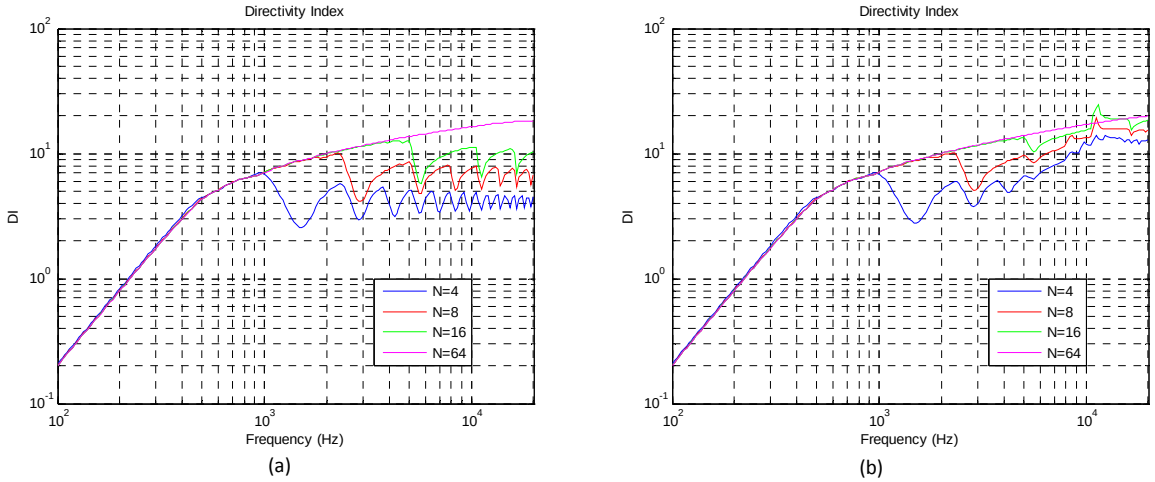

Figure 2.26 DI as a function of frequency on discrete array (a) and phased array (b)

2.11 Quarter power angle

The Directivity Index determines how directive is a source, but does not give information about the width of the main lobe. Thus, the Quarter Power Angle yields the angle where the sound pressure level is -6dB lower than the maximum (0.5 considering the pressure ratio) [9]. To find the angle, the equation of the directivity is set equal to 0.5.

$$D(\phi) = \frac{\sin\left(\frac{\pi}{\lambda} L \sin\theta\right)}{\frac{\pi}{\lambda} L \sin\theta} = 0.5 \tag{2.41}$$

Solving above equation numerically it is obtained

$$\frac{\pi}{\lambda} L \sin\theta = 1.895 \tag{2.42}$$

The angle in radians or degrees is given by

$$\theta_{-6dB} = \sin^1\left(\frac{0.6\,\lambda}{L}\right)\ (rad) \tag{2.43}$$

$$\theta_{-6dB} = \sin^1\left(\frac{0.6\,\lambda}{L}\right)\frac{180}{\pi}\ (degrees) \tag{2.44}$$

Figure 2.27 (a) shows the -6dB angle as a function of L/λ. When L/λ is large, the line array is long and the frequency is high, the angle is small and the beam is more directive.

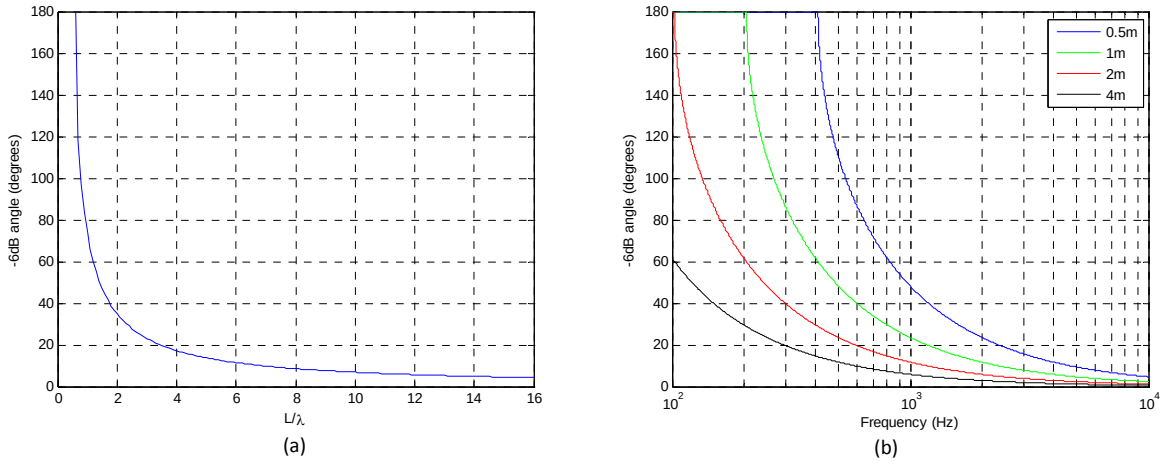

Figure 2.27 -6dB angle as a function of: (a) L/λ (b) frequency

Also the relation between the quarter power angle and the frequency can be plotted. Replacing $\lambda = c/f$ and $c = 340\ m/s$ the function becomes

$$\theta_{-6dB} = \sin^1\left(\frac{0.6\ \lambda}{L}\right) = \sin^1\left(\frac{205}{L\ f}\right) \quad \textbf{(2.45)}$$

The directivity response is shown on Figure 2.27 (b) for different line array lengths. It is observed that the quarter-power angle becomes very narrow at high frequency or if the length of the array increases.

2.12 Amplitude shading

By applying different amplitude values to each source, it is possible modify the shape of the directivity beam [13]. A tapered line array, where the center has more amplitude than the sides, greatly suppresses the side lobes, although produces a wider central lobe than a uniform array of the same length [14]. This effect can be observed in Figure 2.28 (a) and (b), where a discrete amplitude tapering is represented. In Figure 2.28 (c) the same result is obtained for a continuous tapered line array.

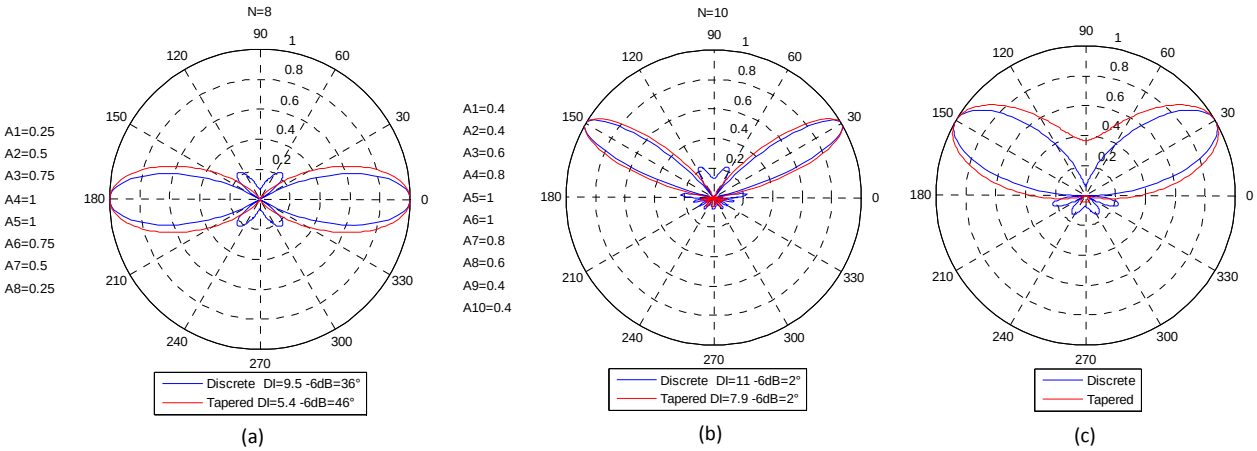

Figure 2.28 Polar patterns of tapered arrays: (a) discrete 8 elements (b) discrete 10 elements (c) continuous

For a discrete line array, the amplitudes can be proposed as a linear function of the amplitude. Then, the amplitude values can be obtained by solving the amplitude function with the spacing x values. For a symmetric tapered array, the function is given as

$$A(x)\ for -\frac{L}{2} \le x \le 0 \tag{2.46}$$

$$-A(x)\ for\ 0 \le x \le \frac{L}{2} \tag{2.47}$$

The directivity function of the tapered line array is obtained by substituting $A(x)$ in Eq. (2.15). An example of triangular amplitude function and its discretization on nine elements is shown in Figure 2.29. In this example, the first and the last elements take zero value; this situation would wastes two sources. This problem will be solved to optimize the pressure performance of the line array.

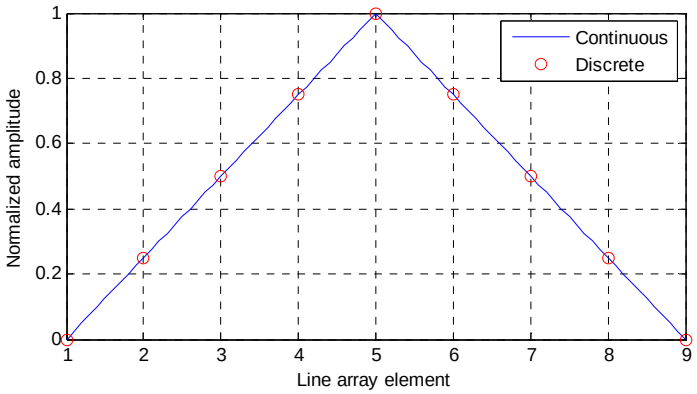

Figure 2.29 Triangular amplitude function for continuous and discrete line array

The Quarter Power Angle and Directivity Index are useful to analyze the tapered line array. Figure 2.30 (a) represents the improvement of the directivity at low frequencies on a 50 cm array. Also, the undulation on the DI at medium frequencies (coming from the grating lobes) is avoided. The width of the main lobe is considered on the Quarter Power Angle, Figure 2.30 (b) shows how the tapered array produces wider angles than the uniform one.

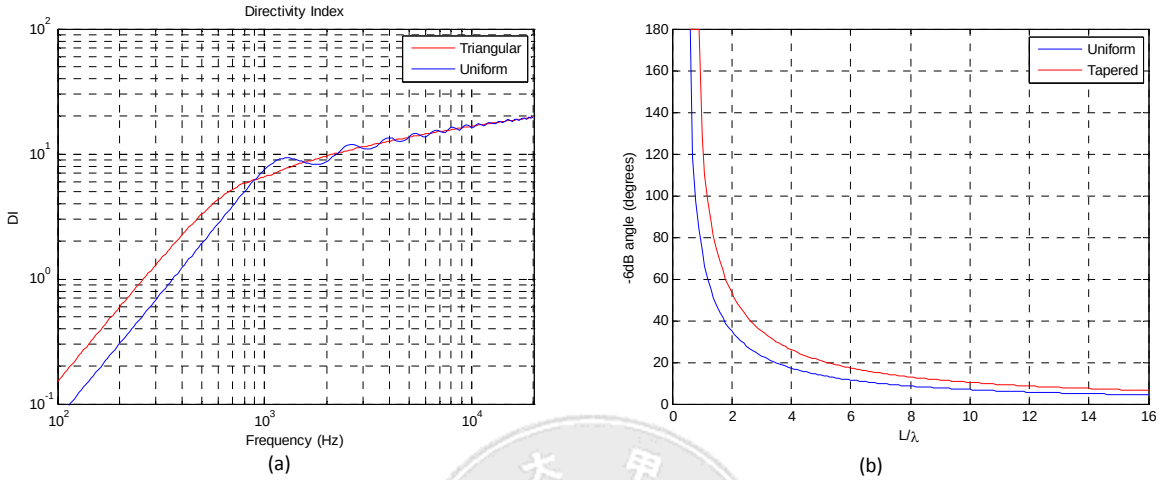

Figure 2.30 Tapered array and uniform array comparison: (a) Directivity Index (b) -6dB Angle

This thesis work compares different amplitude functions by analytic simulation using MatLab. Even though the calculation is programmed for a discrete array, the number of values is increased in order to consider a uniform array result. Then, the functions like triangular, hamming or logarithmic among others are analyzed in directivity and pressure.

2.12.1 Directivity

Initially, Figure 2.31 (a) represents several functions, where all the values have higher amplitude than the triangular function. In Figure 2.31 (b), it is represented that the directivity function varies from 90° and -90° of each amplitude function. The original directivity function with no tapering applied is represented in black color. It is observed that there is a relation between secondary lobes suppression and main lobe width. In other words, there is a balance where one is improved meanwhile the other is degraded.

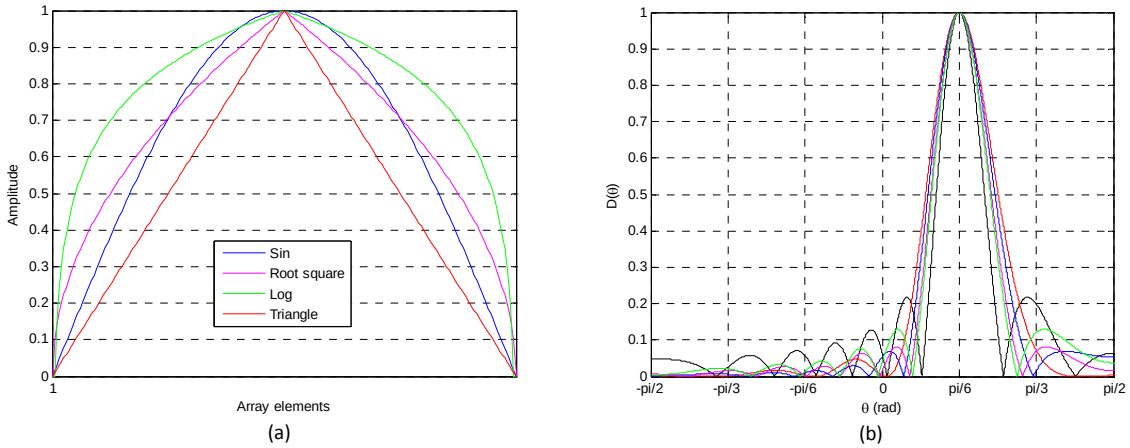

Figure 2.31 Tapering functions comparison 1: (a) Functions (b) Directivity functions

Next, a second group of functions is analyzed in Figure 2-32 (a). All the functions of this group have part of the values below the triangular function. Now, in Figure 2-32 (b), better results for suppressing the secondary lobes are founded. By contrast, the widths of the main lobe are wider.

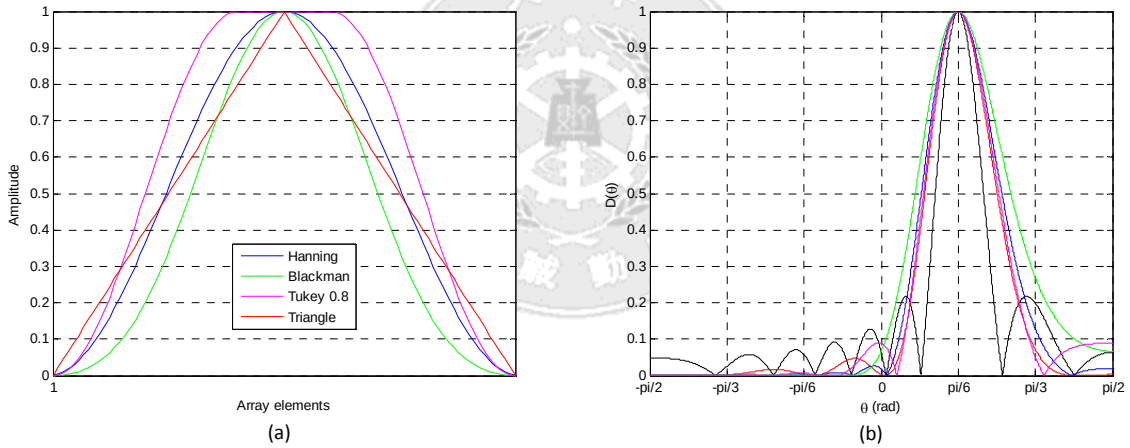

Figure 2-32 Tapering functions comparison 2: (a) Functions (b) Directivity functions

To solve the problem presented previously, where the side speakers would have no amplitude, a slope for the function is introduced. The example plotted in Figure 2.33 illustrates the triangular function with three different slope values. Blue color represents the original triangular function, black a no tapered array. Again, a balance between width and secondary lobes is found. A line array design with maximum suppression of secondary lobes would needs to maximize the relation between the center and the sides amplitudes.

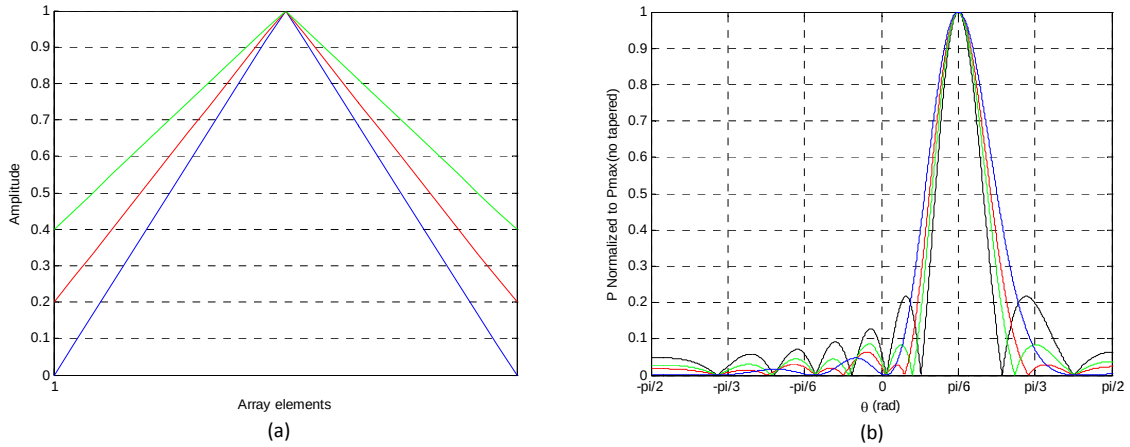

Figure 2.33 Tapering functions comparison 3: (a) Functions (b) Directivity functions

By plotting the directivity as a function of frequency and angle, it is also possible to observe the tapering effect. The directivity with tapering is shown in Figure 2.34 (b), where, the side lobes are less prominent than that obtained by the line array without tapering.

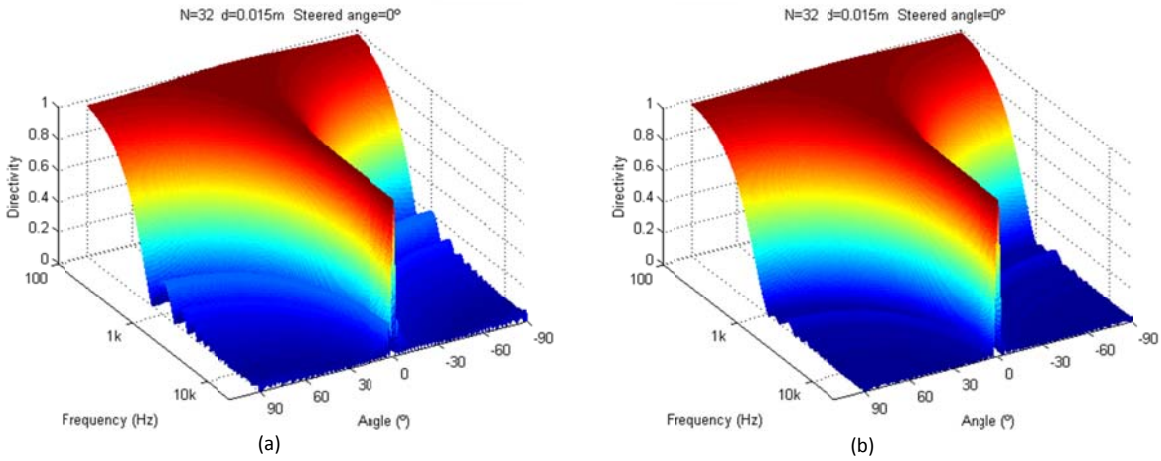

Figure 2.34 3D Directivity function representation: **(**a) without tapering (a) with tapering

2.12.2 Pressure on axis

All that glitters is not gold; the last situation presented has not good performance in a system where all the sources are real. The sound pressure on the listener point is the sum of all the pressures generated by the speakers. Speakers have power limitations; if the central speakers have to generate most of the acoustic pressure a limitation is established for the line array system. In other words, if the suppression of the secondary side lobes is desired the total acoustic pressure of the main lobe is severally degraded. The same last example (of Figure 2.33) is illustrated again in Figure 2.35, but in this case the directivity function is normalized to the maximum pressure. It is observed that the pressure on the main lobe decreases as the value of

the integration of the amplitude function also does. In the case of the original triangle function (blue color), the resulting pressure is reduced to half. This could be deduced by integrating the amplitude function; which also yields half value of unitary constant amplitude function (black color).

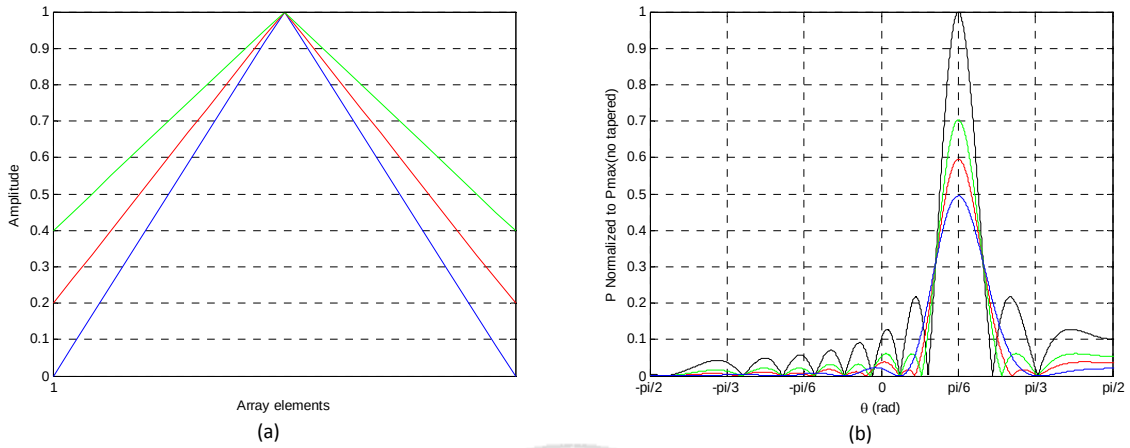

Figure 2.35 Tapering functions comparison 4: (a) Functions (b) Directivity functions

In conclusion, tapering is beneficial to decrease the amplitude of the secondary lobes, and also the performance of a line array system has to be considered. The line array design is a balance between secondary lobes amplitude, main lobe width, and total acoustic pressure.

2.13 Distribution of the inter-element spacing

As shown previously, if the spacing of the elements increases, the frequency where grating lobes appear will be lower. For a good design, small spacing and large array length is desired, in other words, a higher number of elements are better. This point studies with computer simulation the directivity function resulting of different element distributions.

In the next example, it is illustrated a simulation with numerical values. For a 1 m length eight-element array has been considered three spacing situations uniform (blue), increasing (red) and decreasing (green). In Figure 2.36 is shown the distances in meters where is observed the logarithmic progression of the non-uniform distributions. The directivity pattern, in Figure 2.37, shows in different frequencies the better result of the uniform spacing. It obtains lower secondary lobes with almost the same main lobe width.

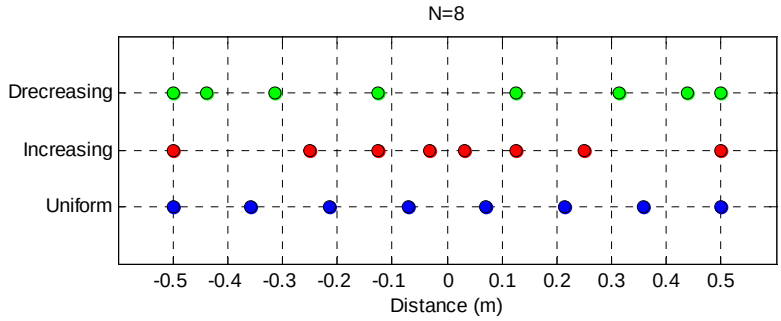

Figure 2.36 Spacing distributions

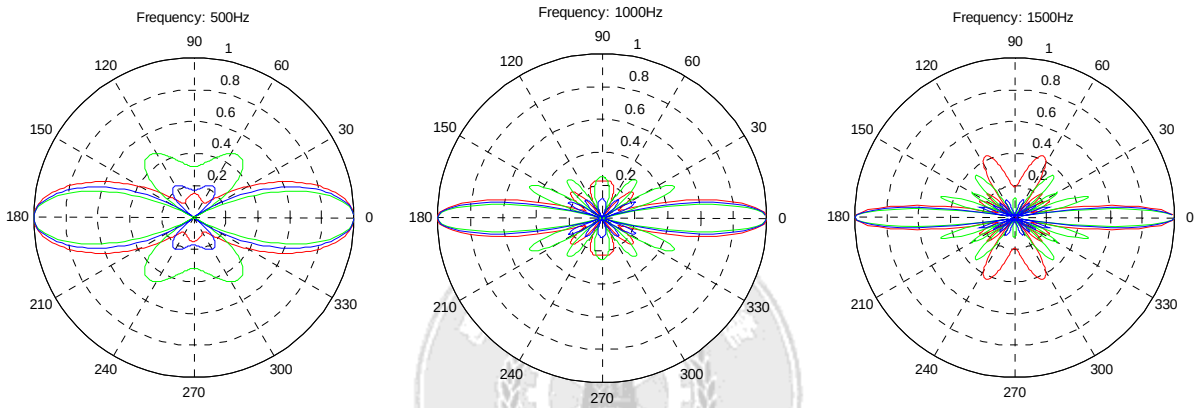

Figure 2.37 Directivity patterns of different spacing distributions

2.14 Nested arrays

Every array is restricted to a frequency range; low frequency limit is given by the array length and high frequency by the distance and size of the elements. In order to achieve a wider broadband response, it is possible to combine the outputs of different band limited arrays. The nested array is combined by others sub-arrays, increasing the length gradually. Then, each sub-array can give a desired response for a frequency range by applying band-pass filter. The overall broad band output is the result of combining the output of the band limited sub-arrays. The advantage of the nested array is the possibility to extent the working frequency range with the same number of elements.

The example shown on Figure 2.38 covers three frequency bands. All the sub-arrays are composed of seven elements and the element spacing is double in each band. The resulting nested array is implemented by 15 sources, where some of them are shared. The distances are given in centimeters.

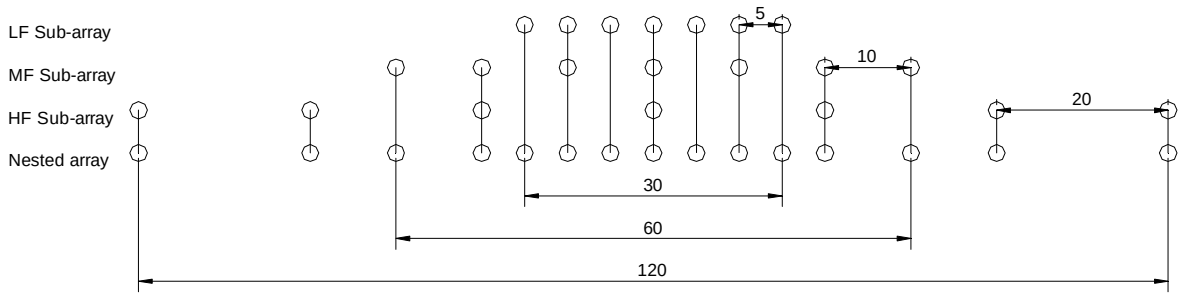

Figure 2.38 Nested array with 3 sub-arrays

In Table 2.2 the frequency limitations of each discrete sub-array at different steered angles are shown. In this design example, the maximum steered angle is 30 degrees, for wider angles grating lobes would appear between frequency bands.

Table 2.2 Nested array: frequency limitations at 0, 10 and 45 degrees

			Angle 0		Angle 10		Angle 30	
	N	**d (m)**	**F_{max} (Hz)**	**F_{min} (Hz)**	**F_{max} (Hz)**	**F_{min} (Hz)**	**F_{max} (Hz)**	**F_{min} (Hz)**
LF Sub-array	7	0.05	5880	980	5010	1186	3920	1960
MF Sub-array	7	0.1	2940	490	2505	593	1960	980
HF Sub-array	7	0.2	1470	245	1253	296	980	490

In order to compare with other discrete arrays, Table 2.3 shows the frequency limitations of other arrays with the same uniformly distributed number of elements.

Table 2.3 Comparison uniform distribution and nested array

	N	**L (m)**	**d (m)**	**F_{max} (Hz)**	**F_{min} (Hz)**
Uniform distributed array	15	1.2	0.086	3722	266
Uniform distributed array	15	0.7	0.050	6403	980
Nested array	15	1.2	0.05 / 0.1 / 0.2	5880	245

It is observed that the working frequency range on the nested array is extended. But the penalty paid is an abrupt change of directivity on the frequency limits of each sub-array. This is caused by the band pass filters necessary to separate the bands. In order to avoid it, the filter can be designed with a low order. This makes the most directive part of a band mix with the less directive of the next one, obtaining a softer directivity change for each band.

If phased array configuration is considered, the high frequency limit is extended depending on the size of the source element. Each phased sub-array directivity, with 4.5 cm of size element, is plotted in Figure 2.39 (a), (b) and (c). In addition, Figure 2.39 (d) and (e) presents the overall

directivity for 0 and 30 degrees. It is noted that, at 30 degrees the apparition of grating lobes even if a phased array is used.

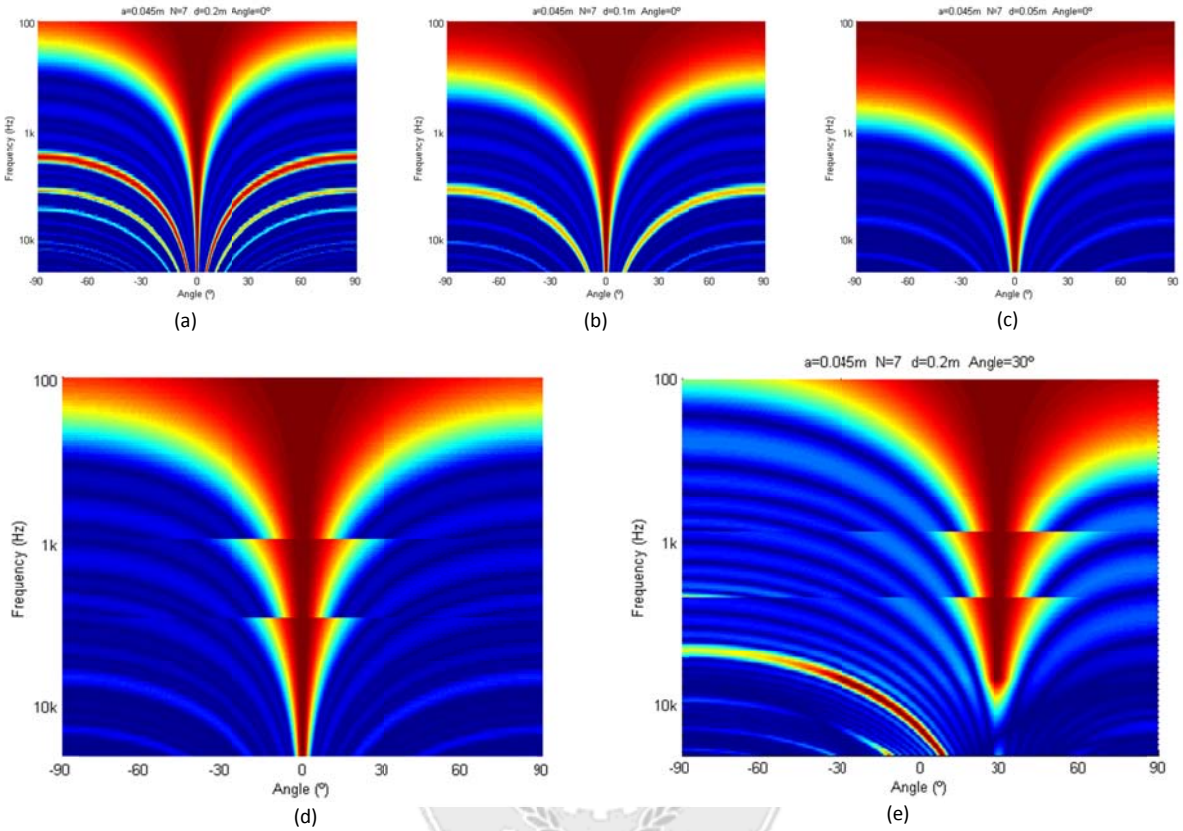

Figure 2.39 Directivity: (a) sub-array LF (b) sub-array MF (c) Sub-array HF (d) Nested 0° (e) Nested 30°

2.15 Far field

In the designing of line array, it is important to define the difference between near and far field. In the near field, the sound pressure level decreases by 3 dB per doubling the distance and an interference pattern is created producing the sound pressure level undulation. However, in the far field the sound pressure level decreases 6 dB per doubling the distance.

A continuous line source can be modeled as a line of infinite point sources. This yields a source of cylindrical waves in the near field, which transforms to a spherical at some point. This is a point is where the far field begins, which depends on the length of the line and the frequency [15].

A single speaker can be modeled like a piston, and the apparition of the far field can be found as a line array. Since the far field distance of the single speaker is smaller than the speaker array, the simplification it is not considered.

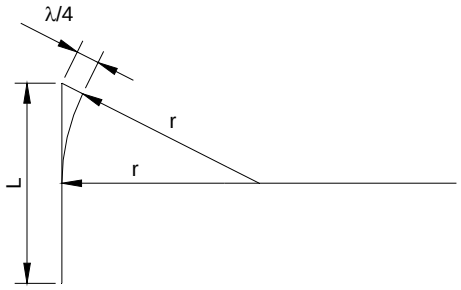

Figure 2.40 Far field calculation graphic

The far field distance (r) is estimated by the criterion that the far field begins when the distance to P from the center of the line array is $\lambda/4$ of the distance to P from the endpoint of the array (r') [9]. As geometrically illustrated in Figure 2.40 it can also be expressed mathematically as

$$r = r' - \frac{\lambda}{4} \tag{2.48}$$

Solving the geometry,

$$r' = \sqrt{\left(\frac{L}{2}\right)^2 + r^2} \tag{2.49}$$

where L is the length of the array. Combining above equations, it is obtained

$$r = \frac{L^2}{2\lambda} - \frac{\lambda}{8} \tag{2.50}$$

where $L \geq \lambda/2$. Considering $\lambda = c/f$ and $c = 343\, m/s$. Eq. (2.50) is written in terms of frequency

$$r = \frac{L^2 f}{686} - \frac{43}{f} \tag{2.51}$$

The distance to the far field increases with the frequency and the length of the array. Figure 2.41 represents where the far field begins with different line array lengths.

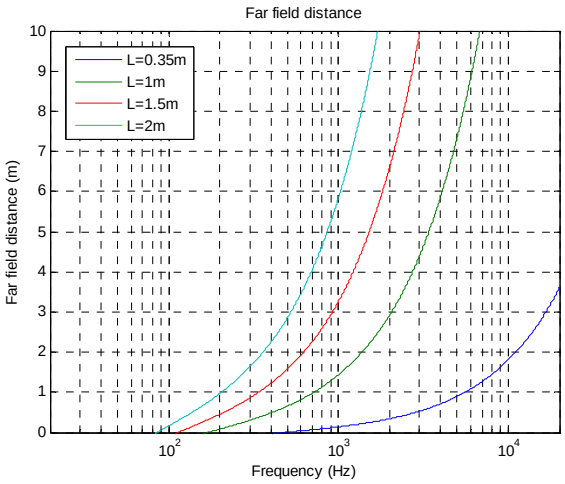

Figure 2.41 Comparison of distances to the far field for different array lengths

2.16 On-axis response

Considering the far field of each individual source, the on-axis response can be calculated by rewriting (2.17) in terms of the distance to the listener (*r*) [7, 18, 19]. Considering equal amplitude along the line array $A(x) = 1$ and the distance to the listener point at *r* from any segment *dx* along the line array as $r'(x) = \sqrt{r^2 + x^2}$, the pressure function becomes

$$P(r) = \int_{-L/2}^{L/2} \frac{e^{\frac{j2\pi}{\lambda}\sqrt{r^2+x^2}}}{\sqrt{r^2 + x^2}} dx \qquad \textbf{(2.52)}$$

By solving numerically, the on-axis response for different line array lengths is shown in Figure 2.42 (a). The distance to the far field increases as length and frequency increases. The magnitude decreases at a rate of -3 dB per doubling of distance in the near field and -6 dB in the far field. The inflexion point position is given by Eq. (2.52). Finally, on-axis response for a 50 cm uniform line array at different frequencies is represented in Figure 2.42 (b).

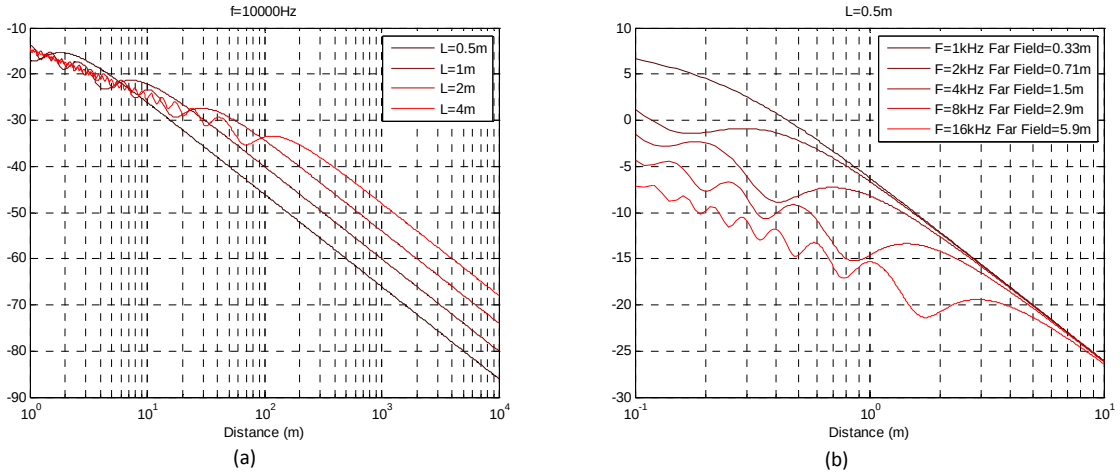

Figure 2.42 (a) On-axis response at 10 kHz (b) On-axis response for L=0.5 m

2.17 Sum of signals

If two identical signals are emitted in phase from the same source, the result is the sum of both signals. In other words, double pressure with the same directivity pattern. It is possible to emit different beams from the same line array at different angles, in this case also the result is the sum of individual directivity functions. But in this case the directivity has several main lobes, and depending on the frequency these are independent. The resulting directivity function is the sum of all individual ones.

$$D(\theta) = D_1(\theta) + D_2(\theta) + \cdots + D_n(\theta) \tag{2.53}$$

The Figure 2.43 presents an 8 elements discrete array with 1 cm of inter-element spacing and two beams at 20 and -20 degrees. In low frequencies, where the line array behaves as an omnidirectional source, the resulting signal has an omnidirectional pattern and the sound pressure is the sum of each individual signal. Then, when frequency increases and the individual beams become directive the resulting signal has main independent beams. For better representation the resulting directivity function is not normalized. Figure 2.44 shows the same example with normalized polar representation.

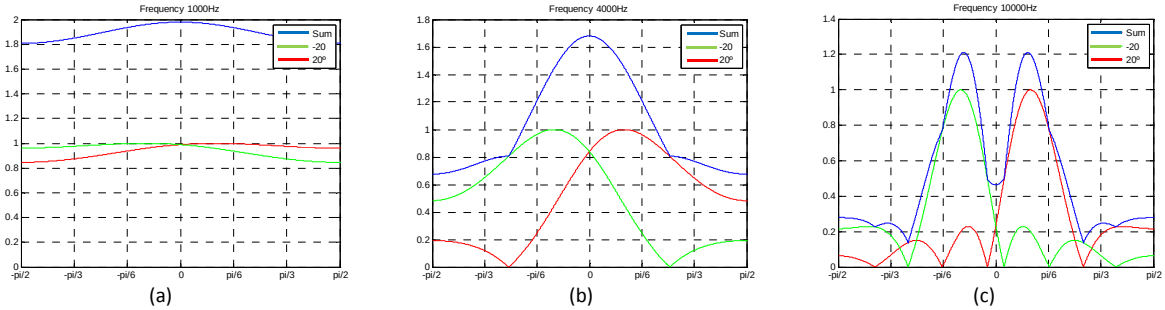

Figure 2.43 Non-normalized directivity patterns of the sum of 2 signals: (a) 1 kHz, (b) 4 kHz (c) 10 kHz

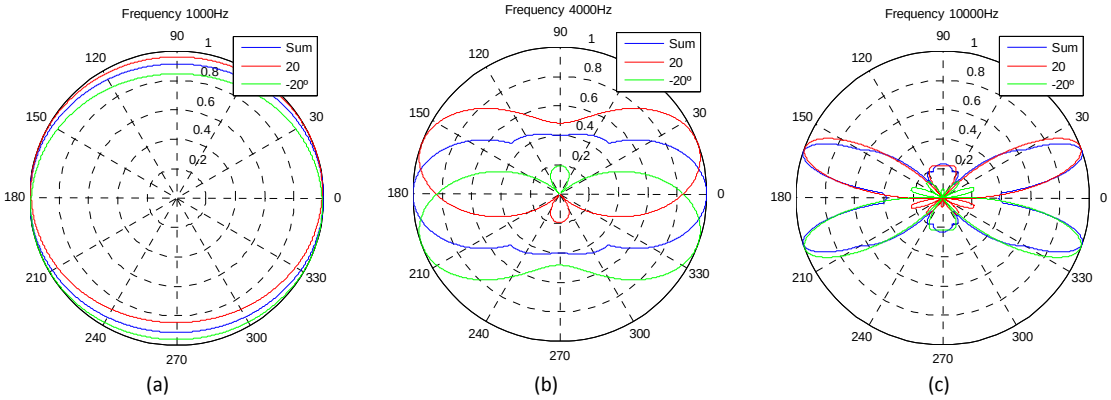

Figure 2.44 Normalized polar pattern of 2 signals: (a) 1 kHz, (b) 4 kHz and (c) 10 kHz

An example of the same line array beaming 3 signals steered at 45°, -45° and 0° is given in Figure 2.45. The same observations of the last example are presented in this one.

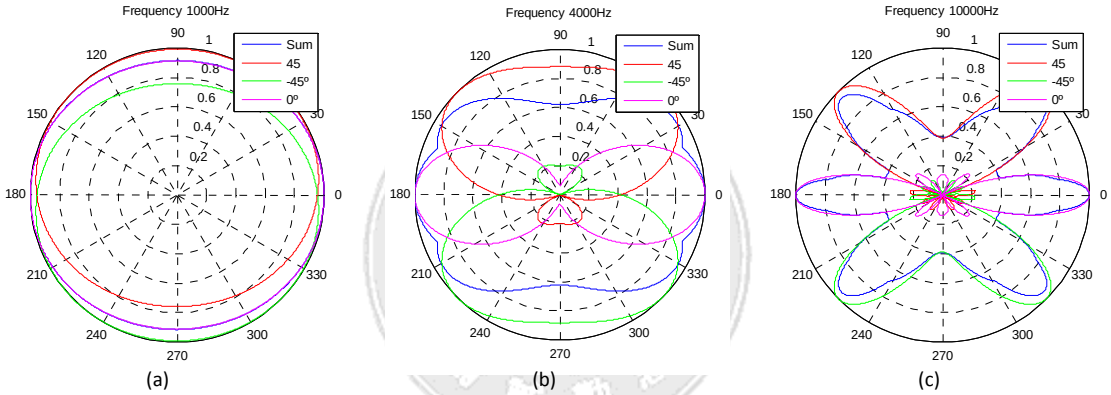

Figure 2.45 Normalized polar pattern of 3 signals: (a) 1 kHz, (b) 4 kHz and (c) 10 kHz

Figure 2.46 illustrates the last two examples of directivity pattern as a function of the frequency and steering angle. The frequency is logarithmically set from 100 Hz to 20 kHz and the directivity is not normalized. It is observed the omnidirectional behavior of the directivity at low frequency, meanwhile at high frequency the different beams are perfectly separated.

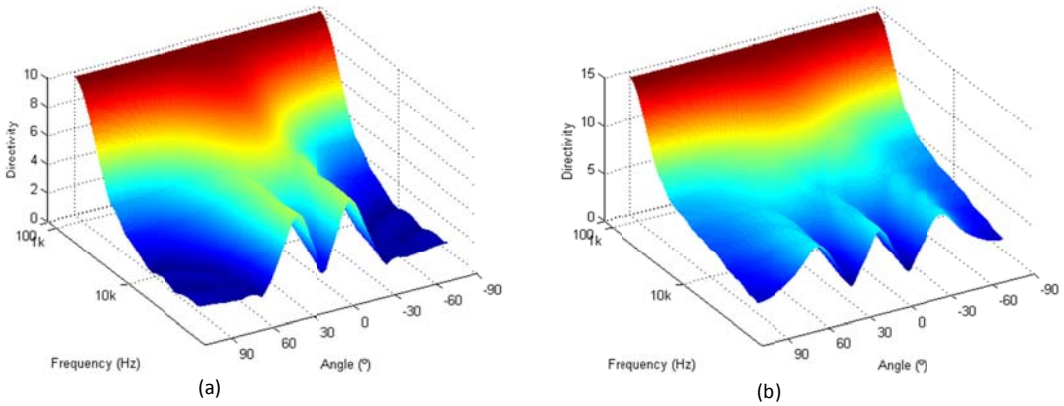

Figure 2.46 Tridimensional polar patterns: (a) Two beams (c) Three beams

Furthermore, two signals can also be emitted in opposite phase. In this case the resulting signal is the subtraction from the original ones. By using this technique it is possible to attenuate the overall level of pressure at one direction. As an example, in Figure 2.47, it is represented the attenuation of signal of an array emitting two beams. The signal at 0° has opposite phase of the signals at 45° and -45°. It is noted that the wave cancellation effect is more notorious at high frequency. This technique, called as crosstalk cancelation and its applications will be explained in detail in Chapter 3.

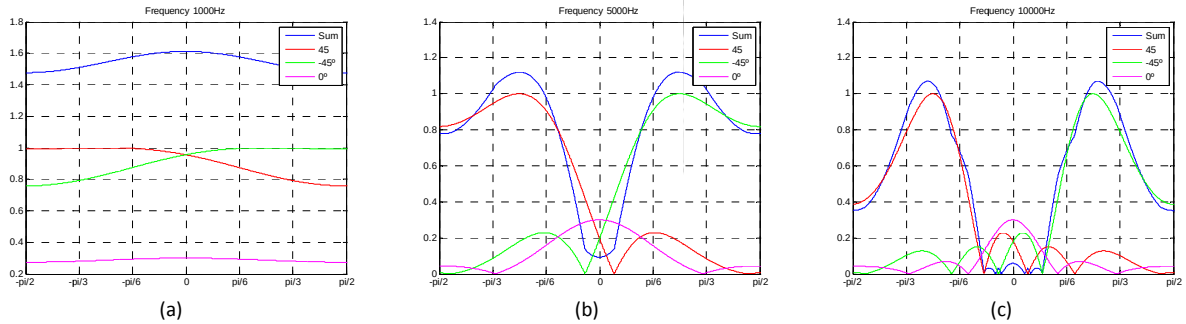

Figure 2.47 Crosstalk cancelation at 0 degrees: : (a) 1 kHz, (b) 4 kHz and (c) 10 kHz

2.18 Conclusions

All the points explained in this chapter can be used to design a line array with a desired directivity and performance. Beyond the simulated design, for a real situation where directional sources are used, the model can be approximated to a phased array. Considering the frequency where grating lobes appear is the same, just the amplitude of the lobes is adjusted by varying the element source size. This allows reasonable predicted results without previously obtaining the directivity of the sources.

To design a line array, the most important is to obtain the directivity function and the working frequency range. Also, a flat frequency response and enough sound pressure level for the

considered application. The equations and methods in this chapter explained will be used to develop two Graphical User Interfaces and predict the directivity function of a real line array configuration.

3 Beamforming algorithms and applications

This chapter presents different applications of beamforming and the algorithms to generate the signals. First, mono-channel and single steered angles will be presented. Then, several beams will provide a multi-channel beamformer. Finally, in order to obtain a transaural audio reproduction on speaker line arrays, methods for crosstalk cancelling and virtual loudspeaker implementation will be addressed.

3.1 Single beam

To obtain electrical steering, the signals sent to each speaker are separately delayed [21, 22, 23]. The mono-channel input signal is converted in eight-channel signal, one for each speaker. The delay in seconds of each channel, it is given by the relation of the inter-element spacing d, sound velocity c and the steered angle θ_s as

$$Delay(s) = \frac{d}{c}\sin\theta_s \tag{3.1}$$

Because the signal processor works digitally, the analog input signal is converted to digital at the sample frequency (F_s) of the A/D converter. Then, the delay can be expressed in samples as

$$Delay\ (Samples) = F_s\frac{d}{c}\sin\theta_s \tag{3.2}$$

To obtain the delay applied to each element, the position e is considered; then the above equation is modify as

$$Delay\ element\ (Samples) = (e-1)\ F_s\frac{d}{c}\sin\theta_s \tag{3.3}$$

The number of delayed samples has to be a whole number, then, the steered angle has to be approximated to the closest one given by a whole number sample. The desired steered angle can be obtained as

$$\theta_s = \sin^{-1}\frac{c\ Samples}{(e-1)\ F_s\ d} \tag{3.4}$$

Next, an example for an eight-element array of 5 cm inter-element spacing is presented. Considering the sample frequency of the DSP (48 kHz) and 4 samples delay a 16.5° steered angle is obtained. The delay applied to each element is represented in Table 3.1.

Table 3.1 Delay applied to each element

Element	1	2	3	4	5	6	7	8
Time delay (μs)	0	41	83	125	166	208	250	291
Samples delay	0	4	8	12	16	20	24	28

Figure 3.1 represents a block diagram of the algorithm. The input signal is separated and the different delays are applied to each output. The measurement results obtained by applying this algorithm can be found in Chapter 6. This technique is useful for applications where a monophonic signal has to be delivered to a specific area, like live sound or sound cancelling.

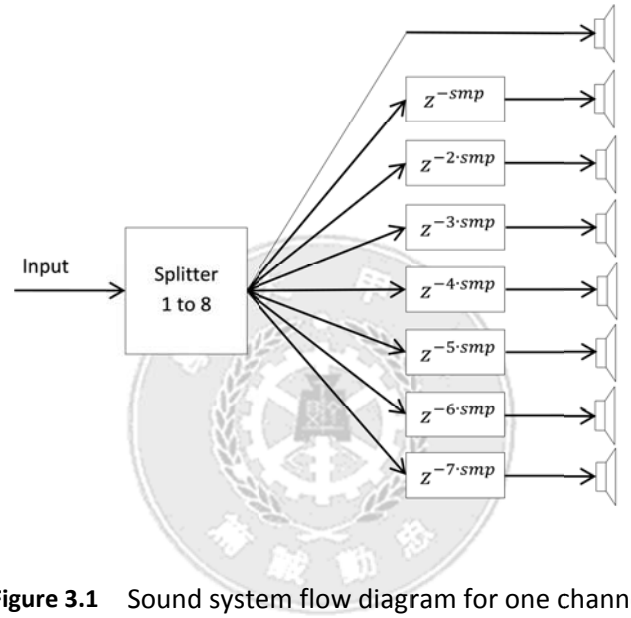

Figure 3.1 Sound system flow diagram for one channel

3.2 Multiple beam

As previously presented in Chapter 2, several steered beams can be emitted by the same beamformer. Then, for multi-channel audio reproduction each channel can be emitted at different angle. Figure 3.2 shows a representation of a stereophonic signal delivered to both ears in binaural audio reproduction.

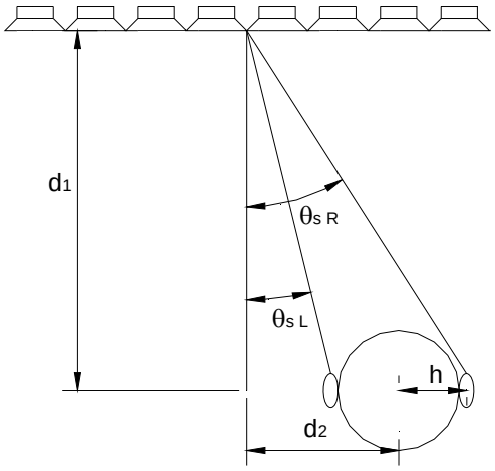

Figure 3.2 Stereo line array and head

d_1 is the distance from the array to the head, h half the distance between the ears and d_2 the distance from the center of the head to the center of the array. By solving the geometric problem the steering angles can be expressed as

$$\theta_{s\,L} = \tan^{-1}\left(\frac{d_1}{d_2 - h}\right)$$
$$\theta_{s\,R} = \tan^{-1}\left(\frac{d_1}{d_2 + h}\right) \quad \textbf{(3.5)}$$

Once the angles are obtained, the delays can be calculated by using Eq. (3.3). Figure 3.3 shows the block diagram designed with the software Pure Path for the DSP TAS3108. In this example, first the two input signals are separated delayed. Then, they are mixed before sending them to the speakers.

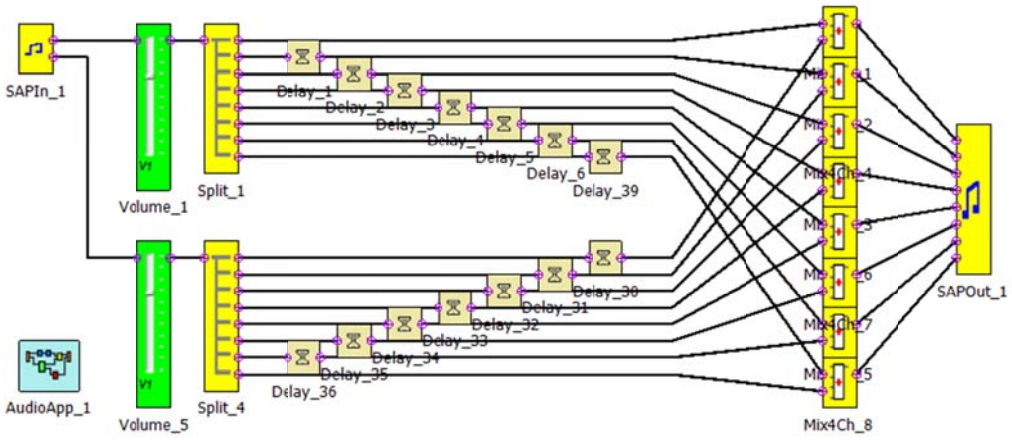

Figure 3.3 Stereo beamformer algorithm programmed on Pure Path GUI

This example provides a stereophonic audio reproduction by steering the beams to each ear, offering more directional sources than two loudspeaker system. Then, less undesired signal will be present in the opposite ears and the crosstalk will be lower. In contraposition the listener has to be situated in the correct position or “sweet spot”. This algorithm is implemented in the DSP and measurement results will be presented in Chapter 6.

3.3 Bouncing beams

More channels can be emitted at different angles. A 5.1 surround audio system provides a 6 channel audio reproduction: front left and right, a center channel, and two surround channels. Center, and front channels can be directly emitted to the listener. Then, the surround channels can be delivered by bouncing the beams on the walls of the room.

Next, a typical distribution is illustrated in Figure 3.4. A ray emitted at point A arrives to the point B by bouncing in two walls. L_1 represents the distance between the source and the listener and $L_2$the distance from the listener to the back wall. d_1 represents the distance between the source and the lateral wall and d_2 the distance from the listener to the lateral wall. L_1 and L_2 are the distances from the back wall to the source and listener respectively.

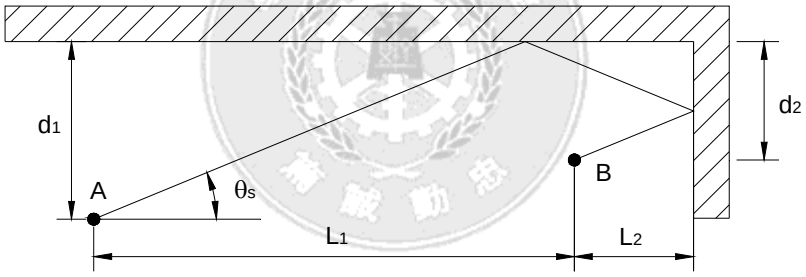

Figure 3.4 Beam bouncing in two walls

Geometric Acoustics assumes that the wavelength is small compared to the dimensions of the room, that is, the low frequency will not efficiently deliver to the listener. By solving the trigonometric problem presented in Figure 3.4, the steering angle can be expressed as

$$\theta_s = \tan^{-1}\left(\frac{L_1 + L_2}{d_1 + d_2}\right) \tag{3.6}$$

If the distance travelled by the surround channel is much longer than the direct one, a delay has to be applied in order to let them arrive simultaneously. The distance difference can be calculated as

$$D = \frac{L_1 + 2L_2}{\cos\theta_s} - \sqrt{L_1^2 + (d_1 - d_2)^2} \tag{3.7}$$

Then, the delay in time can be obtained by using the velocity of the sound *c.*

$$Delay\ (s) = \frac{D}{c} \tag{3.8}$$

This technic presents different disadvantages. The geometry of the room has to be known in advance to calculate the steering angles. Also it has been considered perfect reflective walls, but real situations present elements on the walls with absorption and scattering properties.

3.4 Crosstalk cancellation

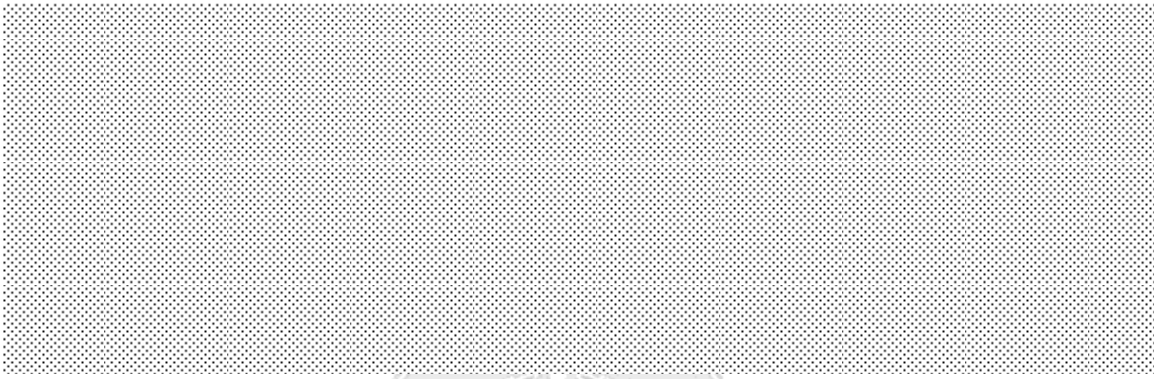

3.4.1 Constant amplitude canceller

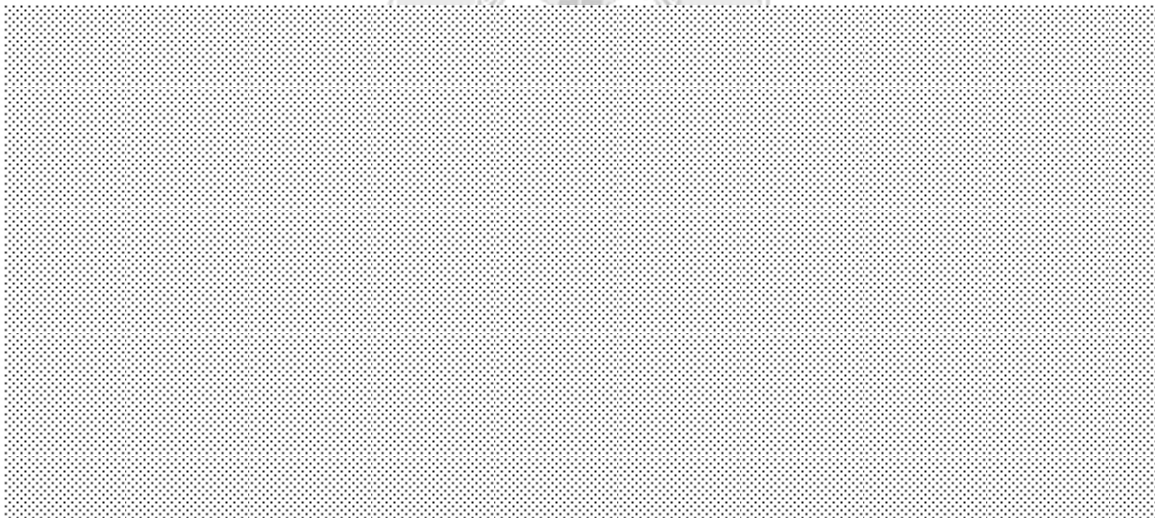

Figure 3.5 Line array speaker with crosstalk canceller

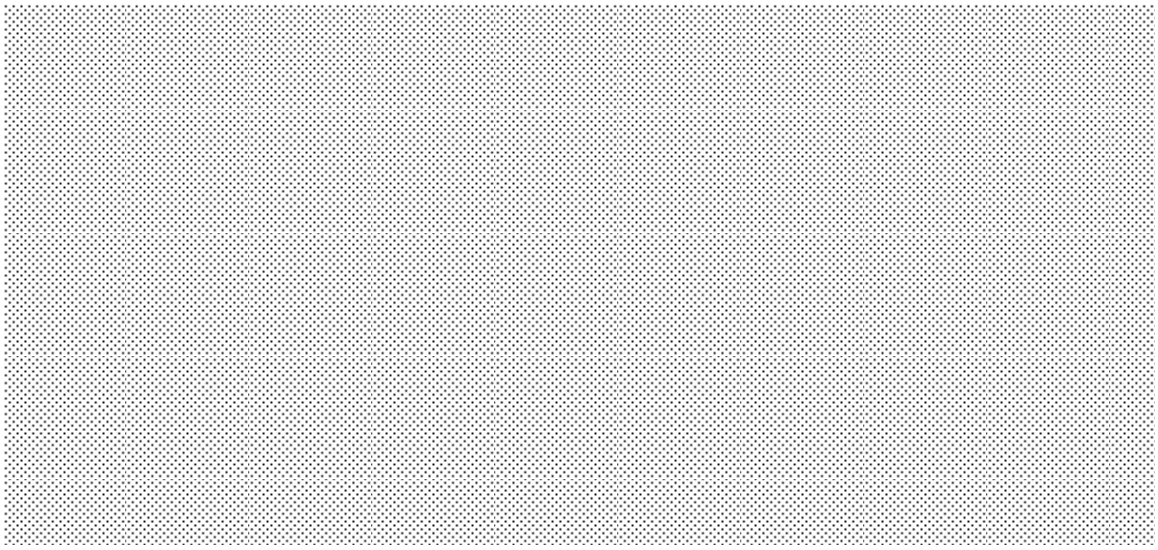

Figure 3.6 Directivity function of crosstalk canceller: (a) 0 dB (b) -6 dB

3.4.2 Frequency canceller

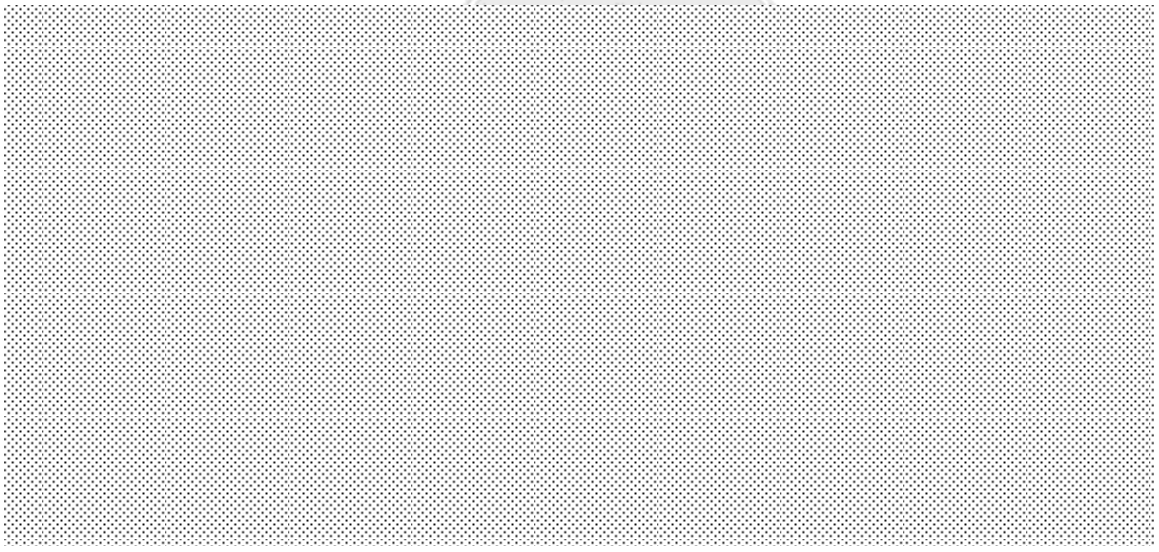

.

Figure 3.7 (a) Frequency response at -10° (b) Directivity function of a 8-element line array

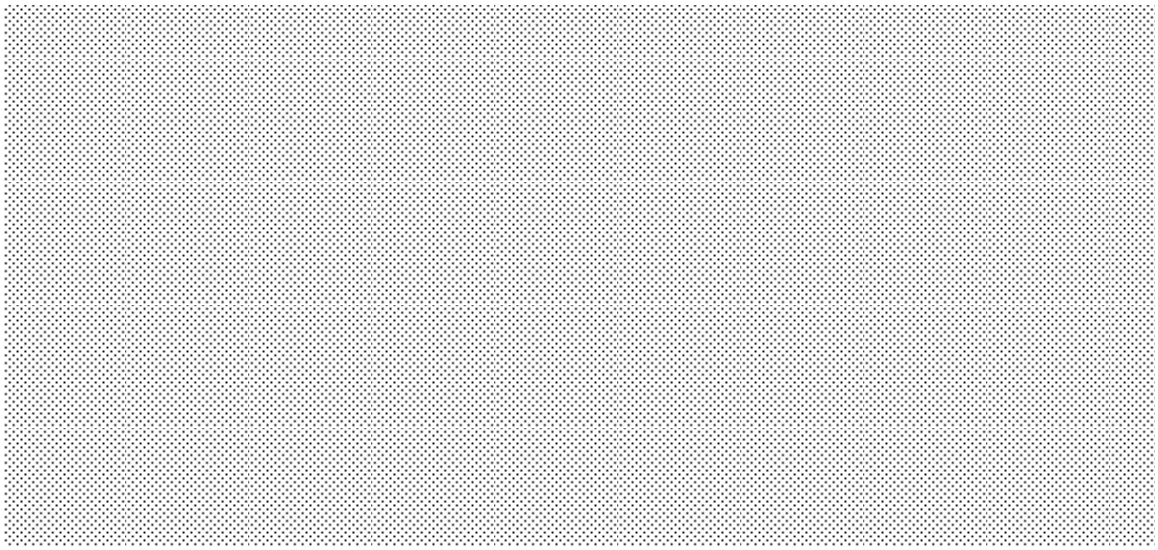

Figure 3-8 Crosstalk canceller with frequency filter

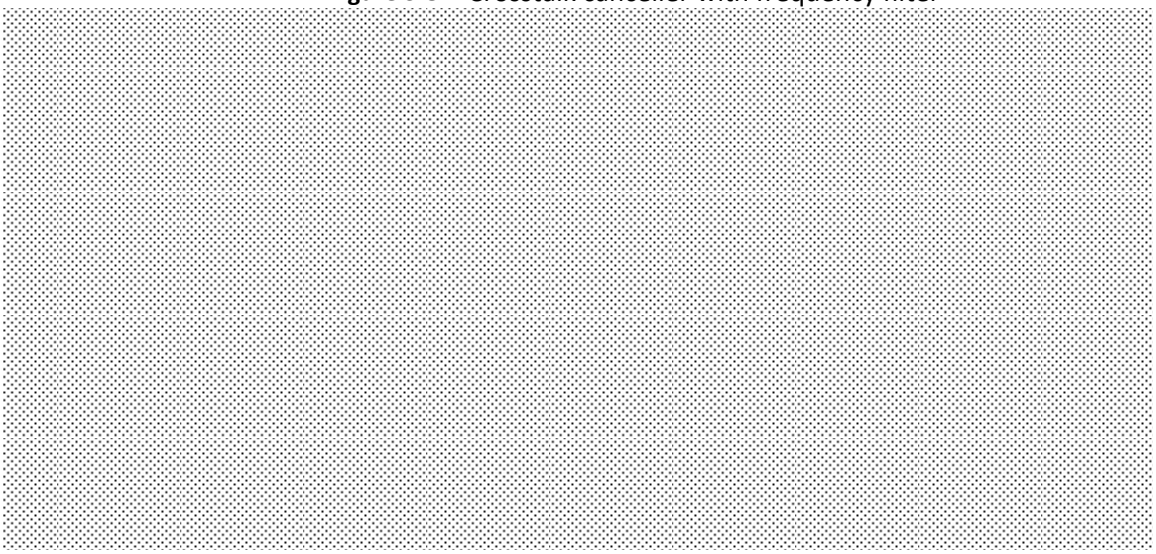

Figure 3.9 (a) Directivity of crosstalk canceller with frequency response (b) Frequency response at -10° and 10°

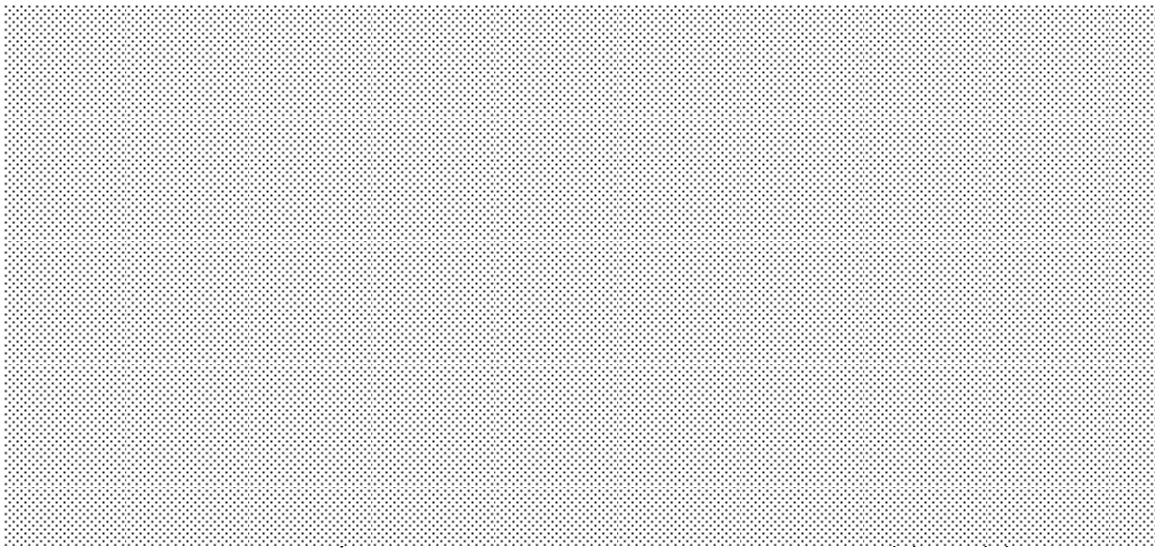

3.4.3 Equalization filter

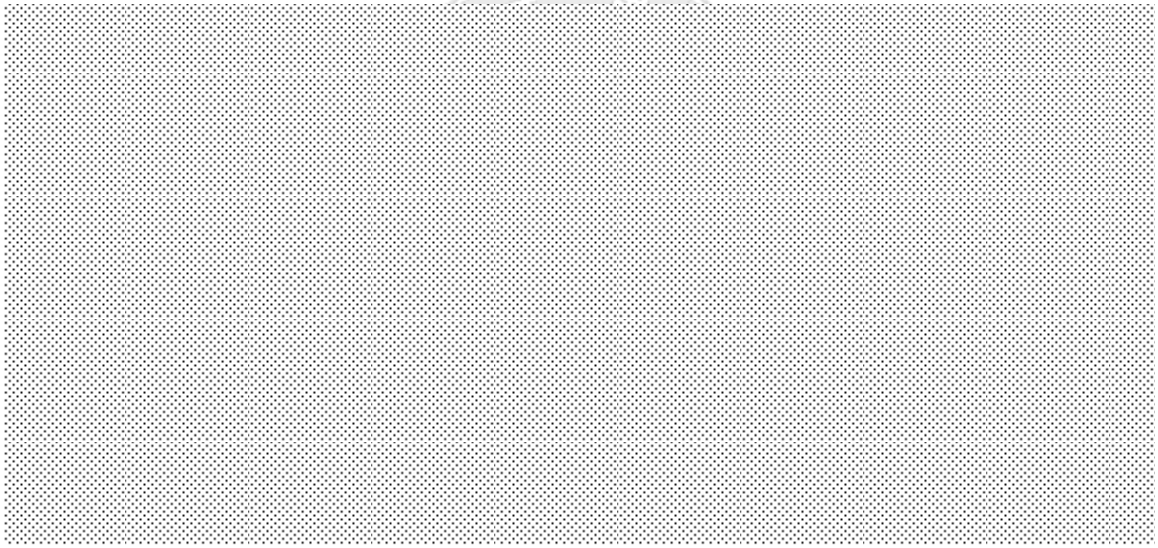

Figure 3.11 Crosstalk cancellation with equalization filter

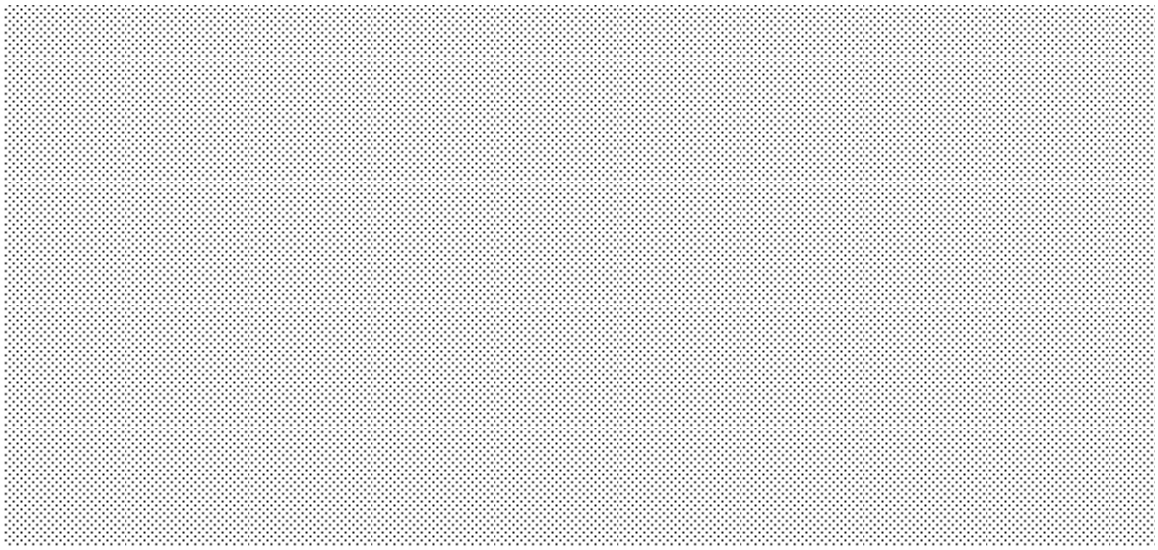

Figure 3.12 Directivity function of crosstalk cancellation with equalizer

3.4.4 Stereo crosstalk canceller

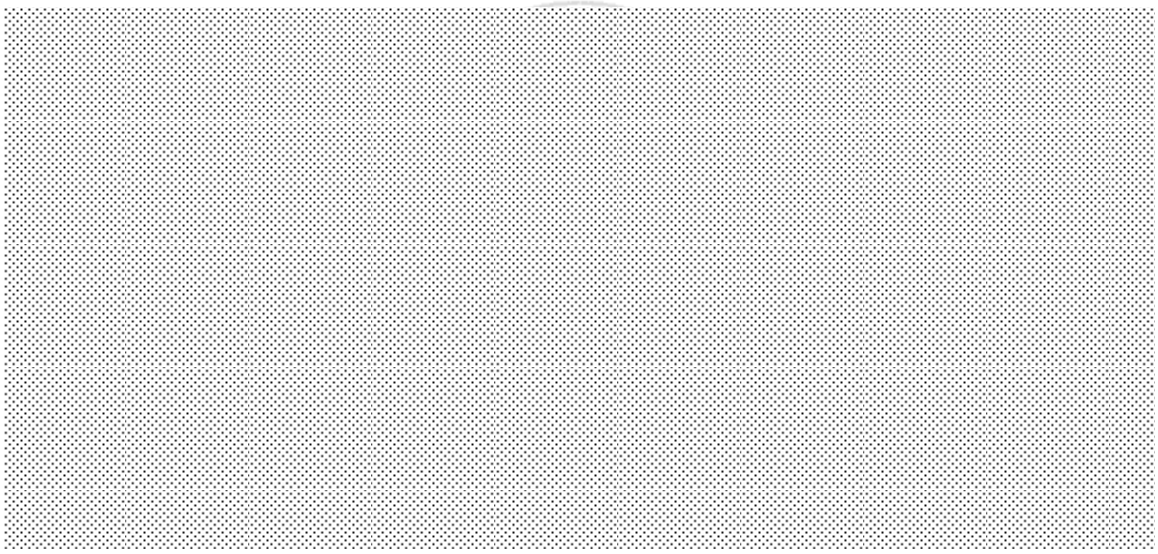

Figure 3.13 Crosstalk cancellation with one line array

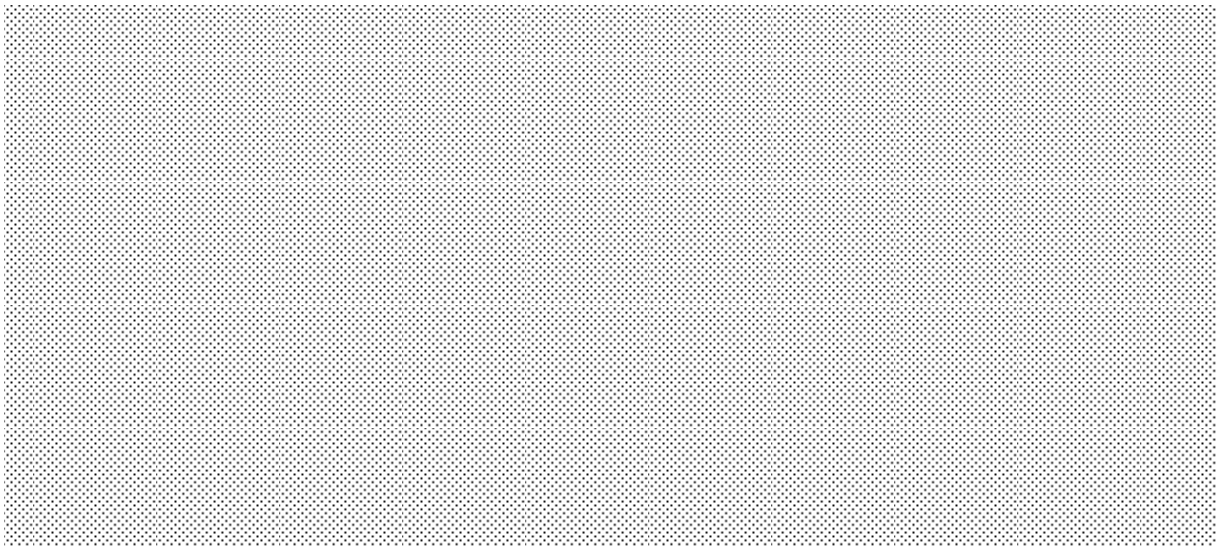

Figure 3.14 Two speaker line arrays and head position

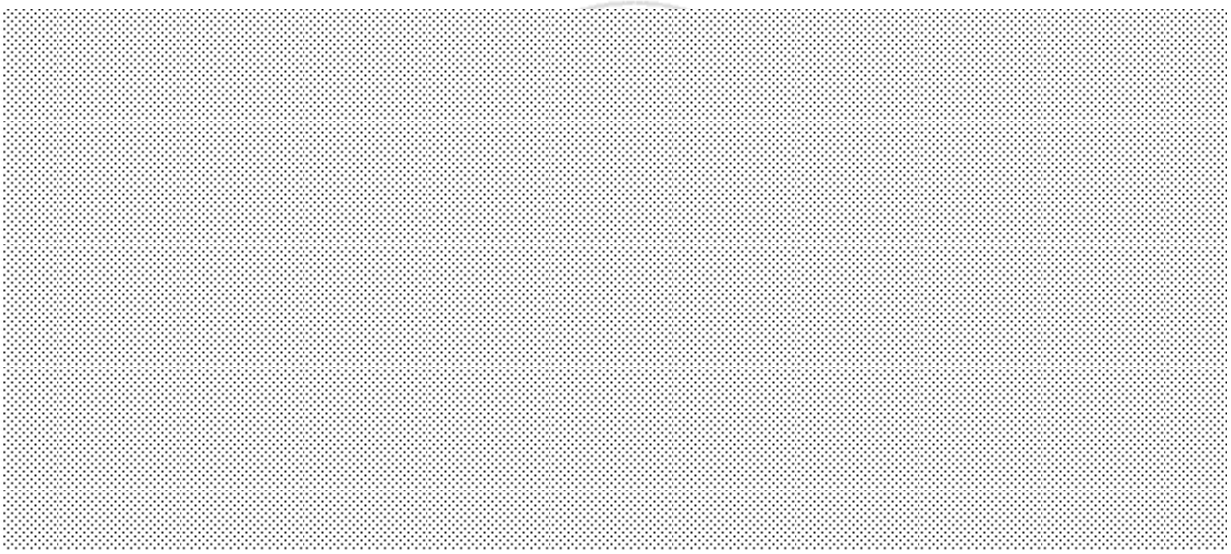

Figure 3.15 Simplified crosstalk cancellation with two speaker arrays

3.4.5 Transaural stereo

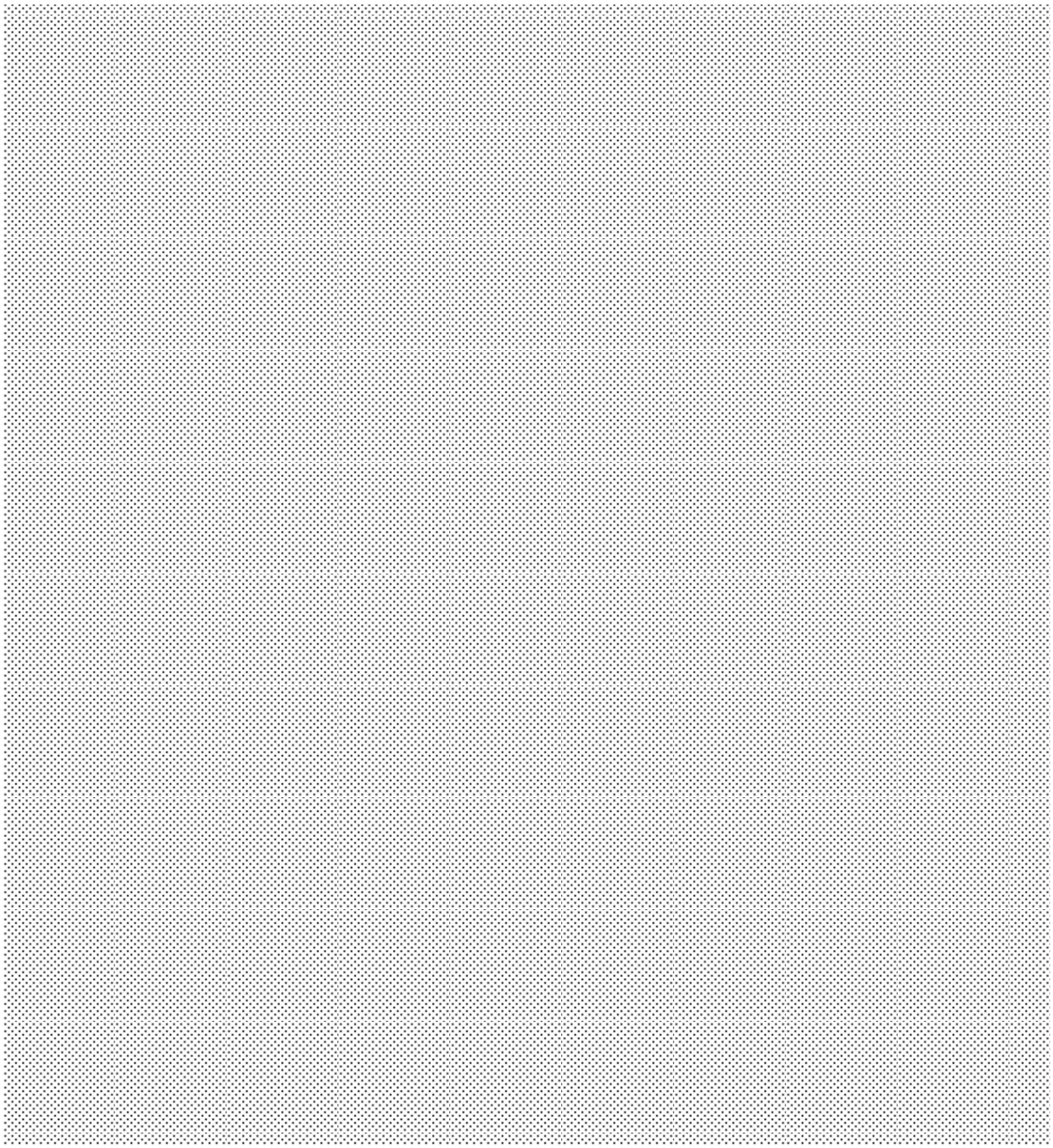

Figure 3.16 Impulse responses of HRTFs

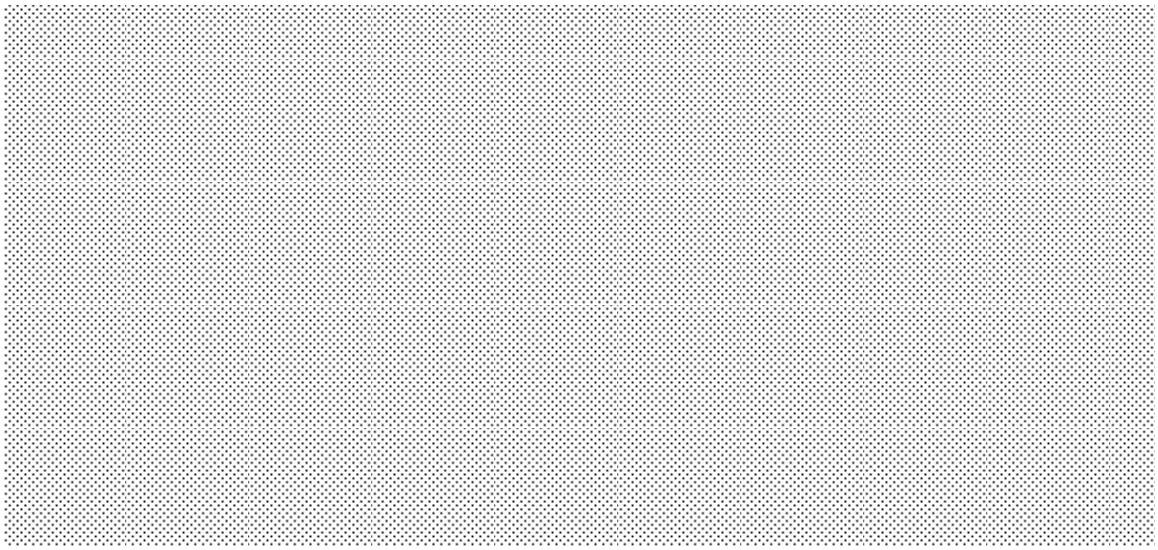

Figure 3.17 Crosstalk cancellation with HRTF

3.5 Putting it all together

Several of the presented algorithms can be implemented together in order to achieved the requirements of a specific situation. There are multiple options and possible configurations that are tested with the DSP and amplifier.

For example, a multichannel audio system can be implemented by two speaker arrays. The left and right channels can be emitted directly to the ears meanwhile the surround channels can be filtered by HRFT with a specific angle. Also the speaker arrays offers natural crosstalk cancelation or the possibility of increasing it by using the equalization filter.

If it is only available a stereo input signal, it is also possible to obtain surround channels by using commercial algorithms like Dolby Stereo Decoder or algorithms from scientific publications [30, 31, 32, 33]. Then, each channel can be emitted by using the different methods presented in this chapter.

3.6 Conclusions

In this chapter, methods for crosstalk canceling and transaural audio reproduction were presented. All the crosstalk cancellers presented are symmetric; the listener is situated on the middle axis of the speakers. However, it is possible to design them for other listener positions by considering the angles for the filters.

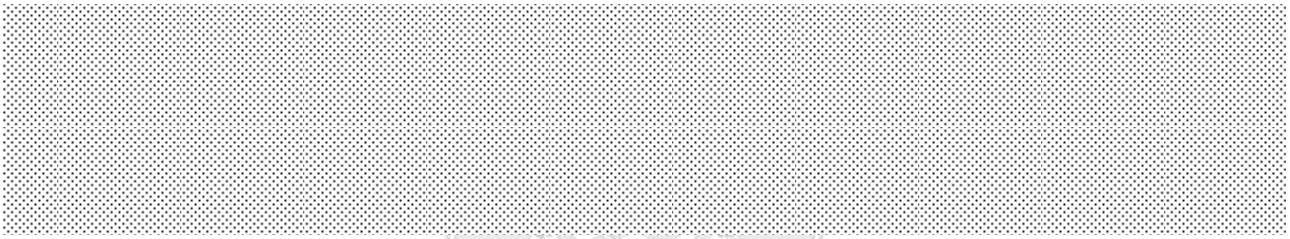

The presented algorithms are implemented in a DSP in order to test and measure them. The directivity functions of the single and double channels can be found in chapter 6. In this thesis work, for the crosstalk cancellation algorithms, the implementation is not possible in real time due to the memory limitation of the DSP, therefore, they are tested in non-real time by programming in Matlab.

4 Beamforming simulation

This chapter will present different methods to simulate the beamforming theory. Most of the figures presented in this thesis work are created by functions programmed in MatLab. Furthermore, as an extension of the functions, Graphic User Interfaces will be presented. These tools will provide a convenience method to design and simulate line arrays. Finally, by simulating with Finite Element Method (FEM) some comparisons will be presented.

4.1 Line array speaker simulator

MatLab (MATtix LABoratoy) is a numerical computing software convenience for matrix operations and data representation. Also it is useful for algorithm implementations and creation of Graphic User Interfaces. Due to its flexibility and versatility most of the figures and examples in this thesis are created with this software.

In order to simulate different line array configurations a Graphic User Interface (GUI) is programmed. This GUI is composed of functions that operate with the numerical methods previously presented in Chapter 2. It obtains the directivity functions of continuous, discrete, phased and directional sources line arrays. In addition, it finds the frequency working range by equation or threshold and provides the Directivity Index and -6 dB angle. Figure 4.1 shows the welcome screen, where a brief introduction is displayed.

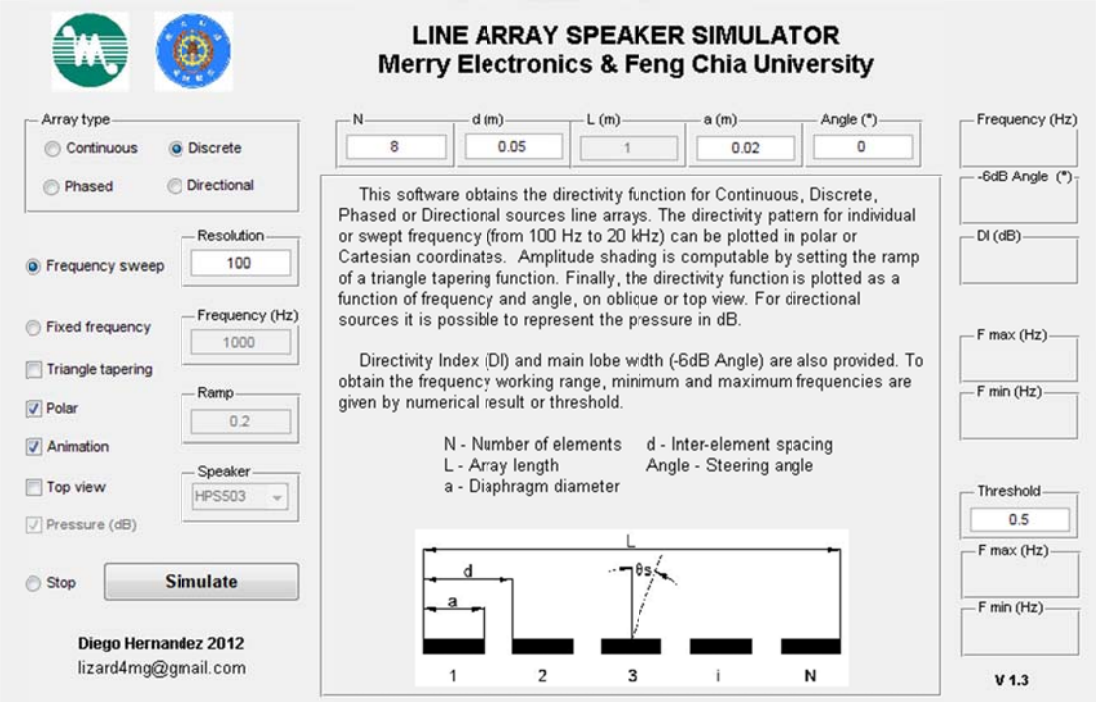

Figure 4.1 Welcome screen of the Speaker Line Array GUI

By selecting the different checkboxes and round selectors it is possible to set the configuration of the desire line array. The GUI automatically activates and deactivates the checkboxes depending on the available options for each line array type. For a uniform line array only the length (L) is necessary. Then, the directivity pattern can be obtained for a single frequency represented in polar or Cartesian coordinates. By activating the checkbox “Animation” an animated evolution of the frequency is plotted. This provides an easy visual method to understand and study the directivity pattern. The GUI allows introducing frequency resolution as a number of elements in logarithmic increment from 100 Hz to 20 kHz. As the resolution increases the computational time increases, requiring more time to generate the final matrix before plotting it. The frequency for each calculation of the directivity is indicated on the panel “frequency”. Figure 4.2 (a) shows a continuous line array at one fix frequency in polar coordinates.

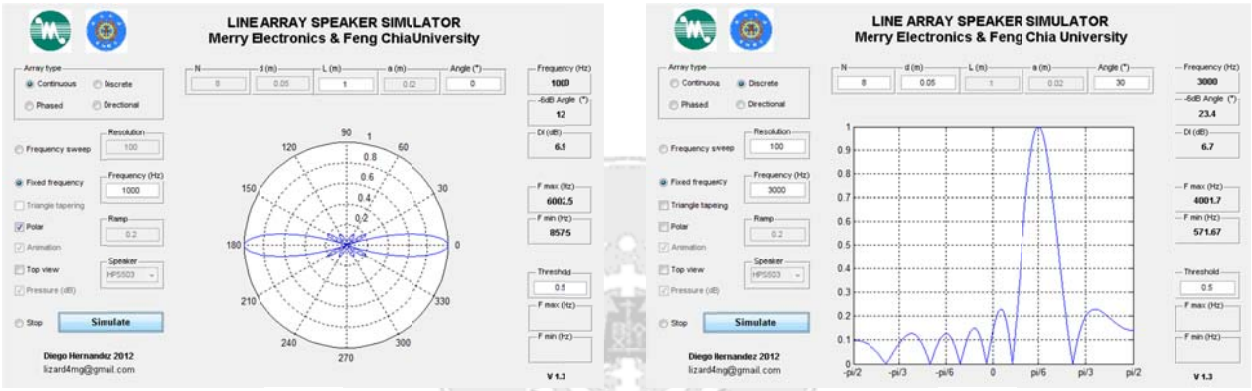

(a) (b)

Figure 4.2 Line array GUI screenshots: (a) Continuous array (b) Discrete array

For a discrete line array number of elements (N) and inter-element spacing (d) is needed. Furthermore, the length of the source element (a) is necessary to design phased line array. If an amplitude shading is desired the checkbox “Triangle tapering” has to be activated. That is, a triangular tapering function with the step as a variable in order to avoid zero amplitude values for the side elements. The amplitude shading is computable for all types of line array. Figure 4.2 (b) shows the frequency response at 3 kHz of an 8-element discrete line array steered 30 degrees in Cartesian coordinates. When all directivity functions of all the discrete frequencies are calculated, a three-dimensional graphic represents the directivity as a function of frequency and angle, as given in Figure 4.3 (a). By selecting the checkbox “top view” the point of view is moved to the top of the figure, offering an easier visualization depending on the circumstances.

For a directional source line array simulation, the selection for each speaker is available on the pop-up menu “speaker”. The available speakers are HPS503, HPS131, DSH624, DSH715 Vertical and DSH715 Horizontal, as previously presented in section 2.6. In addition, also the number of elements (N) and the inter-element spacing is required. Because the speaker presents a frequency response, the information of the pressure can be represented in decibels or linear. If

the number of elements (N) is set equal to 1, the directivity function of the individual speakers can be represented. Figure 4.3 (b) shows the top view directivity of a 12-element array composed of DSH624 speakers.

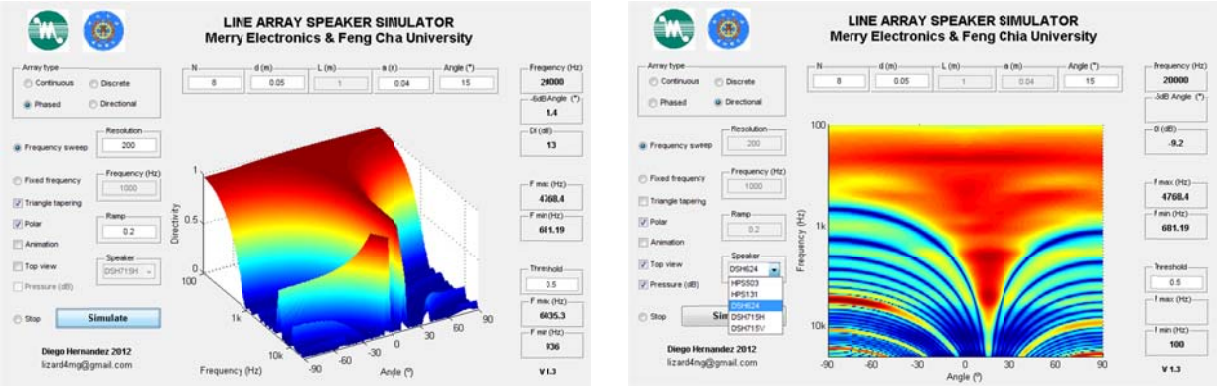

(a) (b)

Figure 4.3 Line array GUI screenshots: (a) Phased array (b) Directional sources array

Also other useful parameters to design line arrays like DI and -6dB are provided. These, are represented automatically for each frequency. The quarter power angle is obtained by finding the main lobe angle and the angle where the pressure becomes half amplitude. To obtain the frequency working range, the minimum and maximum frequencies are provided; these can be calculated by Eq. (2.32) and Eq. (2.37) or by setting a threshold in the GUI.

4.2 Finite Discrete Time Domain simulation

Finite Discrete Time Domain (FDTD) is a simulation technique proposed by Kane Yee (1966). It is a versatile technique to solve problems with differential equations. This method is widely used in the electromagnetic field with Maxell equations. Furthermore in acoustics, it is possible the implementation by using the equation that describes the wave motion in the air. Because this technique works in time domain, it is possible to study the evolution of the wave front with an animation. Considering a two-dimensional medium where ρ is the air density and c the sound speed, the wave equation can be expressed as

$$\frac{dp}{dt} + \rho c^2 \left(\frac{du_x}{dx} + \frac{du_y}{dy} \right) = 0 \qquad \textbf{(4.1)}$$

Then, the pressure in the different positions and time can be calculated. FDTD technique requires high memory resources to compute due to the discretization has to be small in comparison with the wavelength. High frequency requires small distance between modes, that is, a large grid has to be created. The same problem appears if the domain is too large and the frequencies to study too high. Therefore, the presented GUI is restricted to 1 kHz signal in a 9 m^2 domain. To assure a correct simulation at that frequency, each wavelength has 20 elements, that is, they are separated 1.7 cm each other. In order to simulate free field conditions, a Perfect

Matched Layer (PML) is created around the domain. This PML provides the necessary absorption to avoid reflections that could interact and produce interferences. The GUI simulates the beamforming phenomenon on an eight-element line array. The Sound Pressure Level is displayed on the two-dimensional domain as an animation. Figure 4.4 shows the GUI welcome screen.

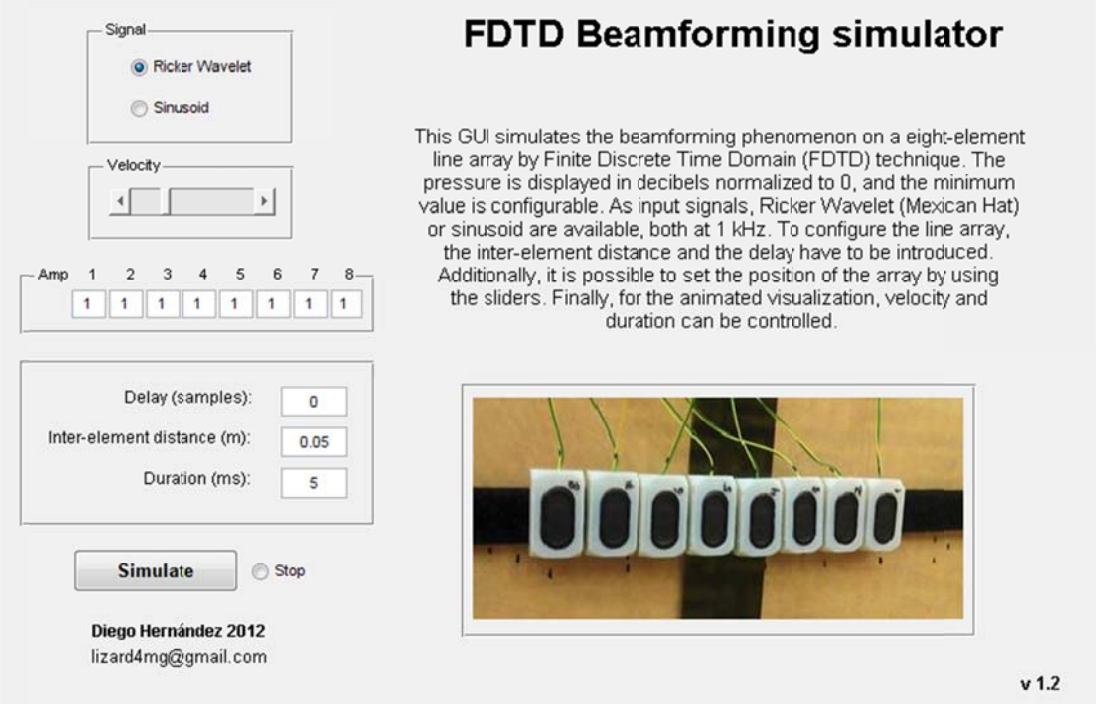

Figure 4.4 Welcome screen of the FDTD Beamforming GUI

The position of the line array on the 2D domain is configurable by the sliders. As input signals, 1 kHz sinusoid or Ricker (Mexican Hat) wavelets are available. Figure 4.5 (a) shows the line array situated on the left and emitting the sinusoidal signal. The amplitude of each element of the eight-element line array is configurable in order to test the attenuation of the side lobes, also it is possible to give amplitude zero and obtain a line array with lower number of elements. To obtain a steered angle the delay has to be introduced in samples. Figure 4.5 (b) shows a line array composed of eight elements with amplitude shading and delayed five samples.

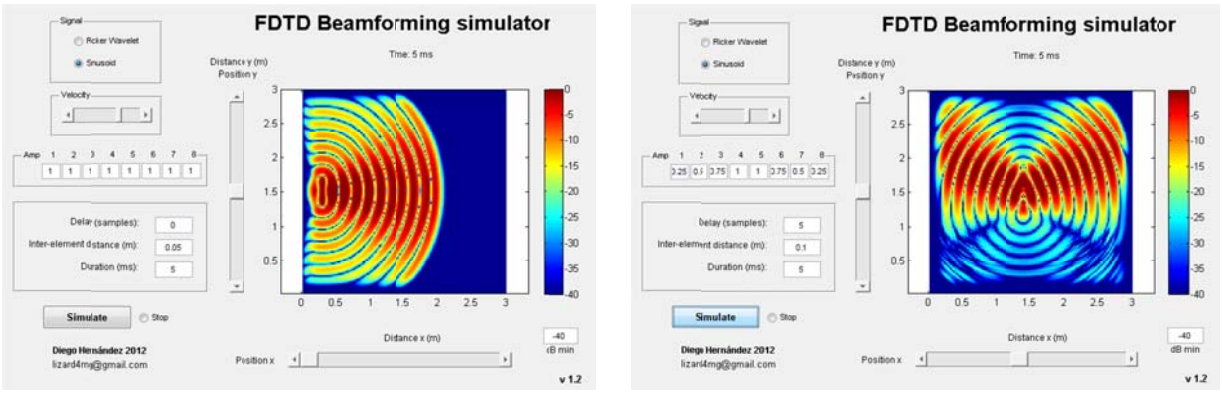

(a) (b)

Figure 4.5 FDTD GUI screenshots: (a) Sinusoid (b) Sinusoid steered

The Ricker wavelet is useful to study the formation of the wavelet and analyzed its the distortion. In order to improve the visualization, the velocity and duration of the animation can be configurable. The pressure is displayed normalized to 0 dB and its minimum value can be adjusted. Figure 4.6 (a) shows the Ricker wavelet emitted with five samples delay. Additionally, it is also possible to vary the inter-element distance to study different distributions. Figure 4.6 (b) shows the wavelet front coming from a line array with the elements separated 15 cm each other.

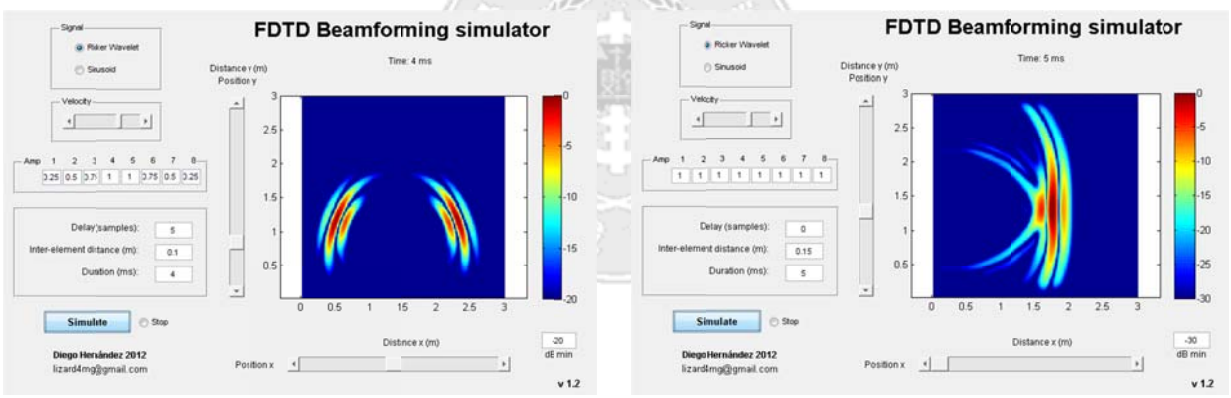

(a) (b)

Figure 4.6 FDTD GUI screenshots: (a) steered Ricker wavelet (b) 15 cm inter-element spacing

4.3 Finite Element Method simulation

Finite Element Method (FEM) is a numerical process to solve problems with differential equations. The simulation software COMSOL offers a user interface where the geometry of the problem can be graphically created. As an example, a discrete line array composed of 8 elements with 5 cm of inter-element distance is disposed at the center of a circle of 4 m diameter. All the elements radiate with same energy and phase, forming the beam at 0 degrees. Once the proposed problem is solved, the results can be visualized in different ways. By representing on a 2D plane, the Sound Pressure Level can be displayed inside the circular domain previously defined. In Figure 4.7 (a), (b) and (c) is represented the directivity at 500, 1000 and 2000 Hz

respectively. It is observed that as the frequency increases the array becomes more directional and secondary lobes appear.

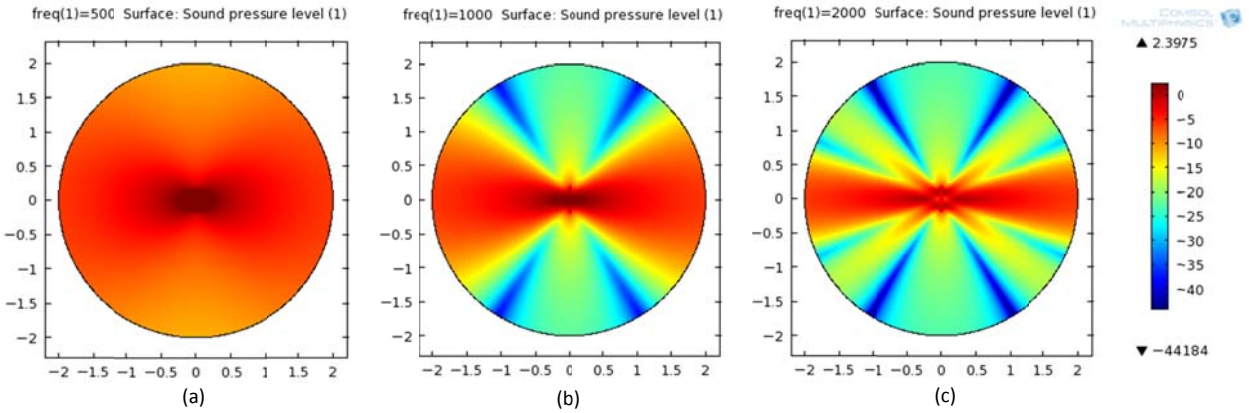

Figure 4.7 Pressure level (dB) representation: (a) 500 Hz (b) 1 kHz (c) 2 kHz

Also it is interesting to represent of the pressure in order to observe the wave interference phenomenon. The maximum and minimum pressure values are spaced as a function of the wavelength and this helps to understand the beam formation. Figure 4.8 (a), (b) and (c) shows the pressure normalized between -1 and 1 at 500, 1000 and 2000 Hz respectively. It is observed that when the waves are opposite phased a minimum is generated, if the waves are in phase the energy is summed and the pressure becomes maximum.

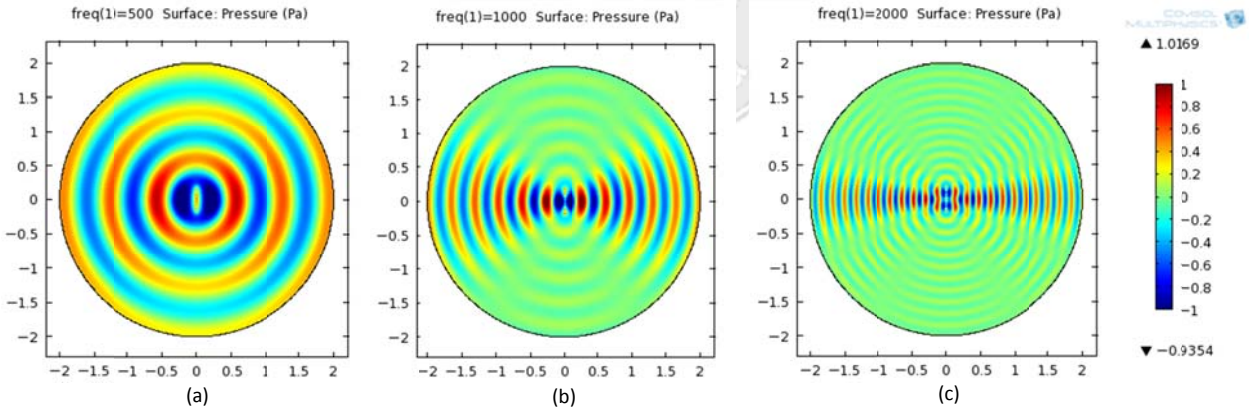

Figure 4.8 Pressure representation (a) 500 Hz (b) 1 kHz (c) 2 kHz

By representing the normalized absolute pressure present around the egde of the circle on a polar chart, the directivity function can be obtained. Figure 4.9 shows the comparasion of the directivity at 500, 1000 and 2000 Hz obtained by COMSOL and MatLab. It is observed that both results are similar.

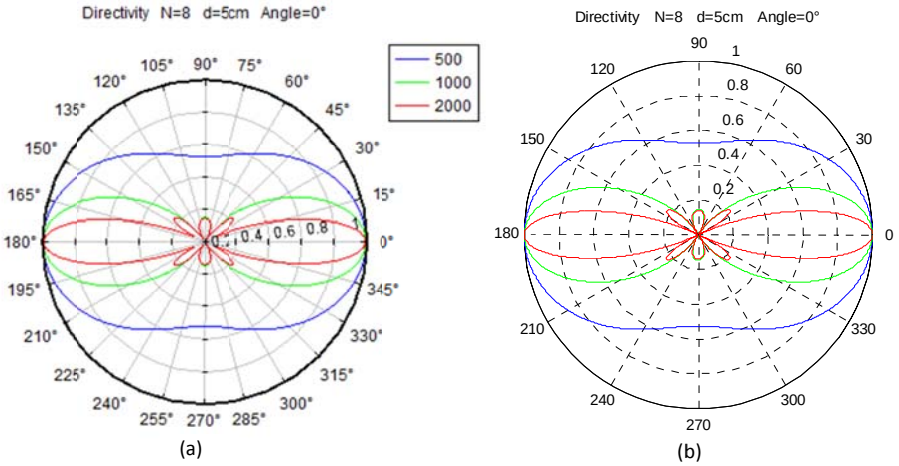

Figure 4.9 Directivity comparison (a) COMSOL (b) MatLab

Next, amplitude shading is simulated in the same array by setting the amplitude configuration presented in section 2.12. Figure 4.10 shows the resulting directivity function at 2 kHz.

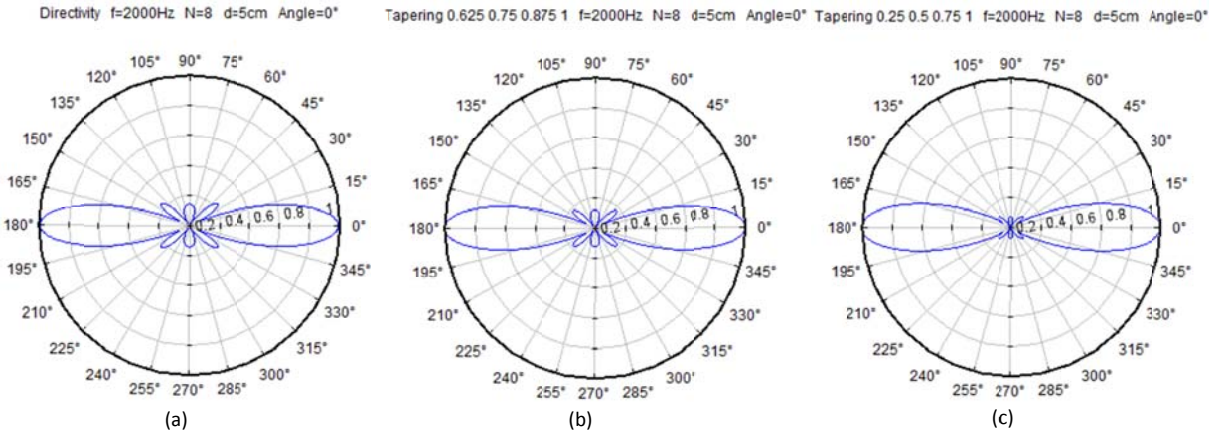

Figure 4.10 Stereo line array. DSH715: (a) 16.5° (b) 29.7°. DSH705: (c) 16.5° (d) 29.7°

The main advantage of FEM is the possibility to obtain the pressure as a function of the distance and simulate complex array configurations. But limited by the memory required and the minimum element size of the mesh additionally, this method presents limitations for application at high frequency. Also the time required for the computing increases if the domain is large or the element size is small. In conclusion, in order to compute the equations presented in chapter 2, MatLab offers a more convenience method to study the beam forming phenomenon.

5 Electro-acoustic design

In order to test different line array configurations and algorithms it is necessary to design an audio system. The sound system is composed in general terms, as shown on Figure 5.1, by a signal generator, signal processor, amplifier, and speakers.

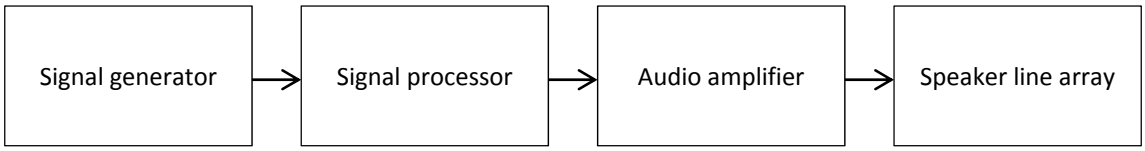

Figure 5.1 Sound system flow diagram

A personal computer is used as the signal generator; depending on the situation, the reproduced signal consists of noise, tones, voice or music. As the signal processor, either a Digital Signal Processor board or an audio card is used. The audio amplifier is designed and built for the purpose of this thesis. Lastly, the line array is composed of (correct others) 8 speakers in two different sets; 8 DSH624 speakers are mounted in a methacrylate enclosure and 8 DSH715 speakers are mounted in individual enclosures. Next, the different parts of the sound system will be explained in detail.

5.1 Digital Signal Processor

By using a Digital Signal Processor (DSP), the signals to the individual speakers can be separately delayed before being sent to the speakers. This processing allows the shaping of the directivity pattern of the line array. Depending on the application, several steered beams can be emitted at the same time. Also, other signal treatments like frequency filtering, dynamic processing, inversion or gain are considered depending on the algorithm [36].

Two different DSPs are considered in this thesis work. A DSP evaluation board is used for simple algorithms in real time processing and an audio sound card for elaborate algorithms in non-real time processing.

5.1.1 DSP Evaluation Module

The Texas Instrument TAS3108EVM2 DSP Evaluation Module (Figure 5.2) is composed of three boards: a DSP chip TAS3108; an input with SPDIF, ADCs, and USB for PC control; and an output with DACs and a SPDIF transmitter [37]. The TAS3108EVM2 allows a complete 8-channel digital audio processor system that includes digital input/output (S/PDIF), analog inputs/outputs and interface to a personal computer. In this work only analog inputs/outputs are used.

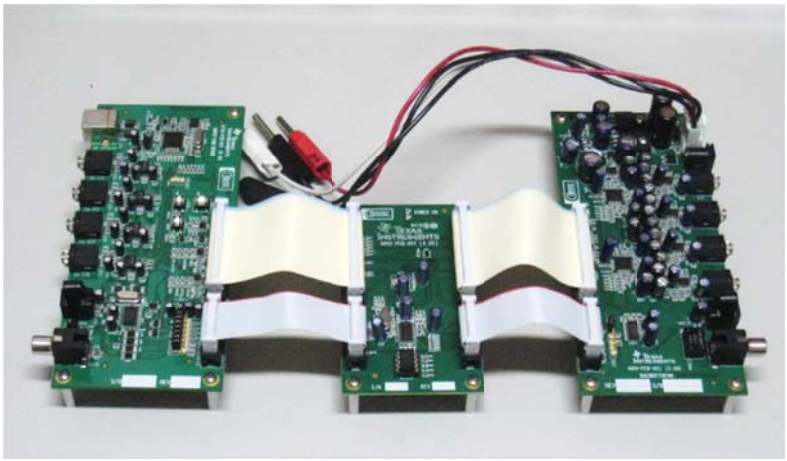

Figure 5.2 TAS3108EVM2 DSP Board

The main disadvantage for the TAS3108 is its memory limitation and programming tool. An 8 speaker line array needs 7 delays per beam formed (consider for the first speaker 0 samples delayed). The TAS3108 has a 20-delay memory limitation, then, only two off-axis beams can be formed simultaneously. The maximum number of FIR filters (at 364-tap) is two and the IIR filters are limited to order two [38]. Also, the GUI Pure Path Studio does not have the flexibility to create complex algorithms via C or MatLab. In summary, this DSP board is useful for measurement in the laboratory where real time processing is necessary and complex algorithms needed.

5.1.2 Sound card

To program more complex algorithms with MatLab, alternatively, an 8-output channel sound card is used. The Vantec NBA-200U (Figure 5.3) is a USB audio adapter that allows 8-channel output for 7.1 audio reproduction. It supports 48/44.1 kHz sampling rates for both playback and recordings, and also SPDIF optical digital input and output. In addition, this audio adapter is used to send the different channels or a multi-channel audio 5.1 to the DSP board. This allows each channel to be emitted at a different angle.

Figure 5.3 Vantec NBA-200U USB Audio Adapter

The main disadvantages are the non-real time processing and the size limitation in processing a matrix in MatLab. The input signals are transformed to 8-channel WAV file (Waveform Audio File Format). Then, the sound file is played by a multimedia player and each channel is sent to each speaker.

5.2 Audio amplifier

In order to connect the line level output of the DSP board and sound card to the speakers, it is necessary to amplify the signal [34], [35]. The speakers considered in this project are less than 3 Watts; a 2-Watt amplifier is powerful enough for this purpose. Next, the design and construction of the amplifier is explained in detail.

5.2.1 Circuit

For convenience, the amplifier system is designed with Integrated Circuits (IC). The LM380 is an IC power audio amplifier with an internally fixed gain, low distortion and wide band width [39]. This IC is designed for audio applications and is suitable for amplifying the signal of each speaker in the line array. In the 14 pin package version (LM380N), the central pins on either side are used as heat sinks. Main specifications and features according to the datasheet are given in Table 5.1.

Table 5.1 Specifications of the LM380

Parameter	Conditions	Value
Output power	3%THD, R_L=8Ω	2.5W_{RMS}
Gain	3%THD, R_L=8Ω	40V/V
Input impedance		150kΩ
Total Harmonic Distortion (THD)	1W	0.2%
Bandwidth	R_o=2W, R_L=8Ω	100kHz

The output power (therefore gain) is related to the power supply voltage (V_{cc}), but the manufacturer does not give information of the power at different voltages. These values, among others, will be obtained by measuring the amplifier.

The amplifier system has eight identical channels, one per speaker. To simplify, Figure 5.4 shows the circuit of one channel and the connectors for audio I/O and power supply.

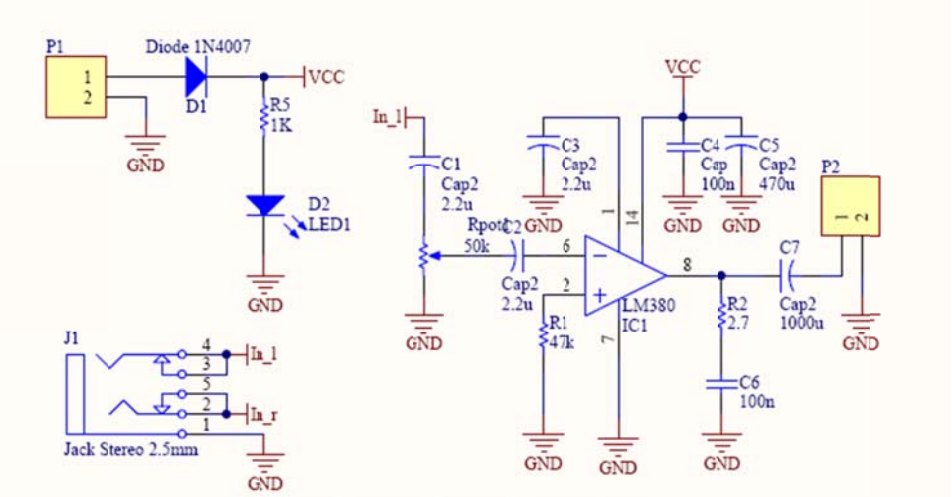

Figure 5.4 Circuit of one channel of the amplifier

In the presented circuit, the signal coming from the DSP enters in the amplifier through the J1 connector. P2 is the output connector where the speaker is connected. The power voltage that the amplifier requires to work comes from the P1 connector. D1 prevents damage if the power supply is connected incorrectly. R5 and D2 are resistor and diode led to indicate when the circuit is working. C1 and C2 are the input coupling capacitors, they block any DC that could be present at the input. C7 is the output coupling capacitor, which blocks the DC level that is present at the amplifier output. C4 and C5 provide power supply filtering. R2 and C6 form a Zobel network for frequency load stability. C3 provides extra supply decoupling. Finally, the potentiometer controls the input level, allowing attenuation in case the voltage excursion of the input signal is too high.

5.2.2 Printed Circuit Board design

The Printed Circuit Board (PCB) is designed via computer using the software Altium Designer. The audio system amplifier has eight similar channels, one power supply connector in common for all the amplifiers, four stereo inputs and eight mono outputs. Altogether, it has to be organized and distributed on a board of reasonable size and proportions.

First, for the design of the PCB it is necessary to know the dimensions of the components, then the footprints can be created. The spacing and widths of the pins and the room for the components has to be considered. Once the footprints are created, these are distributed as close

as possible to avoid long paths and radiations. The decoupling capacitors are situated near the IC in order to obtain maximum power supply filtering. The central pins on both sides of the IC are used as heat-sink; these are also connected to the ground plane to obtain more dissipation. The V_{cc} net has a thicker width for the traces due to higher current circulation.

The board is a single side design, with common ground plane to increase the stability and reduce noise. Figure 5.5 shows the bottom and silk-screen layer, where the distribution of the elements and paths can be observed.

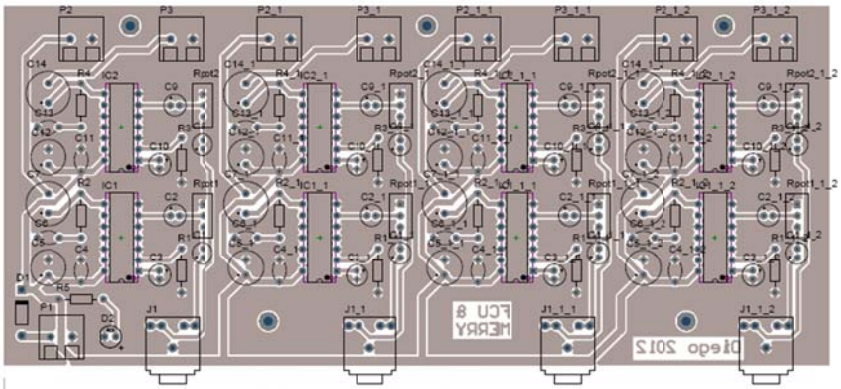

Figure 5.5 Layout of the PCB with footprints

Finally, the design ready to be printed and transferred to the board is shown on Figure 5.6

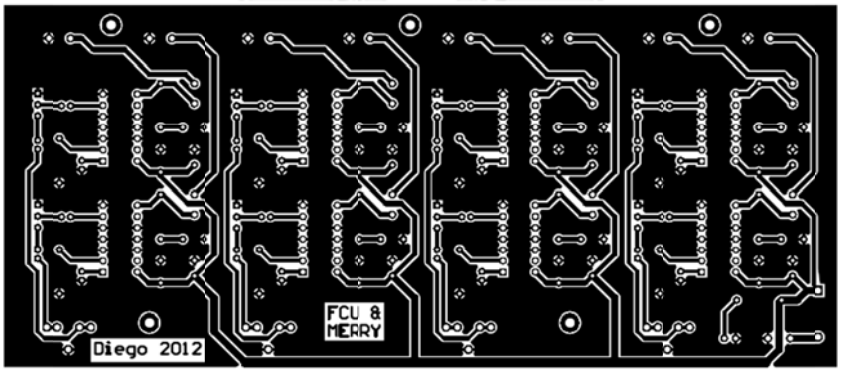

Figure 5.6 Layout of the PCB ready to print

5.2.3 PCB construction

To make the PCB a fiberglass photoresist laminated board is used. The board needs to be exposed to ultra violet light for 2 minutes in the UV exposure box (Figure 5.7 (b)), the PCB design is printed in transparent paper for this purpose. After the exposure, the developing is made by a mix of Sodium Hydroxide and water. Once the photoresist material is removed, for the etching an industrial machine is used. Finally, the components holes are drilled with different sizes depending on the component (Figure 5.7 (a)). After removing with acetone the photoresist

material that protects the copper (Figure 5.7 (c)) the board is ready (Figure 5.7 (e)) and the components can be placed on it (Figure 5.7 (d) and (f)).

Figure 5.7 Images of the PCB construction: (a) Drilling (b) Ultra-violet enclosure (c) Placing the components (d) Cleaning photo-resist material (e) PCB without components (f) PCB with all the components

5.2.4 Power supply

The power supply has to provide the required current to all the ICs. According to the datasheet provided by the manufacturer, the LM380 consumes a quiescent current of 25 mA. At the same time, it is needed the current to amplify the signal. The amplifier can work with a wide voltage range, from 8 V to 22 V. Higher the voltage, higher the output power, therefore higher current consumption. Even though the efficiency of the amplifier has to be considered, an estimation of the required current I_{RMS} can be calculated by knowing the maximum output power P_{RMS} and the load R as

$$I_{RMS} = \sqrt{\frac{P_{RMS}}{R}} = \sqrt{\frac{2.5\ W}{8\ \Omega}} = 0.56\ A \qquad \textbf{(4.1)}$$

Consequently, the 8 channels at this theoretical maximum power would consume $(0.56 + 0.025) \cdot 8 = 4.68\ A$. In this case a power supply of 22 V and 5 A would be necessary. But, for the real case the amplifier should not work more than 1.5 W to avoid the using of heat-sinks, where 3.5 A would be demanded.

For convenience a bench laboratory power supply is used, with the possibility of controlling the voltage and also limiting the current to protect against short-circuit. The power supply is the GPS-4303 of GW Instek (Figure 5.8). It provides 4 independent outputs: 2 outputs 0-30 V 1 A, 1 output 8-15 V (1 A) and 1 output 2.2-5.2 V (1 A). It also allows bridge mode with a maximum of 60V and 6A. This equipment is suitable to power more devices at the same time, like a DSP board.

Figure 5.8 GW Instek GPS-4303 Power supply

5.2.5 Test

The measurement process is in accordance with the standard UNE-EN 60268-3 [40]. Because the audio power amplifier with the LM308 has a fix gain and it varies depending on V_{cc}, not all the items can be measured. The laboratory equipment used for the measurement of the items is composed of oscilloscope (Tektronix TDS1012B), power source (GW Instek GPS-4303) and signal generator (GW Instek SFG-2100). Additionally, audio sound card and the software ARTA are used to measure the items related with frequency response.

Maximum output power

It is interesting to measure first this item in order to set the optimum output power. Because the IC is working using the copper of the PCB as heat-sink, it should not work more than 1.5 W for a long period of time. The output power is calculated by measuring the maximum voltage excursion at the output on an 8 Ω load. The signal generator introduces a 1 kHz sinusoidal signal in the amplifier, its voltage is gradually increased meanwhile the output voltage is measured by the oscilloscope. The voltage value at the output just before the clipping is the maximum output excursion. Then, the output power is calculated by using $P_{RMS} = V_{RMS}^2 / R$. This operation is executed from 8 to 20 V with steps of 1 V. The representation of the output power as a function of the power supply voltage is illustrated on Figure 5.

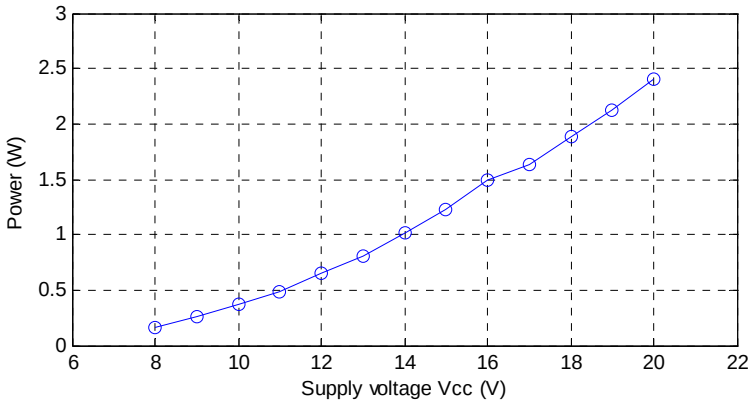

Figure 5.9 Output Power of the amplifier

Other parameters as a function of the supply voltage

At the same time of the maximum output voltage measurement, the maximum input voltage and the noise presented at the output were measured. To measure the noise a 1 kΩ resistor is connected at the input. With these measurement results, it is also possible calculate the Dynamic Range (DR) as a function of V_{cc}. The DR is the relation between the maximum excursion voltage and the output voltage without signal.

$$DR = 20 \log \left(\frac{V_{0\,max}}{V_{0\,noise}} \right) \quad \textbf{(4.2)}$$

The measured and calculated parameters dependent on V_{cc} are shown in Table 5.2.

Table 5.2 Parameters of the amplifier

V_{cc}	Noise	V_{in} max	V_{out} max	Output Power	DR
V	mV_{rms}	mV_{rms}	V_{rms}	W_{rms}	dB
8	2,0	25,9	1,1	0,2	54,9
9	2,2	33,0	1,4	0,3	56,6
10	2,2	39,3	1,7	0,4	57,8
11	2,4	46,4	2,0	0,5	58,1
12	2,7	53,6	2,3	0,6	58,6
13	2,8	55,4	2,5	0,8	59,3
14	2,8	64,3	2,8	1,0	60,1
15	3,0	67,9	3,1	1,2	60,5
16	3,0	76,8	3,5	1,5	61,2
17	3,1	82,1	3,6	1,6	61,3
18	3,2	89,3	3,9	1,9	61,7
19	3,3	96,4	4,1	2,1	62,0
20	3,4	100,0	4,4	2,4	62,3

In order to measure the next items, the power supply is set with 15 V, this value yields a nominal power of 1.2 W.

Input Sensitivity

The input sensitivity is defined as the RMS voltage applied at the input to obtain 1 W at the output, in this case with an 8 Ω load. To obtain 1 W at the output is it measured the voltage as follows,

$$P_{rms} = \frac{V^2}{R} \tag{4.3}$$

$$V_{rms} = \sqrt{P_{rms} R} = \sqrt{1W \cdot 8\Omega} = 2.81\, V_{rms}$$

As shown in Figure 5.10, the RMS voltage value at the input is measured at channel 2 of the oscilloscope. Then, the sensitivity is:

$$Sensitivity\ (1W) = 58\ mV$$

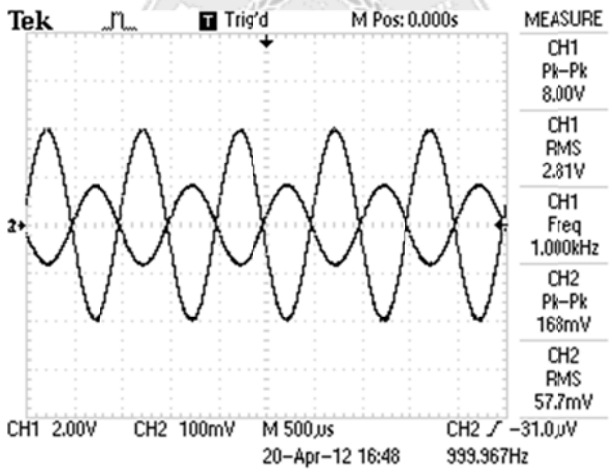

Figure 5.10 Measurement of the sensitivity

Input impedance

Even though the impedance depends on the frequency, the standard requires the measurement to be done at 1 kHz. For the measurement, a resistor is placed in series before the input as shown on Figure 5.11 (a).

(a)

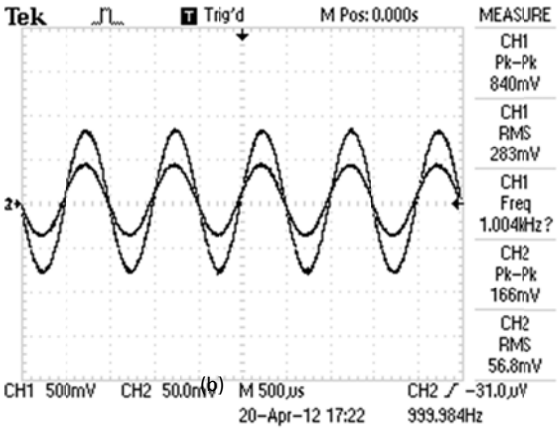

(b)

Figure 5.11 (a) Circuit for the impedance measurement (b) Measurement of the input impedance

The input impedance of the signal generator (Rx) is 50 Ω, small enough to omit it. After measuring V_1 and V_i (Figure 5.11 (b)) the value of the impedance is calculated as

$$R_i = \frac{V_1}{V_i - V_1} R_x = \frac{0.165}{0.283 - 0.165} 150 \cdot 10^3 = 210\ k\Omega \quad \textbf{(4.4)}$$

Output impedance

To measure the output impedance, first the output with the load and a 1 kHz sinusoidal input signal is measured. According to the circuit shown in Figure 5.12 (a) the impedance is obtained as

$$R_o = \frac{V_x - V_2}{V_2} R_L \quad \textbf{(4.5)}$$

The V_x value is unkown, but it is possible to measure it by taking out the load ($V_x = V_{2\ no\ load}$). Then, after measuring V_2 and $V_{2\ no\ load}$ (Figure 5.12), the value of the output impedance is calculated as

$$R_o = \frac{V_{2\ no\ load} - V_2}{V_2} R_L = \frac{6.4 - 6.24}{6.4} 8 = 200\ m\Omega \quad \textbf{(4.6)}$$

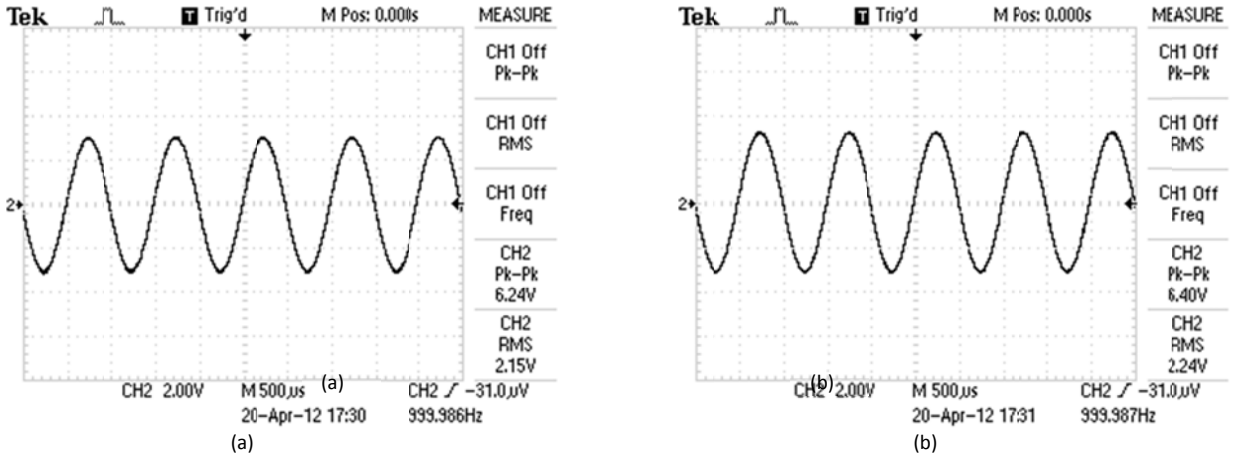

Figure 5.12 Measurement of the output impedance. (a) V_2 (b) $V_{2\ no\ load}$

Damping Factor

In audio amplifiers the Damping Factor (DF) can be defined as the relation between the load and output impedance. The value has to be as high as possible in order to the amplifier behaves as an ideal voltage source. It is calculated as

$$DF = \frac{R_{speaker}}{R_0} = \frac{8}{0.2} = 40 \tag{4.7}$$

Signal to noise ratio (S/N) at 1W

This ratio is the relation between the output signal and the noise. In this point noise is defined as the output voltage with a 1 kΩ load connected at the input. A 1 kHz sinusoidal signal is used as input to obtain 1 W at the output. After measuring the voltages with the oscilloscope (Figure 5.13), the Signal to Noise ratio at 1 W is obtained as

$$\left(\frac{S}{N}\right) = 20\log\left(\frac{V_{out}}{V_{0\ noise}}\right) = 20\log\left(\frac{2.84}{3.5\cdot 10^{-3}}\right) = 58\ dB \tag{4.8}$$

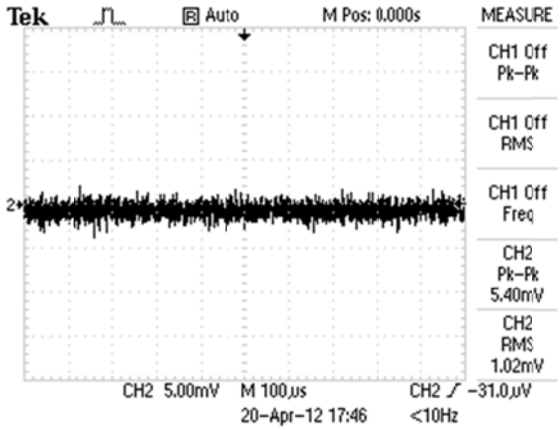

Figure 5.13 Measurement of $V_{0\ noise}$

Crosstalk

The Crosstalk is the no desired signal presented at the output of the not excited channel coming from the exited one. The amplifier has eight channels and it is important to keep the separation to avoid interferences. For the measurement, a 1 kHz sinusoidal signal is applied to one input and the output of other channel is measured. The crosstalk attenuation of two channels is given by the relation of both output voltages

$$A = 20\log\left(\frac{V_1}{V_2}\right) = 20\log\left(\frac{4}{0.025}\right) = 44\ dB \qquad \textbf{(4.9)}$$

Frequency Response

For the frequency domain measurements, the software ARTA and the sound card of the computer are used. ARTA is an application for audio measurements and analysis in acoustical and communication systems provided by ARTALABS. The sound card has limitations in frequency and input voltage range, the voltage of the signal to measure is bigger than the maximum input of the sound card. To avoid saturation, a simple attenuator with resistors is used. For the frequency limitations, it can be observed that the higher frequency limit given by the sound card, and not by the amplifier, which is 18 kHz. In low frequency, the limit is found at 40 Hz. In conclusion, the frequency response of the amplifier (Figure 5.14) is suitable for this purpose.

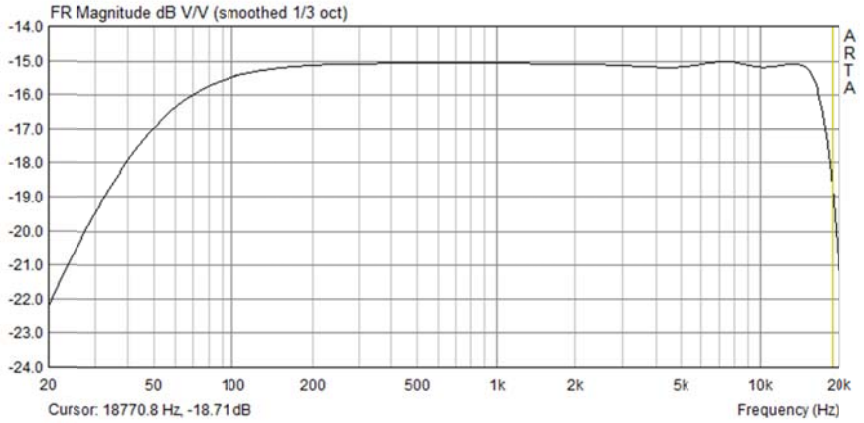

Figure 5.14 Frequency response of the amplifier

Total Harmonic Distortion (THD)

The Total Harmonic Distortion (THD) is defined as the ratio of the sum of all harmonic components power to the fundamental frequency power. This parameter characterizes the linearity of the amplifier, and it is one of the most important to measure the quality of an amplifier. THD+N means the Total Harmonic Distortion plus Noise. To measure it, a 1 kHz sinusoidal signal is generated by ARTA and introduced to the input of the amplifier. Because this amplifier offers a fix gain, the input level has to be adequate to avoid saturation at the output. Then, the output is measured by the spectrum analyzer, and the result $THD + N = 0.24\%$ is shown in Figure 5.15

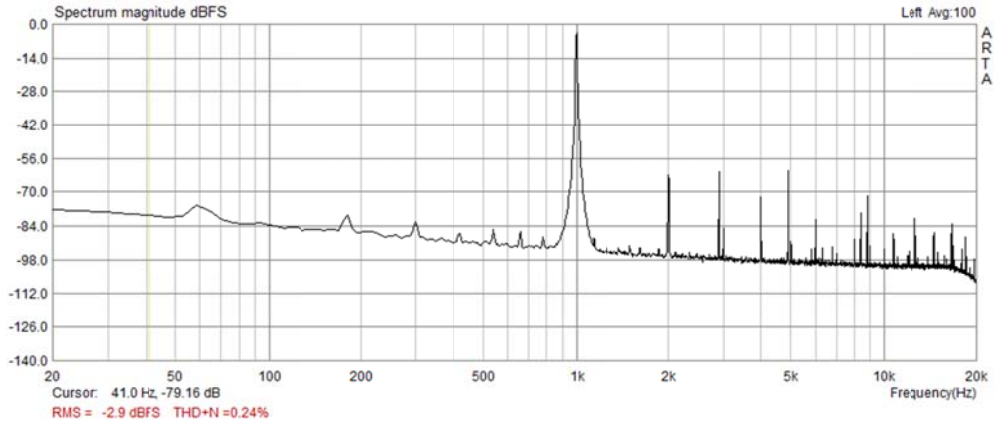

Figure 5.15 THD+N measurement

Intermodulation Distortion (IMD)

The Intermodulation Distortion is an amplitude modulation of two signals in a system with nonlinearities. This introduces additional signals at frequencies that are not only just harmonic frequencies, but also at the sum and difference frequencies of the original frequency. To

measure it, 13 kHz and 14 kHz sinusoidal signals are introduced to the input of the amplifier, the output is measured by ARTA and the 0.065% of IMD is obtained as shown in Figure 5.16

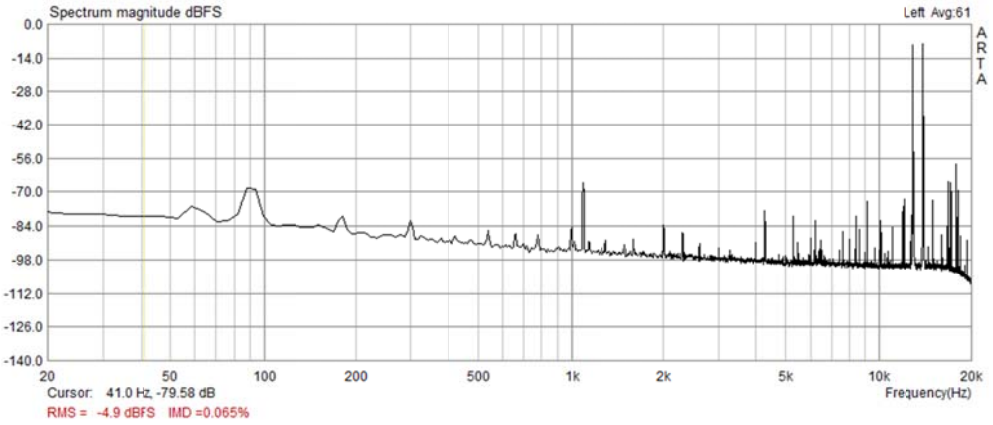

Figure 5.16 IMD measurement

5.3 Speakers

For the testing and measurement of the line array and its algorithms two speaker sets, formed by DSH624 and DSH715, are used. The DSH624 is a 2 W high performance speaker designed for TV and portable audio applications. On the other hand, the DSH715 is a micro-speaker designed for laptops and electronic tablets. More details about their directivity and frequency response can be found in section 6.2.

In order to provide speaker selection, an 8-channel Single Pole Double Throw (SPDT) selector is designed. This allows a combination of speakers or a fast change of set. Each channel of the selector is formed by 2 switches situated between the amplifier and the speakers as represented in Figure 5.17.

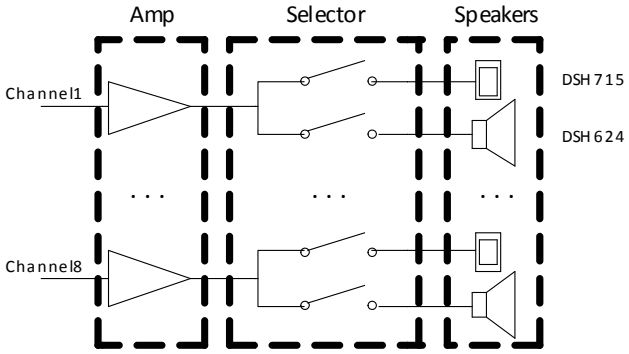

Figure 5.17 Speaker selector diagram

To obtain more versatile equipment, the amplifier and speaker selector are also placed inside. The construction in methacrylate glass (acrylic) is carried out by Merry Electronics. Figure 5.18 shows the resulting enclosure including speakers, amplifier and speaker selector.

(a)

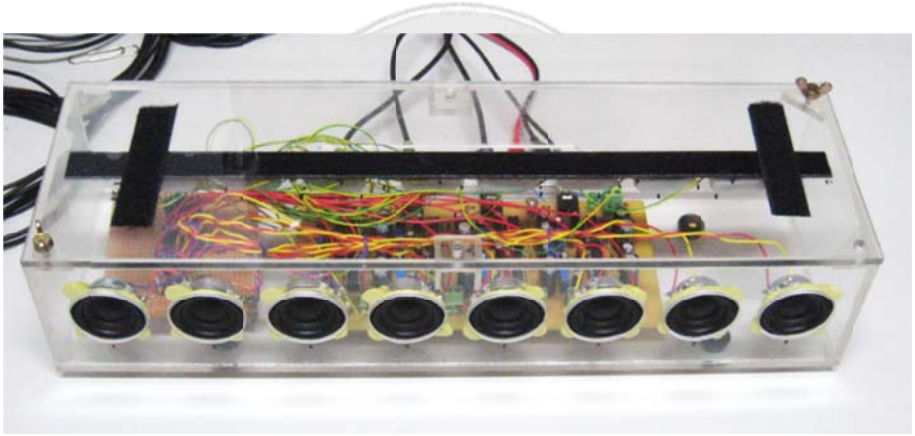

(b)

Figure 5.18 Enclosure with elements inside: (a) Back (b) Front

The DSH715 speakers are mounted in individual enclosures of 3 cm^3 (Figure 5.19 (a)). This offers the flexibility to easily dispose the speakers in different configurations. As shown in Figure 5.19 (b), different inter-element spacing configurations can be easily prepared for test.

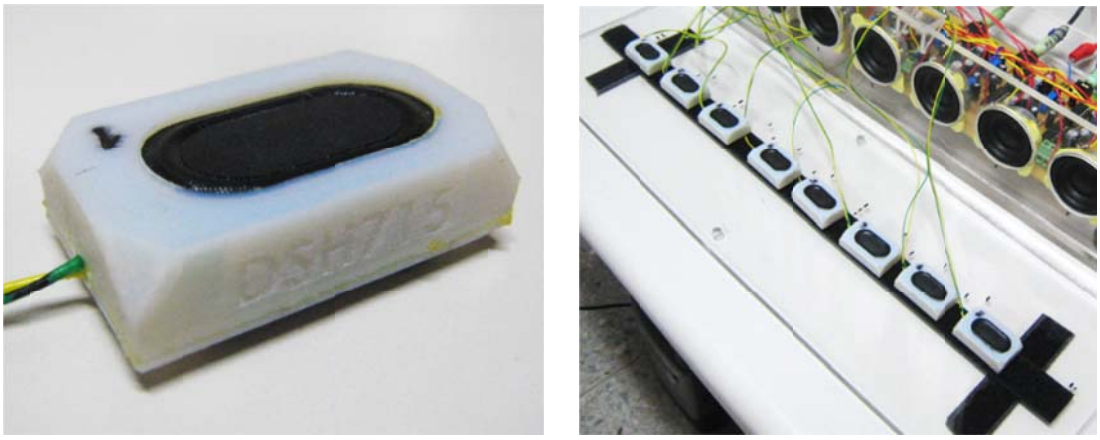

(a) (b)

Figure 5.19 DSH715 micro-speaker: (a) Mounted in individual enclosure (b) Dispose on line array

6 Measurements

This section will present the validity of the mathematical methods to simulate the directivity of line arrays. First, the measurement process will be explained in detail. Then, the directivity and frequency response of the individual speakers used in this thesis will be presented. Lastly, different line array configurations will be compared in order to check the validity of the simulations.

6.1 Measurement process

The measurement process is in accordance with the international standard IEC 60268-5-2003 [41]. The purpose is to measure the directivity and sound pressure resulting from different line array speaker configurations. The Device Under Test (DUT) composed of DSH624 is disposed on a standard baffle in free-field conditions in an anechoic chamber (Figure 6.1 (a)), which is in accordance with ISO-3745 and ISO-7779. The micro-speakers DSH715, mounted in the closed enclosures, are disposed directly on the baffle by using fabric hook-and-loop fastener (commonly known as Velcro). This method allows an easy way to measure different line array configurations (Figure 6.1 (b)). For multi-unit speaker configurations, acoustical interference is created. The measuring distance is chosen to minimize the errors caused by this phenomenon. Due to the heavy weight of the baffle and DUT, the microphone has to be moved by the turntable and the maximum reachable distance is 1.2 meter. According to Eq. (2.51), with a 35 cm length array and the distance of 1.2 m the far field conditions can be found below 6720 Hz.

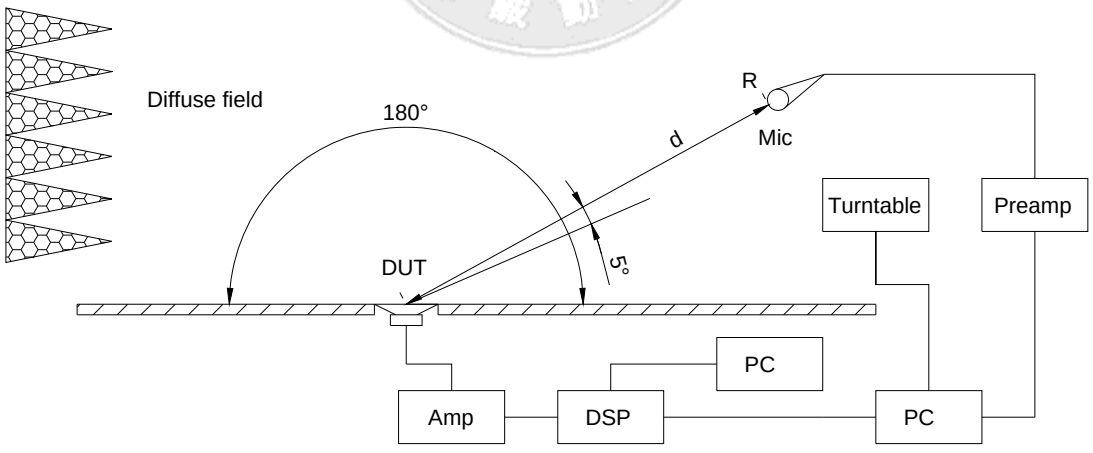

Figure 6.1 Block diagram of the set-up

According to the block diagram presented in Figure 6.1, the DUT is connected to the output of the computer sound card thought the DSP and the 8-channel amplifier. After the calibration, a chirp signal from 100 Hz to 20 kHz is reproduced. The pressure level at the recording point (R) is captured by the microphone Brüel & Kjær (B&K) 4191 and sent back to the computer thought

the pre-amplifier B&K 716. The frequency response is stored by the software Sound Check and the signal is sent to the turntable controller B&K 5997 to turn 5 degrees.

For the representation of the measurement results, the standard indicates that the sound pressure level shall be shown as a family of polar response curves at different frequencies or as a family of frequency response curves at various angles. In this thesis work, for convenience, the pressure level is represented as a function of frequency and angle. This method provides an easier recognition of the directivity and frequency response at the same time.

When the frequency response at all the angles has been measured, Sound Check allows exporting to spreadsheet files. Then, the information is imported into MatLab and the directivity function can be represented. The angular resolution of the measurement is 5 degrees; for the 180 degrees covered there are 37 measurements. The frequency has 83 values, logarithmically increased from 100 Hz to 20 kHz. In other words, a matrix of size 37 x 83 is stored during each measurement. To improve the visualization new values are interpolated between the original values. The angular resolution is increased to 0.1 degrees and the frequency to 500 values. In Figure 6.2 the process of interpolation is represented. The resulting matrix is composed of 500 x 1801 elements, with enough resolution to provide an optimum visualization.

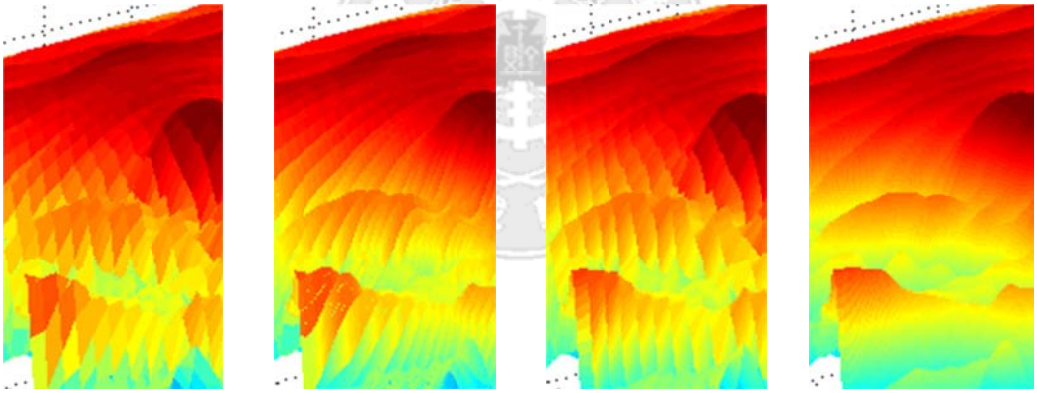

(a) (b) (c) (d)

Figure 6.2 Interpolation: (a) No applied (b) Angular 0.1° (c) Frequency 500 values (d) Angular and frequency

The errors introduced by the measurement cause gaps in the representation. To improve the visualization, it is possible to smooth the surface of the figures. This makes the recognition easier in 3D but the information with low varying amplitude can be lost if the smoothness is too high. In Figure 6.3 (b) and (e) the improvement of the visualization by smoothing the surface is illustrated. Lastly, Figure 6.3 (c) and (f) shows how the side-lobes information can be lost if an excessive smoothing is applied.

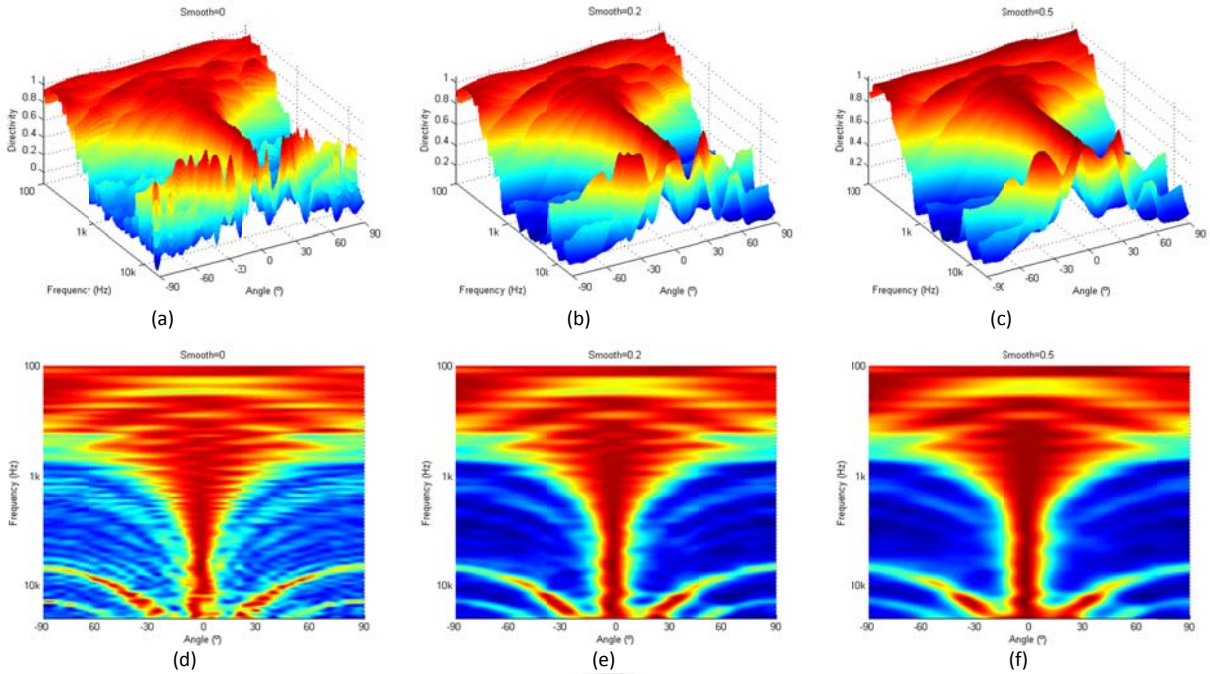

Figure 6.3 Smoothing: (a),(b) and (c) 3D views; (d), (e) and (f) top views

Unless otherwise indicated, all the directivity functions are represented with angular resolution of 0.1°, frequency resolution of 500 values and smoothing of 0.1. The sound pressure level in decibels is scaled between -40 dB and 0 dB, and the directivity normalized at each frequency between 0 and 1.

Figure 6.4 present different pictures of the measurement process. Figure 6.4 (a) shows the front of the baffle where it is also possible to observe the microphone mounted on the turntable. A configuration with 8 DSH715 speakers is displayed in Figure 6.4 (b). Figure 6.4 (c) shows the back of the baffle, where the amplifier and DSP are positioned. Lastly, the measurement of a single speaker is shown in Figure 6.4 (d).

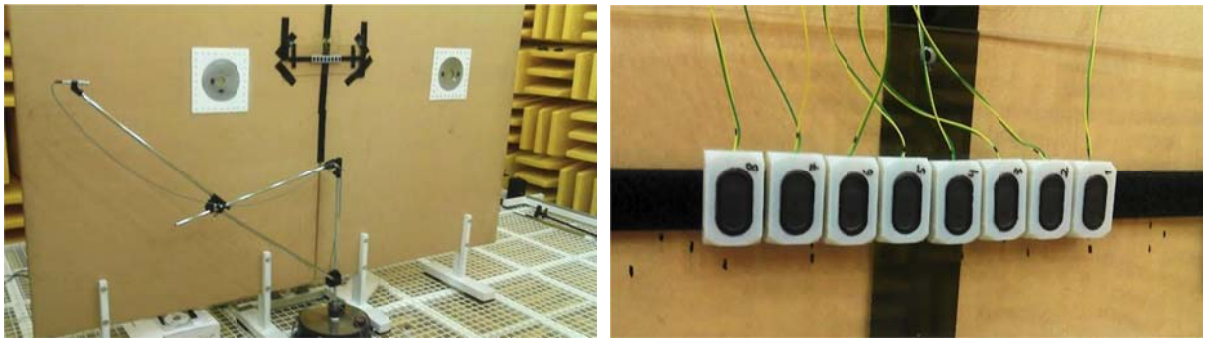

(a) (b)

(c) (d)

Figure 6.4 Images of the measurement process: (a) Front of baffle (b) Line array configuration (c) Back of the baffle (d) Single speaker measurement

6.2 Speaker measurements

Before obtaining the directivity of line arrays, the single speaker measurements are considered. The speaker directivity is measured on a baffle as previously explained. After applying angle and frequency interpolation, Figure 6.5 (a) represents the frequency response of the HPS503 speaker at 90°, 45° and 0°. It is observed that the frequency higher than 3 kHz is attenuated as the angle increases, in other words, the higher amplitude at high frequency is found on-axis at 0 degrees. In Figure 6.5 (b) the Sound Pressure Level (Ref. 20 µPa) is represented on a polar pattern. In this case also it is possible to observe the speaker behaves omnidirectional at low frequency and as the frequency increases it becomes more directional on-axis.

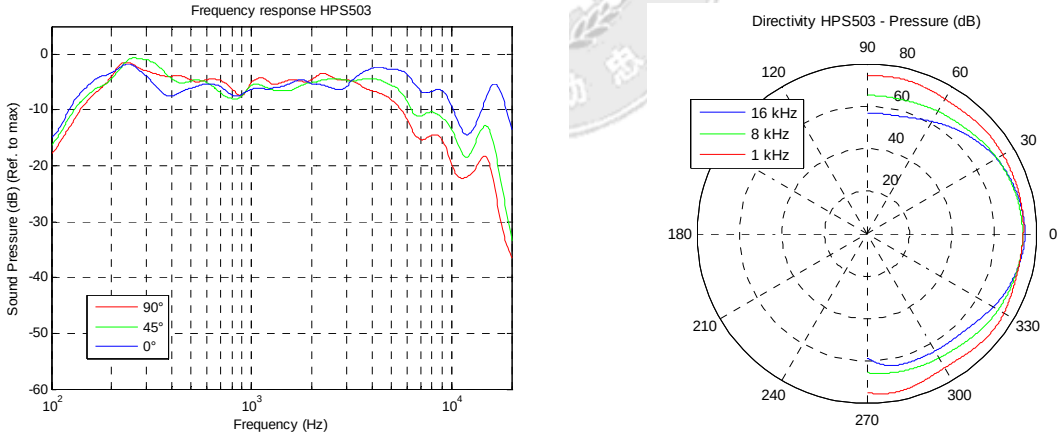

Figure 6.5 HPS503 directivity: (a) Frequency response (b) Polar pattern

To provide a more convenience recognition of the directivity in all the frequency and the angle range, the pressure level is represented as a function of frequency and angle. In this case, for the speaker directivity representation, the measured pressure level in decibels is normalized to its maximum. Next, Figure 6.6 presents the different speakers directivity functions. It is observed that if the size of the diaphragm decreases, the directivity at high frequency also decreases, and the source behaves as a omnidirectional source. The micro-speaker directivity is

measured in the vertical and horizontal positions (Figure 6.6 (d) and (e)). Note the f_0 is found at 800 Hz and its omnidirectional behavior at high frequency. The other speakers present the f_0 at 200 Hz and a directional behavior at high frequency.

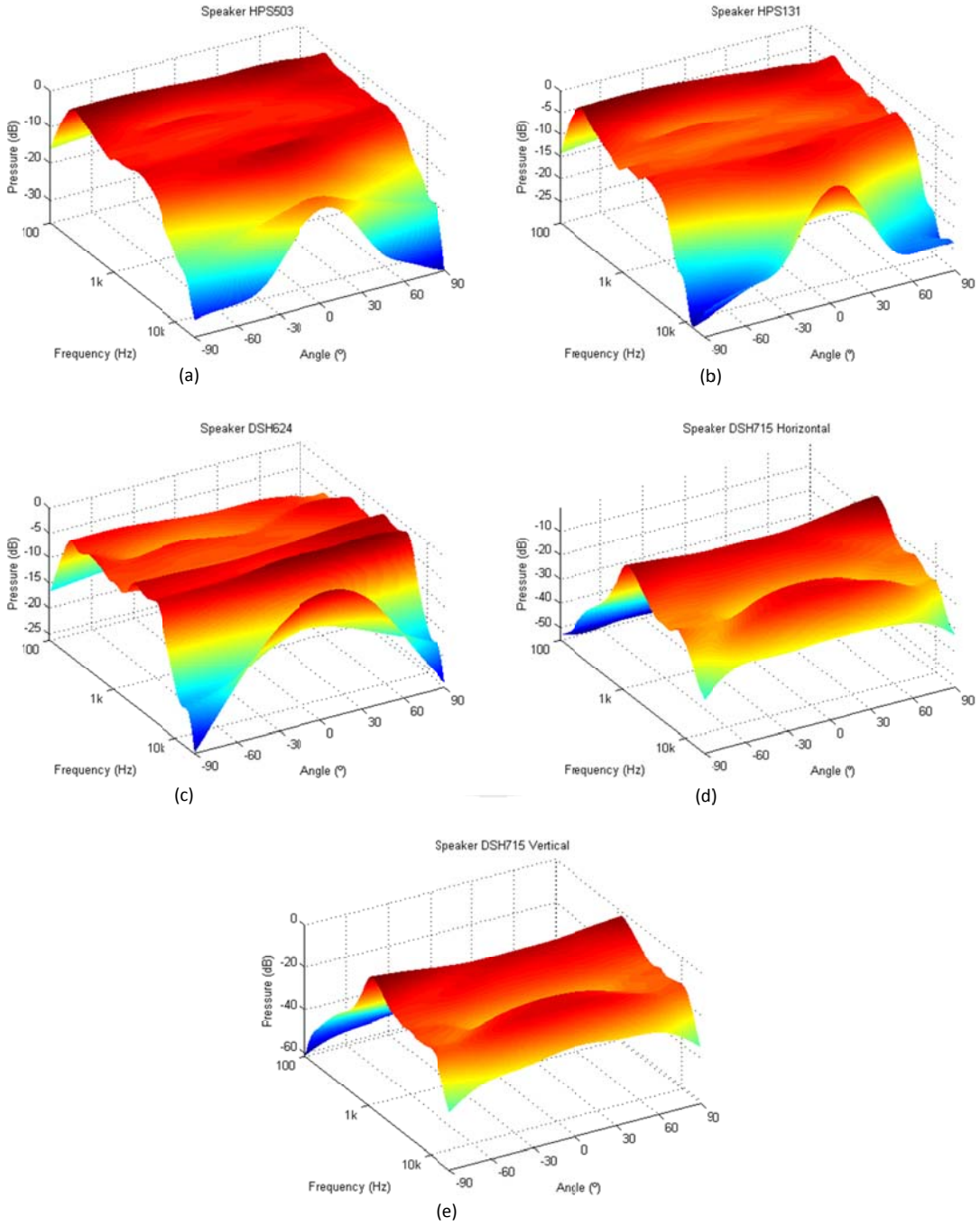

Figure 6.6 Speaker directivity: (a) HPS503 (b) HPS131 (c) DSH624 (d) DSH715 Horizontal (e) DSH715 Vertical

The directivity functions of the speakers above presented are imported as a matrix in the GUI in order to simulate directional source arrays. Also the directivity of a real speaker of diameter *D* can be approximate to a uniform line array of length *a*. The speaker, as the uniform array, behaves omnidirectional at low frequency and becomes more directional as the frequency increases. For the HSP503, HPS131 and DSH624 speaker units the relation *D/a* can be obtained by comparing the simulated and measured results. The HSP503, HPS131 can be simplified as a uniform line array of a=1.5 cm, and the DSH624 as a=1.2 cm. For an overall simplification the *D/a* relation for all these speakers is 2.5. Even though the shape of the diaphragm affects the directivity pattern, in this case, the speaker are similar enough to accept a simplification. To minimize the error, the comparison is realized on an 8 elements line array. Figure 6.7 illustrates the different values of *a* and the line array formed by the HPS503.

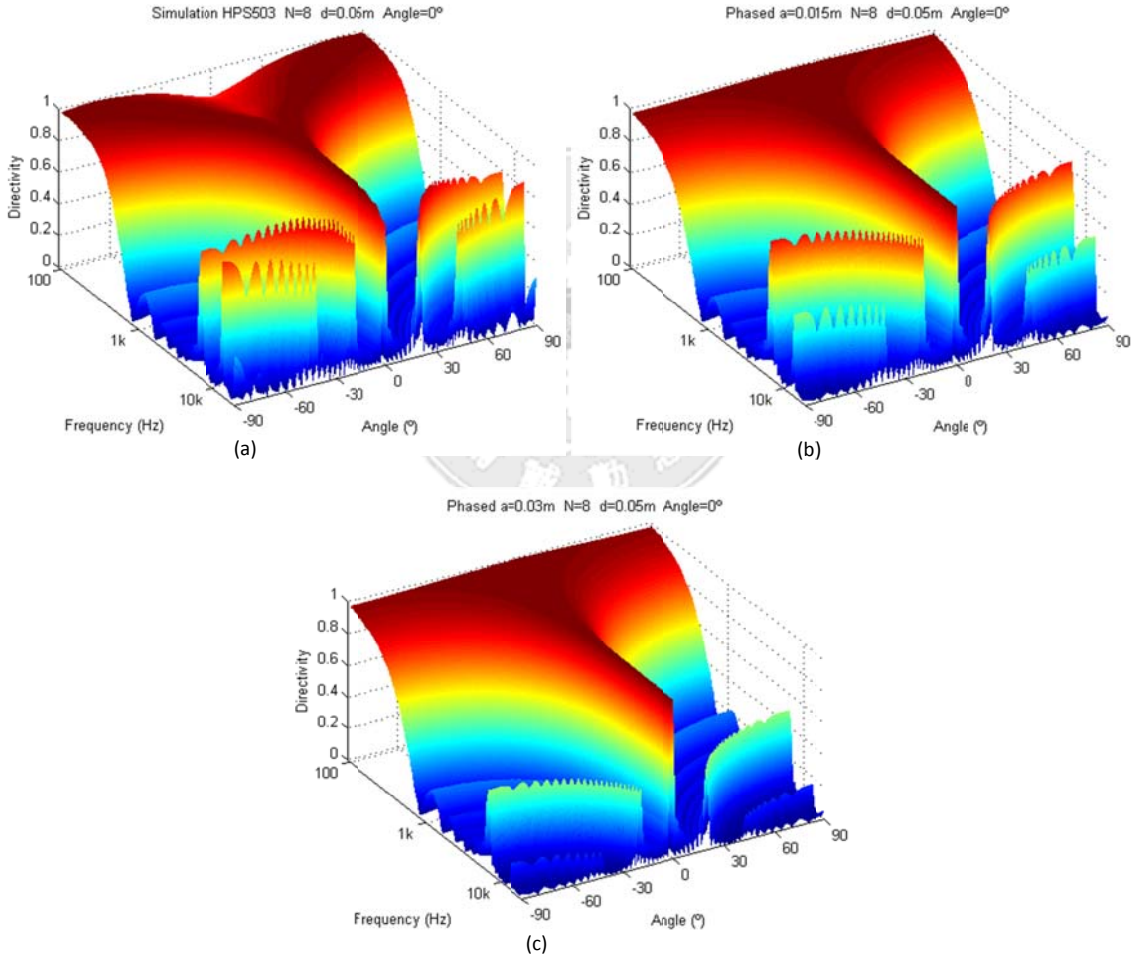

Figure 6.7 (a) HPS503 8 elements line array (b) Phased array a=1.5 cm (c) Phased array a=3 cm

6.3 Measurement results

Different configuration of line arrays and properties of beam forming are measured and presented in order to compare with the simulated results. The GUI and the functions provide a

theoretical result to be compared with the real measurement. This study begins with a detailed comparison of the line array formed by eight DSH624 speakers in the methacrylate enclosure. Then, other configurations with different number of elements and inter-element spacing will be presented. Also, the DSH715 in the individual enclosure will provide other array configurations. Lastly, multiple steered beams, amplitude shading and crosstalk cancellation will be presented.

6.3.1 Eight-element line array

The first measurement presented is a single beam steered at 0 degrees on the 8-elements DSH624 line array. The inter-element spacing given by the enclosure is 5 cm with no delay or filter is applied to any speaker. The directivity function obtained from the measurement is plotted in Figure 6.8 (a) and it can be compared with the simulated phased array on Figure 6.8 (b). For each frequency the directivity function is calculated by normalizing to 1, this provides a good method to observe the apparition of the grating lobes.

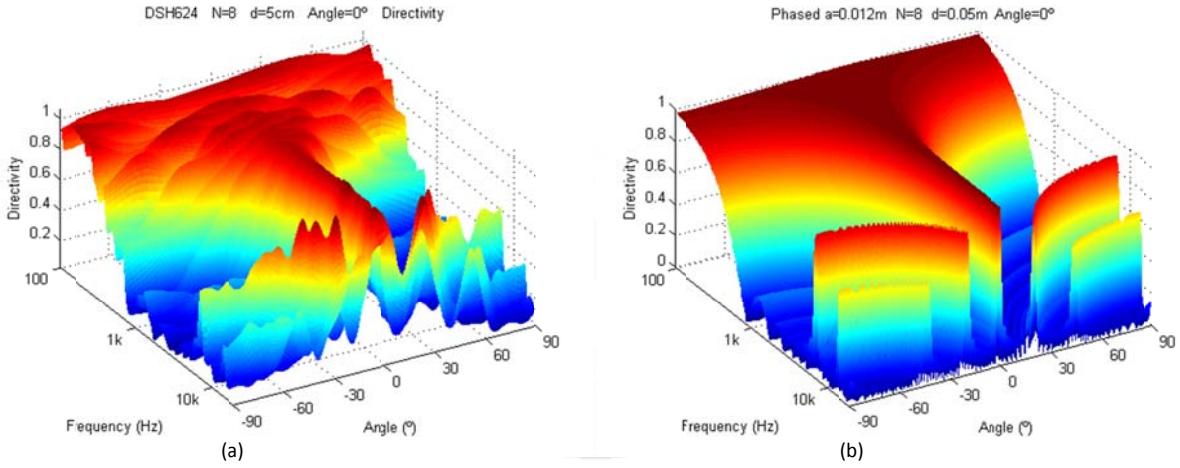

Figure 6.8 Directivity 3D representations: (a) Measured (b) Phased array simulation

Because the measured directivity function presents too many abrupt changes, the comparison can be difficult. For an easier recognition, the point of the observation is moved to the top of the figure. Next, Figure 6.9 (a) represents the top view representation of the Figure 6.8 (a), and it can be compared with the directivity simulation of a directional sources line array shown in Figure 6.9 (b). It is observed that the apparition of side and grating lobes coincide.

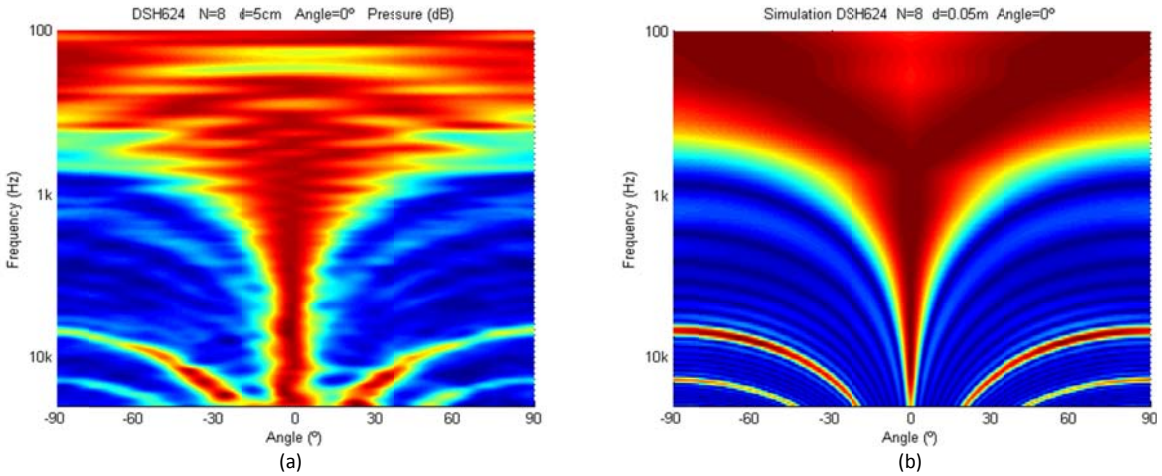

Figure 6.9 Directivity top-view representation: (a) Measured (b) Phased array simulation

If the information about the pressure distribution is needed, the frequency response of the speaker has to be considered. The measured directivity result is presented in Figure 6.10 (a) on a decibel scale (from -40 to 0 dB). By comparing with the simulation shown in Figure 6.10 (b) it can be observed that the maximum pressure is present on-axis once the f_0 of the speaker is reached.

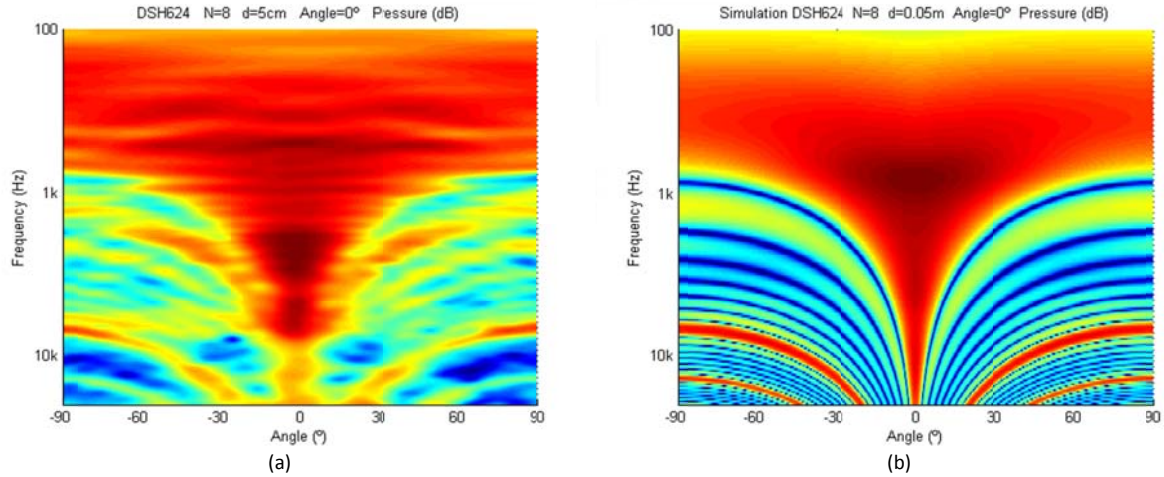

Figure 6.10 Directivity top-view representations: (a) Measured (b) Phased array simulation

6.3.1.1 Steering angle

The steered angle can be calculated as a function of the inter-element spacing and the sample frequency of the DSP by using Eq. (3.3). Because the DSP only allows whole delay values, for 4, 7 and 10 samples; the delay are obtained as 16.5, 29.7 and 45.1 degrees, respectively. The different directivities are shown in Figure 6.11. Measured results are represented on the left side, and in order to compare with the theory, the simulation results can be found on the right side. To obtain a better representation to identify the apparition of the grating lobes and main lobe width the directivity is represented normalized at each frequency. The drawback of this normalization is that the frequency response of the sources is considered perfectly flat in all the

range and the pressure information is lost. By comparing measured and simulated results, it is found that the predictions are correct and the grating lobes and lobe width coincide.

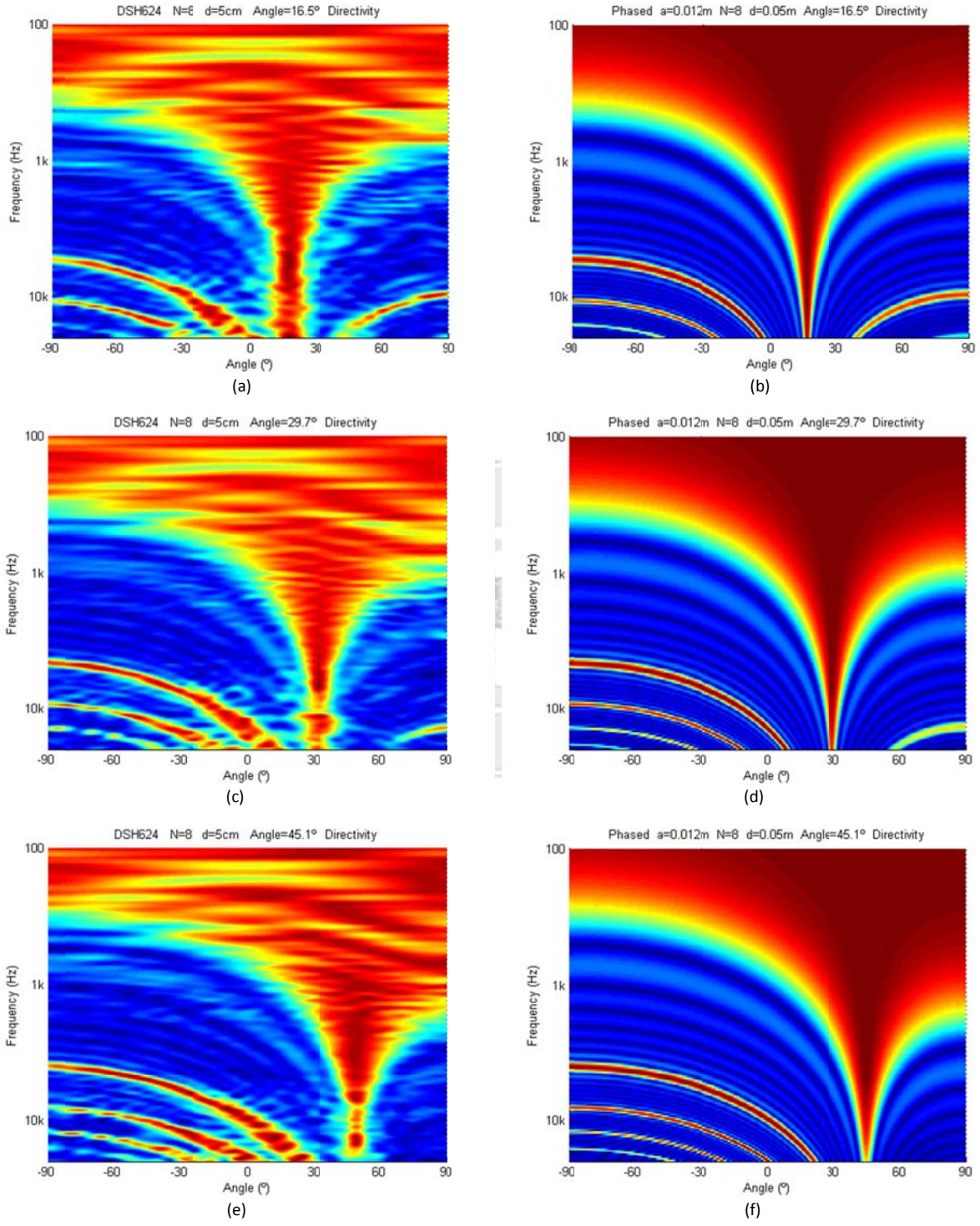

Figure 6.11 DSH624 8-element array: (a) 16.5° (c) 29.7° (e) 45.1°. 8-element array simulation: (b) 16.5° (d) 29.7° (f) 45.1°

6.3.1.2 Micro-speaker array

In order to test the same configuration with micro-speakers, the DSH715 units are disposed with equal inter-element spacing (5 cm). These micro-speakers are not able to reproduce low frequency, then, it may be interesting to plot the directivity as a function of pressure in order to observe the frequency limitations. Figure 6.12 (a) shows the measured directivity function for a steered angle of 0°. It is observed, as predicted by the simulation result shown in Figure 6.12 (b). It is found that the maximum pressure is present on axis and above the f_0 of the micro-speaker.

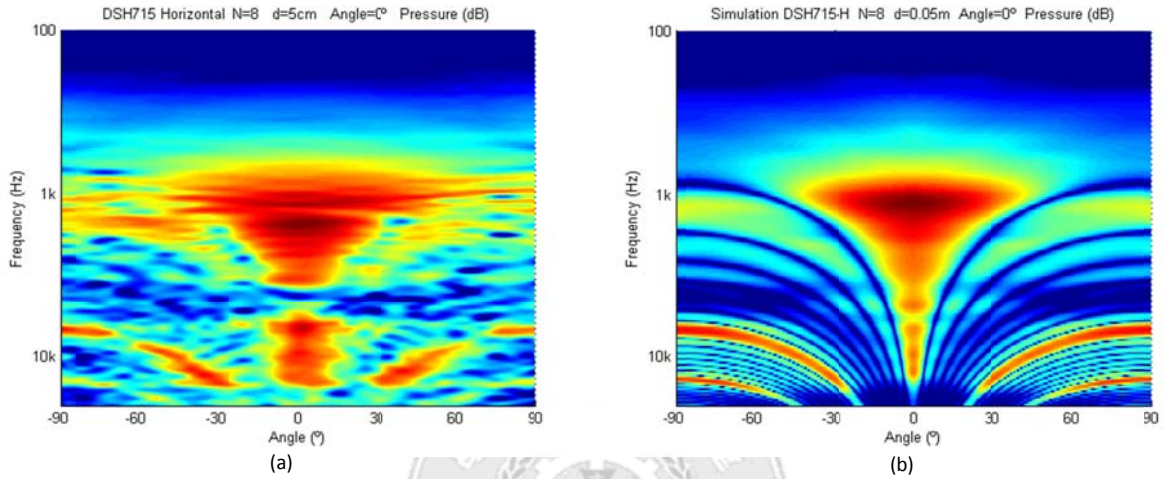

Figure 6.12 DSH715 8-element array pressure level representation: (a) Measured (b) Simulated

The representation of the pressure normalized at each frequency offers a better representation to find the frequency working range. The measurement shown in Figure 6.13 represents a beam steered at -16.5° and its simulation using the DSH715 directivity function.

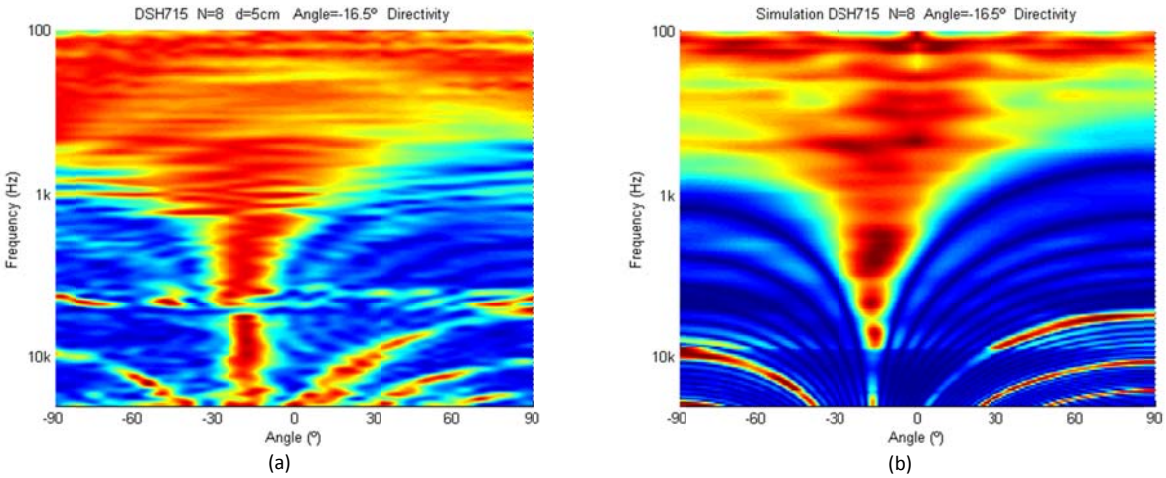

Figure 6.13 DSH715 8-element array normalized pressure representation: (a) Measured (b) Simulated

6.3.1.3 Size element

In order to compare the size of the element, the effect on the grating lobes amplitude, the directivity of the horizontal and vertical DSH715 speaker positions (effective size 1.1 cm and 0.6 cm) are presented in Figure 6.14 (a) and (b). In this case, the relation of *d* and *a* is small enough, so the difference is not easily appreciated. The effect is more notorious by comparing with the DSH624 speaker (effective size 1.2 cm), as shown in Figure 6.14 (c).

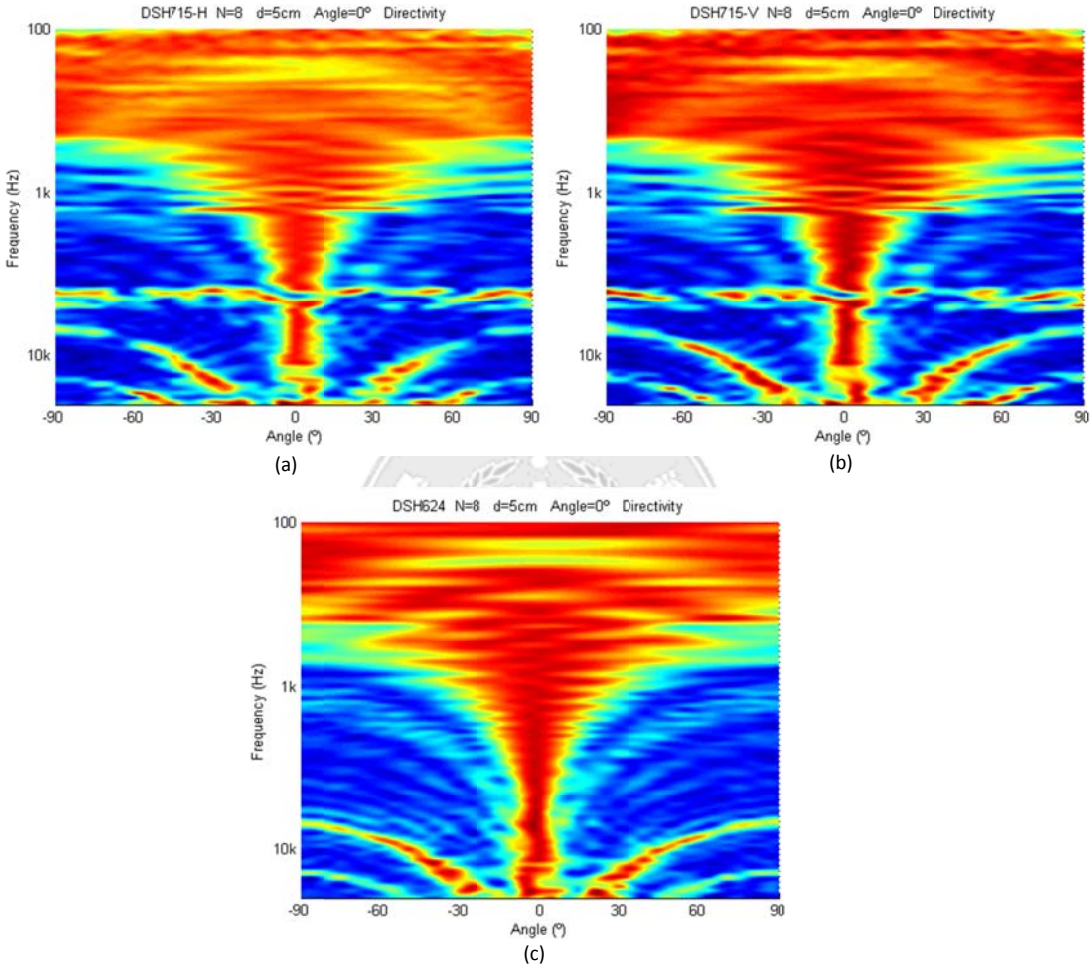

Figure 6.14 Eight-element array: (a) DSH715 Horizontal (b) DSH715 Vertical (c) DSH624

6.3.1.4 Inter-spacing distance

Due to the versatility of the DSH715 enclosure, the directivity with different values of inter-element spacing can be easily measured. The inter-spacing distances analyzed are 5, 4, 3 and 2 cm. The speakers are disposed in horizontal position except for d=2 cm that are disposed in vertical. Figure 6.7 shows the top-view of the directivity measured for the four distances. It is observed, as predicted by the theory, the grating lobes appear at higher frequency as the inter-spacing distance decreases. By plotting the pressure, it can be observed when the distance decreases, the low frequency amplitude is increased and the beam becomes less directive. This

experiment can demonstrate that the ideal line array, in order to avoid the grating lobes, is composed of sources positioned as close as possible. But to keep the low frequency directivity, the array length has to be long and this would require a number of elements too high. This problem can be mitigated by using nested arrays.

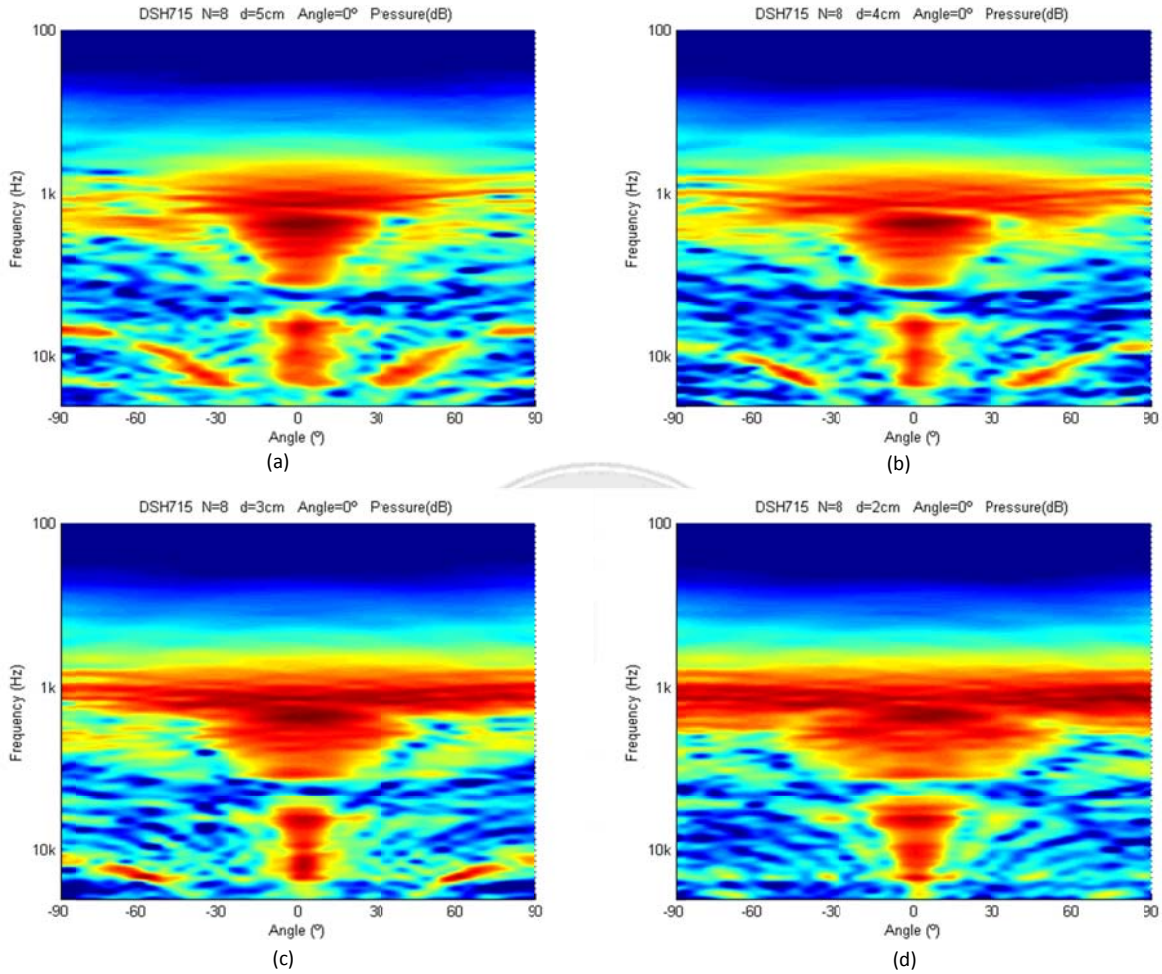

Figure 6.15 Eight-element DSH715 array: (a) d=5 cm (c) d=4 cm (b) d=3 cm (d) d=2 cm

6.3.2 Four-element line array

For the 4-element line array experiment, the speakers DSH624 are considered. Compared with the same length 8-elements line array, the grating lobes appear at lower frequency due to the increment of the inter-element distance d. The inter-element distance in the measurement set-up is 10 cm with the beam steered at 0 and 45 degrees.

Figure 6.16 (a) and (b) shows the directivity function of the measured and simulated 0° steered angle respectively. Directivity is normalized at each frequency in order to observe the apparition of the grating lobes. The directivity of the steering angle set to 45°, measured and simulated, is represented in Figure 6.16 (a) and (b), respectively.

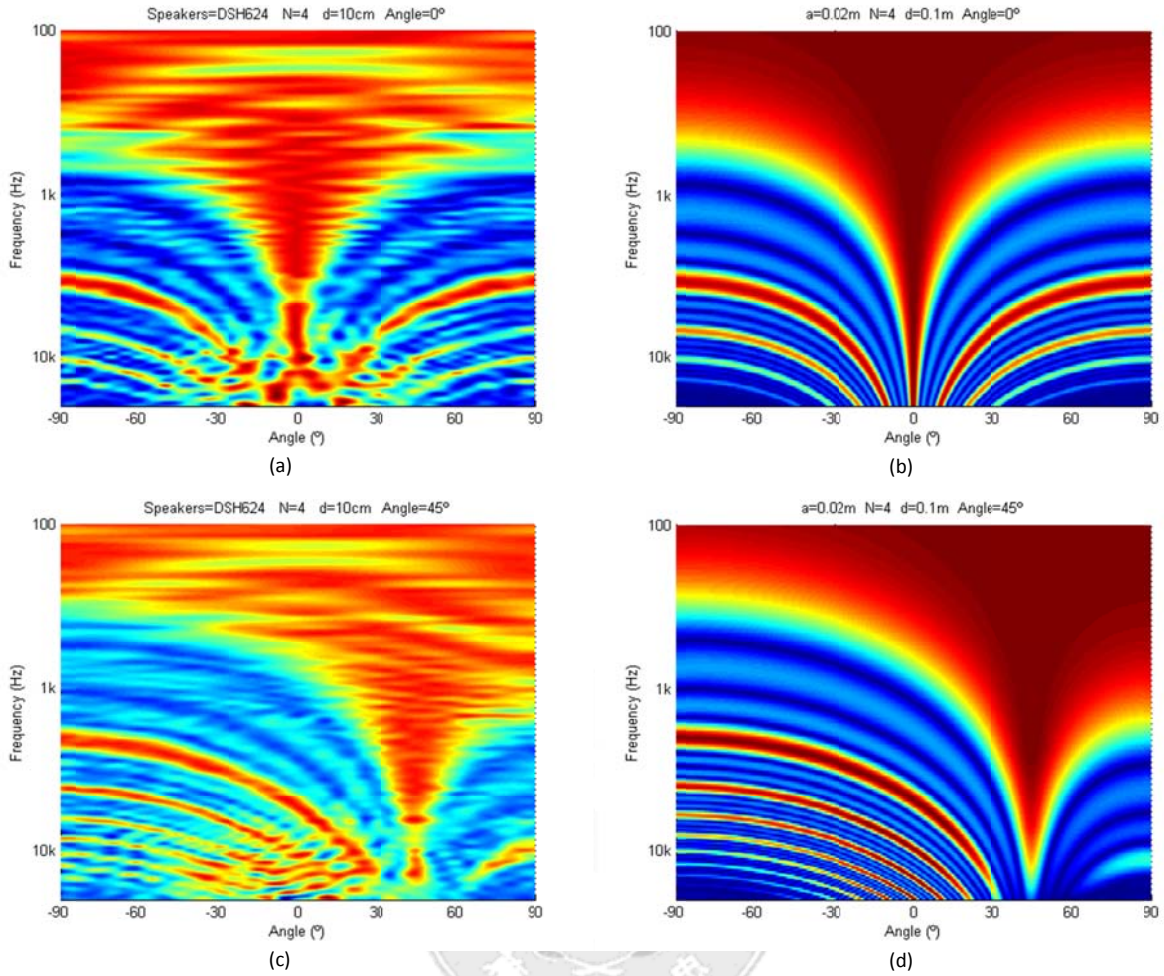

Figure 6.16 Four-element array. Measured: (a) Angle 0° (c) Angle 45°. Simulated: (b) Angle 0° (d) Angle 45°

6.3.3 Two-element line array

Most of the audio systems are composed of two sources separated by a distance d, this provides stereophonic audio reproduction. If the sources are correlated, due to the phenomenon of wave interference the frequency response at the listener point changes as it moves, generating a comb filter. Like in a line array, the interference pattern is given by the inter-element distance and the frequency. It is noted that, in a domestic environment, the system is not in a diffuse field and the reverberation mixes the signals, then, the effect will be attenuated.

This interference is also present in an enclosure with two speakers. The low frequency is increased 6 dB meanwhile the interference is generated in high frequency. This effect is produced on the axis where the speakers are disposed, and because of the listener uses to move in the horizontal plane, the speakers are usually stacked horizontally.

Next, in Figure 6.17 different inter-element distances are presented for a 2-element array. The top-view representation shows that the acoustic pressure normalized from -50 to 0 dB. Noting that the low frequency is increased as the speakers become closer.

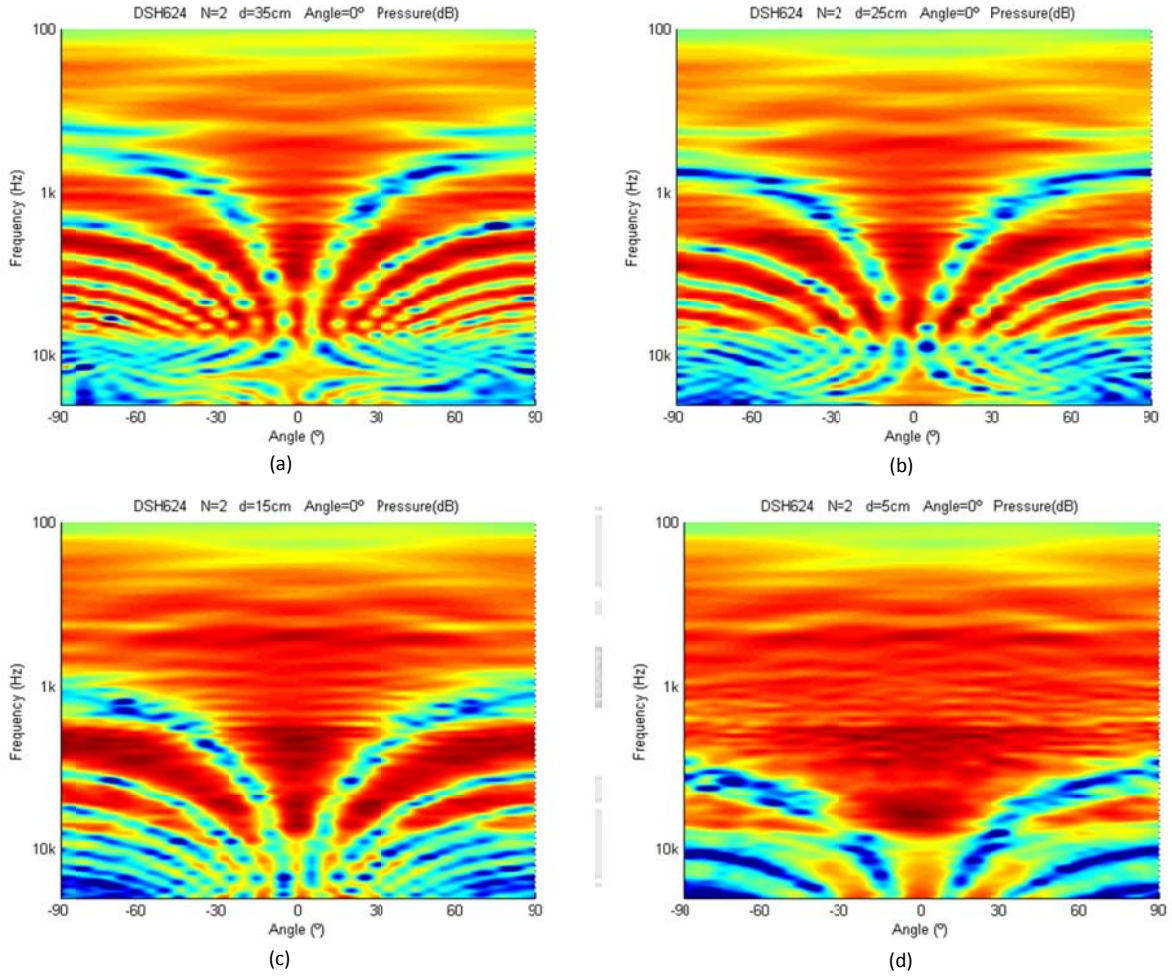

Figure 6.17 Two-element line array: (a) d=35 cm (b) d=25 cm (c) d=15 cm (d) d=5 cm

6.3.4 Amplitude shading

By adjusting the amplitude of each speaker, it is possible to attenuate the side lobes of the directivity function. In order to compare with the simulation, the DSP is programmed with the two amplitude sets presented in Table 6.1. Both sets contain discrete values of triangular functions that avoid zero values on the side elements.

Table 6.1 Tapering amplitude values

Element	1	2	3	4	5	6	7	8
No tapering	1	1	1	1	1	1	1	1
Tapering 1	0.625	0.75	0.875	1	1	0.875	0.75	0.625

Tapering 2	0.25	0.5	0.75	1	1	0.75	0.5	0.25

The proposed configurations are measured by a line array composed of 8 DSH624 speakers separated 5 cm. Figure 6.18 (a), (b) and (c) shows close views of the 3 measured results. The directivity function is normalized at each frequency to improve the visualization of the side lobes. As observed in the simulated results presented in Figure 6.18 (d), (e), and (f), the measured results are coherent and coincide with the estimation. As predicted by the simulation, attenuation of the side lobes and increment of the main lobe width are obtained as the slope of the triangle function decreases.

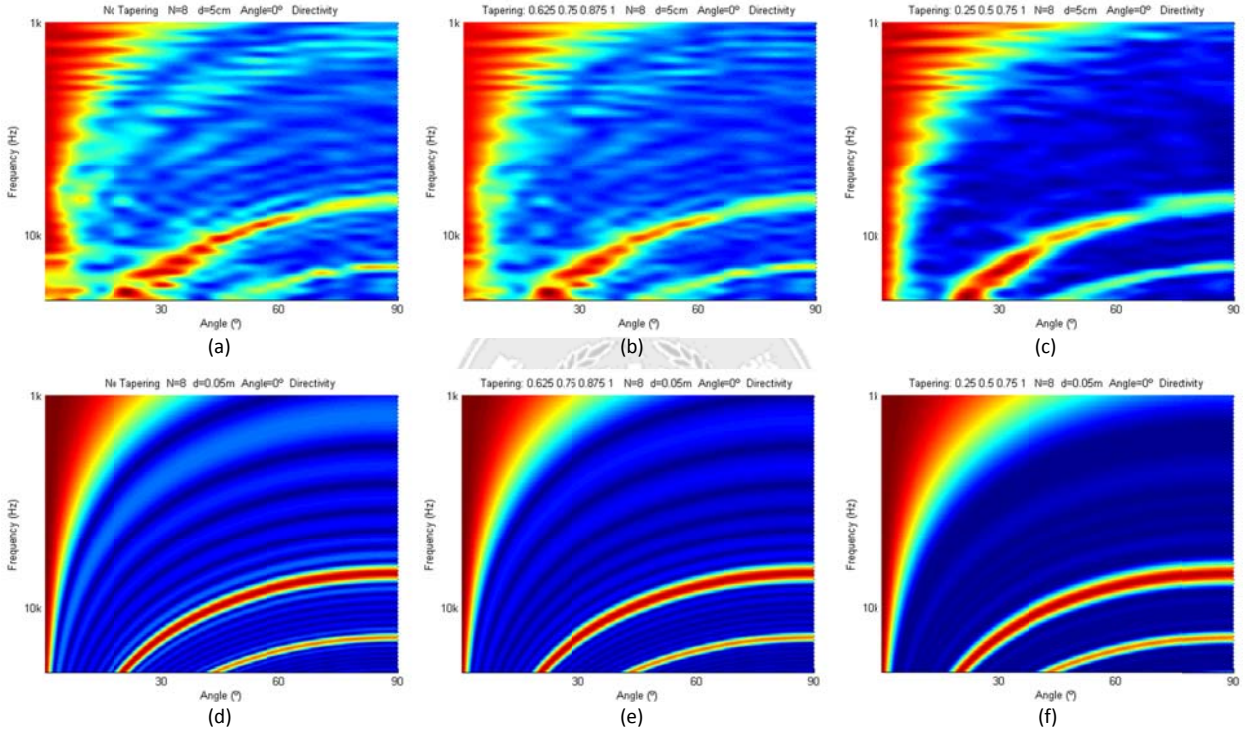

Figure 6.18 Amplitude shading. Measured: (a), (b) and (c) Simulated: (d), (e) and (f)

6.3.5 Nested array

Due to the versatility offered by the DSH715 micro-speaker, the directivity of a nested array configuration can be measured. The proposed array is formed by 2 sub-arrays, as shown in Figure 6.19. The low frequency sub-array is composed of 6 elements spaced 6 cm and the high frequency sub-array by 4 elements spaced 2 cm.

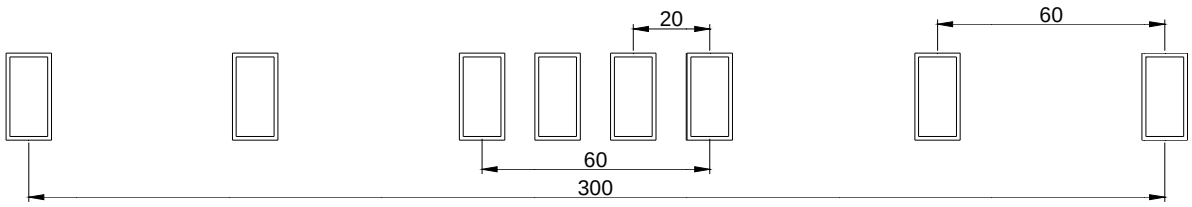

Figure 6.19 Filtered emitted signal (a) High-frequency sub-array (b) Low-frequency sub-array

The frequency limitations of each sub-array are shown in Table 6.2. In this design the steered angle is set at 0 degrees, for wider angles grating lobes would appear between frequency bands.

Table 6.2 Nested array: frequency limitations at 0 degrees

	N	d (m)	F_{max} (Hz)	F_{min} (Hz)
LF Sub-array	6	0.6	4764	953
HF Sub-array	4	0.2	12863	4288

To separate the signal a high pass filter is needed for the high sub-array and low pass filter for the low-sub-array. Both Infinite Impulse Response (IIR) filters are second order Linkwitz Riley type and the cut-off frequency is situated at 4.5 kHz. The second order filter further attenuates the cut-off 12 dB per octave, that is, the two signals are mixed gradually around 4.5 kHz. Figure 6.20 shows the filtered signal emitted by the high and low frequency sub-arrays.

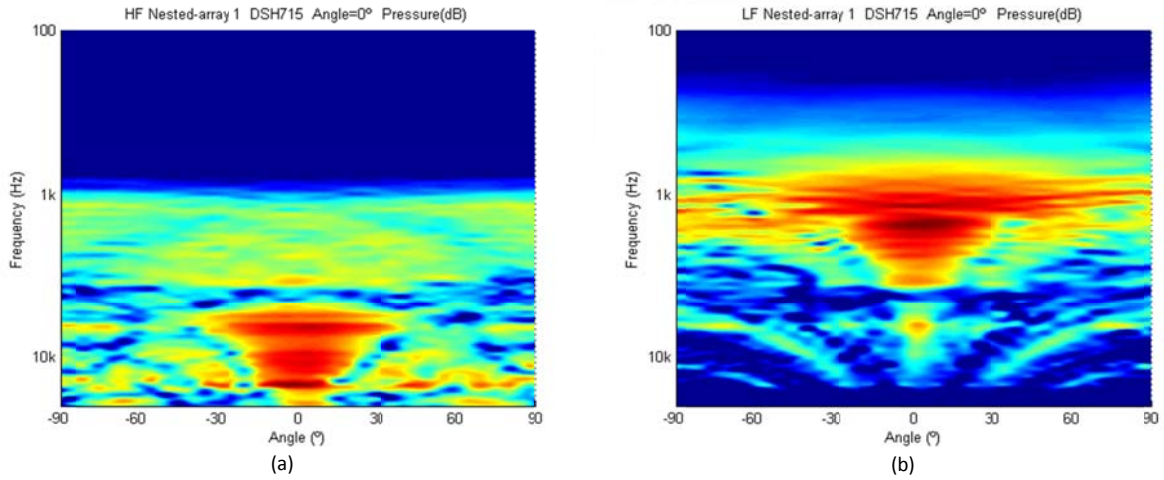

Figure 6.20 Filtered emitted signal (a) High-frequency sub-array (b) Low-frequency sub-array

The directivity function of the nested array is shown in Figure 6.21 (a) and it can be compared with the simulated directivity function in Figure 6.21 (b). Noting that the measured result uses second order filters and the simulated ideal filters to separate the signal of each sub-array. It is observed that no grating lobes are formed as predicted by the theoretical design.

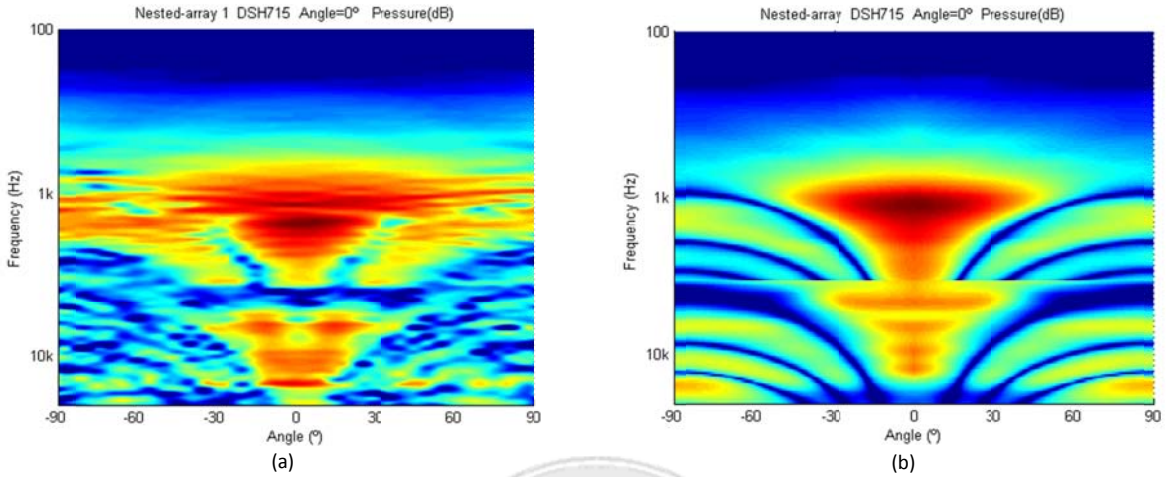

Figure 6.21 Nested-array: (a) Measured (b) Simulated

6.3.6 Multiple beam

By using the algorithm presented in subsection 3.2, it is possible to generate several beams in the same line array. This experiment is measured for 2 different 8-elements line array with 5 cm as inter-element spacing, one composed of the DSH624 speaker and other by the DSH715. The steering angles are set at ±16.5° (4 samples delay) and ±29.7° (7 samples delay) and the two signals emitted have same amplitude and phase. In order to obtain an easier recognition of the 2 beams, the directivity function is normalized. It is observed that at low frequency, the source behaves omnidirectional and the resulting signal has an omnidirectional pattern then the pressure is the sum of each individual signal. As the frequency increases the two beams become more directive and independent.

Figure 6.22 (a) and (b) shows the directivity function generated by the DSH624 speakers at 16.5° and 37°, respectively; and Figure 6.22 (c) and (d) the generated with the DSH715 speakers at the same angles. It is observed that the directivity of both configurations coincides.

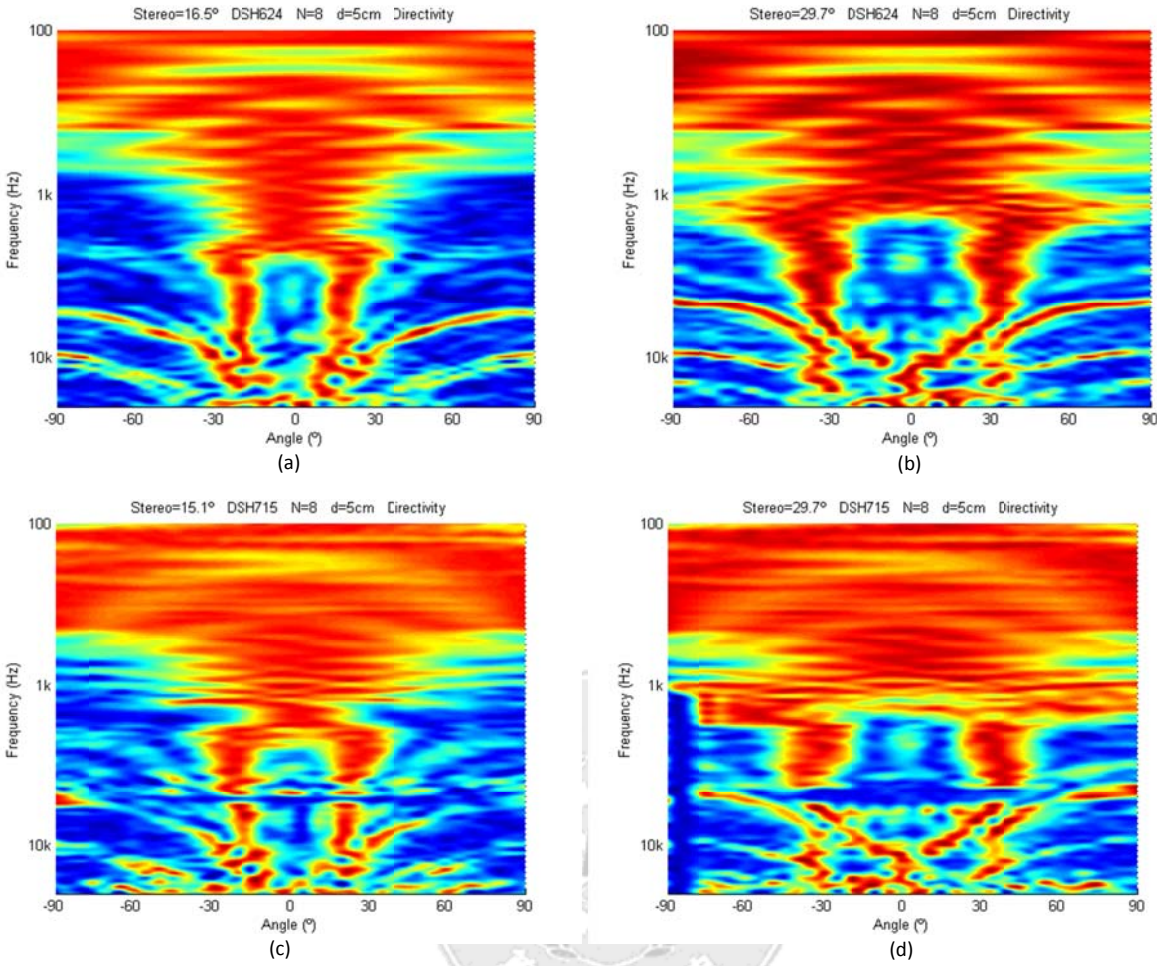

Figure 6.22 Stereo line array. DSH624: (a) 16.5° (b) 29.7°. DSH715: (c) 16.5° (d) 29.7°

6.3.7 Crosstalk cancellation

If one of the beams of a stereo line array is inverted, destructive interferences can be created. A minimum of pressure can be obtained by emitting the signal originally present in one angle with opposite phase. Since the frequency response of any angle in a line array can be calculated, it is theoretically possible to eliminate the signal at that angle. This technique, as presented in section 3.4, is known as crosstalk cancelation. In this measurement no frequency filters are applied to the signals, only steering angle and amplitude are considered. The line array is composed of 8 DSH624 speakers spaced at 5 cm. Figure 6.23 (a) shows the measured directivity (Pressure) of a stereo line array, the angle at -10° is emitted at half pressure that the one emitted at 10°. As predicted by the simulated result (Figure 6.23 (b)), the low frequency response at 10° is attenuated and the medium frequency at -10° is increased.

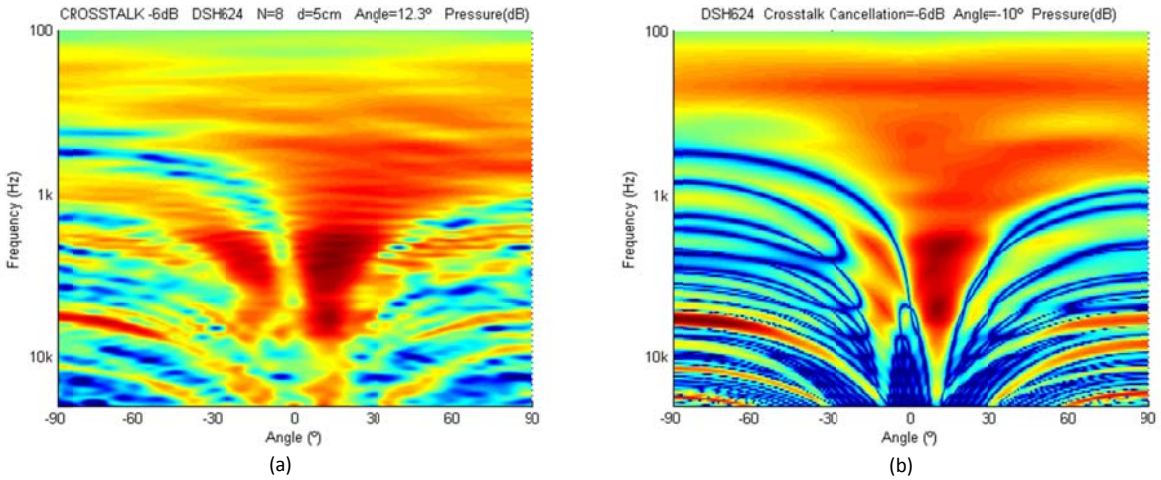

Figure 6.23 DSH624 Stereo line array directivity: (a) Measured (b) Simulated

By plotting the normalized directivity, the interference effect is easily appreciated. Figure 6.24 (a) (b) and (c) represent the directivity for -3, -6, and -9 dB respectively. Nothing that the cancellation is more severe as the amplitude of the phase-inverted beam increases.

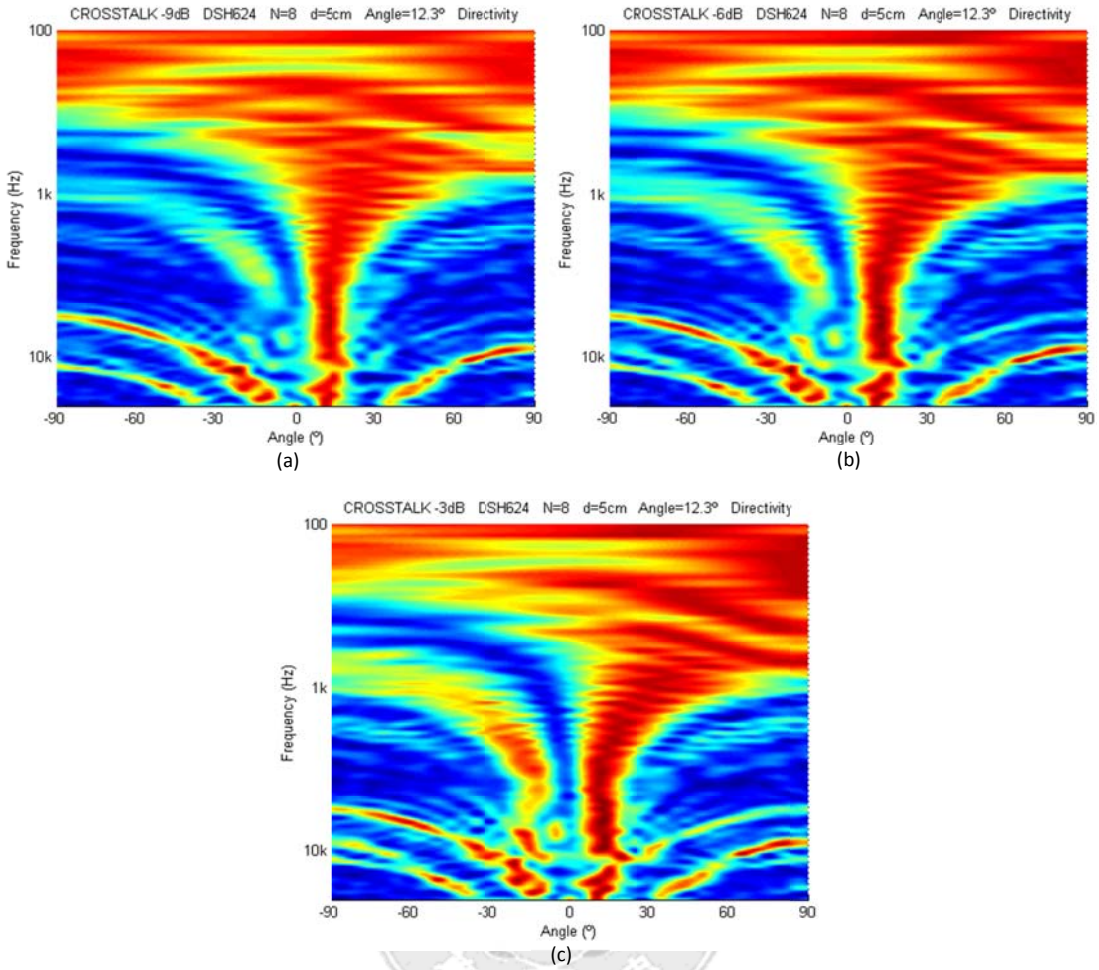

Figure 6.24 DSH624 Stereo array 10°: (a) -3dB (b) -6dB (c) -9dB

Lastly, the experiment is repeated for -30 and 30° angles. The directivity function for -3, -6, and -9 dB is shown in Figure 6.25. By representing the directivity as a function of pressure, it is observed a high attenuation in the low frequency as the inverted beam increases its amplitude.

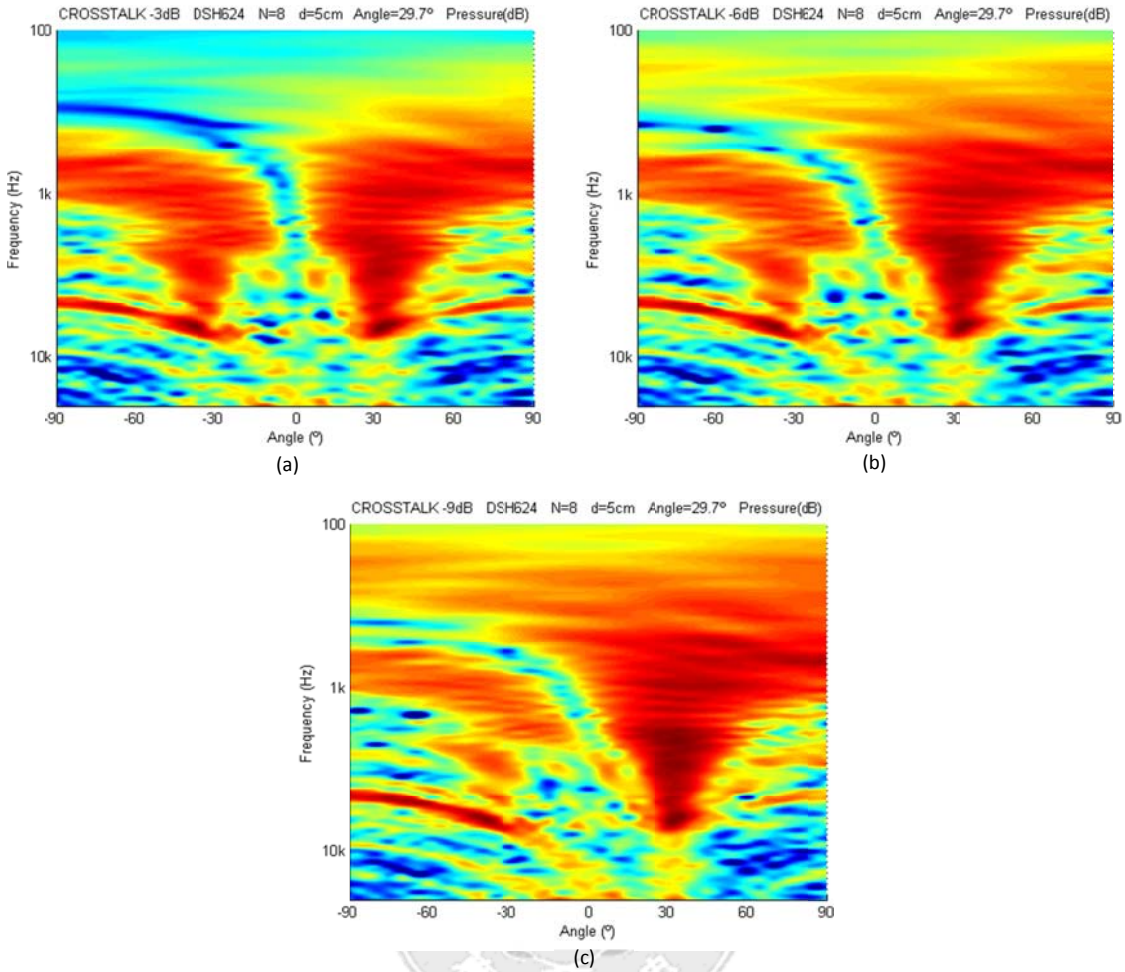

Figure 6.25 DSH624 Stereo array 30°: (a) -3dB (b) -6dB (c) -9dB

7 Conclusions

The thesis presented a wide overview of a beamforming and 3D audio. Focused in line arrays composed of small speakers, a validation of the theory has been offered by comparing simulations with measurements. In addition, applications and algorithms were proposed in order to obtain transaural audio reproduction. This chapter provides the reader an overall summary of the thesis results, contributions, and lines for the future work.

Chapter 2 offered a wide study about the beamforming phenomenon. It was concluded that to design beamformers, it is important to obtain the directivity function and the working frequency range. The information related with the DI and -6 dB angle can provide useful information for the design. Besides, it was also concluded that the directional sources array can be approximated to a phased array. The amplitude of the grating lobes can be adjusted by varying the element source size. This allows accurate predictions without previously measuring the directivity of the sources.

As concluded in Chapter 3, the most important issue in transaural audio reproduction is the crosstalk cancellation. The accuracy of the canceller related to HRTF depends on the functions and the listener. However, the crosstalk cancellation related to the beamforming proposed in this thesis is more accurate because it depends on the measurements of speaker array. Also, the basic crosstalk canceller method related to HRTF takes omnidirectional sources into account. Through the proposed line array speaker technique, a natural channel separation is offered by using its directional proprieties; as a result, this causes crosstalk attenuation.

The electro-acoustic design presented in Chapter 5 has been successfully applied to the measurement of line-array directivity and testing of different 3D audio algorithm. Therefore, it can also be used in future work for applications that require multichannel amplification. Finally, in light of the results obtained in the measurement comparisons presented in Chapter 6, it can be concluded that the theoretical estimations coincide with the measured results.

7.1 Contributions

In chapter 3, a crosstalk canceller algorithm to obtain transaural sound was presented. The proposed method is more accurate than HRTF because depends on the directivity of the speaker array, and it can be known in advance.

The Graphical User Interfaces (GUI) developed in Chapter 4 can obtain the directivity function of multiple line array configurations. The GUI serves as a convenient tool to study and understand the beamforming theory. It also presented a method to improve the representation of the measured results by interpolation and smoothing the original recorded data.

The contribution in Chapter 6 is the presentation of the design, the construction and the measurement of an eight-channel amplifier. It can be used for High Fidelity audio reproduction in low power applications, such as TV, electronic tables, and computers.

In order to validate the theoretical estimations, Chapter 7 compared the simulated with measured directivity functions of the line array speakers. In addition, a relation between the diameter of the speaker diaphragm and the element size of the phased array was proposed by comparing several measurements. This provides a method to predict the apparition of the grating lobes only by knowing the diameter of the diaphragm.

7.2 Future work

This thesis has uncovered many topics to research in this area; some of them are listed below.

Finite Difference Time Domain

Finite Difference Time Domain (FDTD) is a versatile technique to solve problems with differential equations, like the propagation of acoustical waves in the air. By simulating with this technic, the beamforming can be study in time domain. In this thesis, a GUI was presented in order to simulate an eight-element line array at 1 kHz in a 9 m^2 square domain. Therefore, this simulation technique will be an adequate method to simulate and solve complex configurations only previously measured in anechoic chamber.

Noise cancelling

The using of microphone line arrays for noise cancelling has been deeply investigated during the last decades. Most of the research has been related with the recording process. By using beamformers, it is possible to focus the sound pressure at the listener ear in order to attenuate the signal coming from the reflections of the walls. Therefore, the speaker line array can be used to attenuate the noise.

Three-dimensional beamforming

By combining speakers in a line array, a cylinder source is obtained. If the speakers are disposed on a plane, it could be possible to obtain a source that is able to focus in two angles direction. The overall pressure will be the sum of all the pressures produced by the individual speakers. Also, the low frequency will be increased due to the proximity of the speakers. This method would provide new design opportunities for sound sources.

Psycho-acoustical validation

Measurements for transaural audio can be carried out in anechoic chamber with Head and Torso Simulator. Additionally, it would be interesting to prepare an experiment with human listeners. This measurement would require a big group of people, but it can offer a good estimation of the results obtained in this thesis related with 3D sound.

References

[1] B. Webb and J. Baird. "*Advances in Line Array Technology for Live Sound*". Martin Audio Limited

[2] Don Davis and Eugene Patronis, *Sound system engineering*. Burlington: Focal Press, 2006.

[3] David T. Blackstock, *Fundamentals of physical acoustics.* New York: Wiley-Interscience publication, 2000.

[4] Glen Ballou, *Electroacoustic Devices: Microphones and Loudspeakers*. Burlington: Focal Press, 2009.

[5] B. McCarthy, *Sound Systems Design and Optimization*¸ Burlington: Focal Press, 2007

[6] D. Smith, *"Discrete-Element Line Arrays--Their Modeling and optimization*". J. Audio Eng Soc., Vol. 45, No. 11, November 1997

[7] D. Smith, "*Discrete Element Line Arrays (Everything There Is To Know About...)".* AES 99th Convention Paper, 1995, pp. 4060.

[8] M. Ureda, *"Line Arrays: Theory and Applications".* AES 110th Convention Paper, 2001, pp. 5304.

[9] M. Ureda, "Analysis of Loudspeaker Line Arrays". JBL Professional, 2004

[10] L. Azar, Y. Shi and S. Wooh, "*Beam focusing behavior of linear phased arrays*". NDT&E International 33, 2000, pp. 189–198.

[11] S. Wooh and Y. Shi, "*Optimum beam steering of linear phased arrays".* Wave Motion 29, 1999, pp. 245–265.

[12] S. Wooh and Y. Shi, *"Influence of phased array element size on beam steering behavior".* Ultrasonics 36, 1998, pp. 737–749.

[13] R. Schimidmaier and G. Meyer. *"Dynamic Amplitude Shading Of Electronically Steered Line Source Arrays"*. AES 92th Convention Paper, 1992, pp. 3272.

[14] M. Urban, C. Heil and P. Baunan, *"Wavefront Sculpture Technology".* AES 111th Convention Paper, 2001, pp. 5488.

[15] M. Ureda, "*Pressure Response of Line Sources*". AES 113th Convention Paper, 2002, pp. 5649.

[16] J. Werff, "*Electronically Controlled Loudspeaker Arrays without Side Lobes*". AES 110th Convention Paper, 2001, pp. 5322.

[17] C. Neil and M. Urban, "*Sound Field Radiated by Multiple Sound Source Arrays*". AES 92th Convention Paper, 1992, pp. 3269.

[18] Technical Report, "DSP Beam Steering with Modern Line Arrays". Meyer Sound Laboratories, 2002

[19] Y. Shen, D. Ou and K. An, *"The Relation between Active Radiating Factor and Frequency Responses of Loudspeaker Line Arrays".* AES 122nh Convention Paper, 2007, pp. 7058.

[20] C. Jiang, J. Zou and Y. Shen, *"Impulse Response and Frequency Response of A Line Loudspeaker Array"*. AES 117th Convention Paper, 2004, pp. 6248.

[21] D. Meyer, "*Multiple-Beam, Electronically Steered Line-Source"*. J. Audio Eng Soc., Vol. 38, No. 4, April 1990

[22] S. Wooh and Y. Shi, *"A Simulation Study of the Beam Steering Characteristics".* Journal of Nondestructive Evaluation, Vol. 18, No. 2, 1999

[23] N. Sakamoto, W. Kobayashi, T. Onoye and I. Shirakawa, "DSP implementation of low computational 3D sound localization algorithm" IEEE 0-7803-7145-3, 2001

[24] J. Bauck, "A simple loudspeaker array and associated crosstalk". J. Audio Eng Soc., Vol. 49, No. 1/2, January/February 2001

[25] S. Kim, S. Jang, D. Kong and S. Bang, "Adaptive Virtual Surround Sound Rendering Method for an Arbitrary Listening Position". AES 30nd International Conference, 2007.

[26] M. Guldenschuh and A. Sontacchi. "*Transaural stereo in a beamforming approach*", Int. Conference on Digital Audio Effects, 2009

[27] W. Gardner, "3-D Audio Using Loudspeakers" Ph.D. dissertation, Massachusetts Institute of Technology., USA, 1997

[28] U. Zolzer, *Digital Audio Effects*. New York: Wiley, 2000

[29] J. Huopaniemi, "Vitual Acoutcis and 3-D sound in multimea signal processing". Ph.D. dissertation, Laboratory of Acoustics and Audio Signal Processing, Helsinki Univ., Finland, 1999

[30] R. Irwan and R. Aarts, *"A method to convert stereo to multi-channel sound".* AES 19th International Conference, 2001, pp. 5610.

[31] Y. Parodi, "A systematic Study of Binaural Reproduction Systems Through loudspeakers", Ph.D. dissertation, Department of Electronic Systems, Aalborg University, Denmark, 2010

[32] B. Wiggins, "An Investigation into the Real-time Manipulation and control of Three-Dimensional Sound Fields", Ph.D. dissertation, University of Derby, UK, 2004

[33] C. Avenado and J. Jot, "Frequency Domain Techniques for Stereo to Multichannel Upmix". AES 22nd International Conference, 2003.

[34] D. Self, *Audio Power Amplifier Handbook*. Burlington: Focal Press, 2009

[35] Glen Ballou, *Electroacoustic Devices: Microphones and Loudspeakers*. Burlington: Focal Press, 2009

[36] S. Kuo and B. Lee, Real-Time Digital Signal Processing. Chichester: Wiley & sons, 2001

[37] Texas Instruments, "TAS3108EVM2 User's Guide (Rev. A)", November 2005.

[38] Texas Instruments, "AUDIO DIGITAL SIGNAL PROCESSORS", TAS3108 datasheet, October 2005 [Revised November 2007].

[39] National Semiconductor, LM380 datasheet, August 2000 [Revised 2004].

[40] Sound system equipment - Part 3: Amplifiers, IEC 60268-3, 2000.

[41] Sound system equipment - Part 5: Loudspeakers, IEC 60268-5, 2003.

[42] M. Gander and J. Eargle, "Measurement and Estimation of Large Loudspeaker Array Performance". J. Audio Eng Soc., Vol. 38, No. 4, April 1990